FRONTIERS OF PHYSICS

VIEW & PERSPECTIVE
Volume 18 / Issue 6 / 64401 / 2023

On the question of quark confinement in the Abelian $U(1)$ QED gauge interaction

Cheuk-Yin Wong

Physics Division, Oak Ridge National Laboratory*, Oak Ridge, TN 37831, USA
E-mail: wongc@ornl.gov
Received January 14, 2023; accepted March 28, 2023

ABSTRACT

If we approximate light quarks as massless and apply the Schwinger confinement mechanism to light quarks, we will reach the conclusion that a light quark q and its antiquark $\bar{q}$ will be confined as a $q\bar{q}$ boson in the Abelian $U(1)$ QED gauge interaction in (1+1)D, as in an open string. From the work of Coleman, Jackiw, and Susskind, we can infer further that the Schwinger confinement mechanism persists even for massive quarks in (1+1)D. Could such a QED-confined $q\bar{q}$ one-dimensional open string in (1+1)D be the idealization of a flux tube in the physical world in (3+1)D, similar to the case of QCD-confined $q\bar{q}$ open string? If so, the QED-confined $q\bar{q}$ bosons may show up as neutral QED mesons in the mass region of many tens of MeV [*Phys. Rev. C* 81, 064903 (2010) & *J. High Energy Phys.* 2020(8), 165 (2020)]. Is it ever possible that a quark and an antiquark be produced and interact in QED alone to form a confined QED meson? Is there any experimental evidence for the existence of a QED meson (or QED mesons)? The observations of the anomalous soft photons, the X17 particle, and the E38 particle suggest that they may bear the experimental evidence for the existence of such QED mesons. Further confirmation and investigations on the X17 and E38 particles will shed definitive light on the question of quark confinement in QED in (3+1)D. Implications of quark confinement in the QED interaction are discussed.

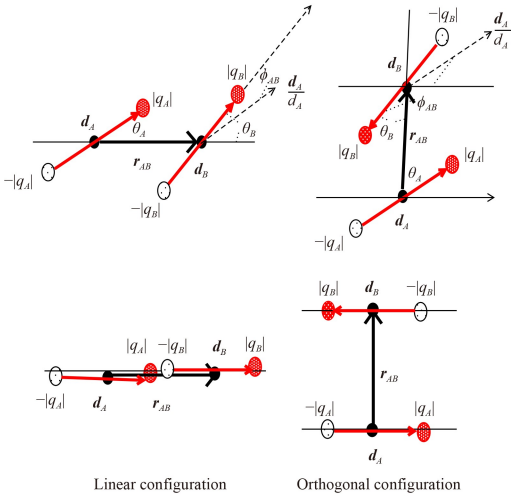

Keywords quark confinement, QCD interaction, QED interaction, Schwinger model, open string model of mesons, QCD molecular states

Contents

*This research was supported in part by the Division of Nuclear Physics, US Department of Energy under contract DE-AC05-00OR22725 with UT-Battelle, LLC. The publisher, by accepting the article for publication, acknowledges that the US government retains a nonexclusive, paid-up, irrevocable, worldwide license to publish or reproduce the published form of this manuscript, or allow others to do so, for US government purposes. DOE will provide public access to these results of federally sponsored research in accordance with the DOE Public Access Plan (URL: energy.gov/downloads/doe-public-access-plan), Oak Ridge, Tennessee 37831, USA.

Higher Education Press

arXiv: 2208.09920
https://doi.org/10.1007/s11467-023-1288-0

1 Introduction

As is well-known, quarks[1)] interact in the QCD (quantum chromodynamical) interaction and the QED (quantum electrodynamical) interaction. The general understanding is that the confinement of quarks arises from the non-Abelian nature of the QCD interaction in which the gluons mediate the QCD interaction between quarks and the gluons also interact among themselves. The self-interactions of gluons build the bridges connecting the quarks and confining the quarks.

The confinement of quarks is a peculiar phenomenon because quarks cannot be isolated. We can get an idea about such a peculiar property by asking whether a quark and its antiquark are confined in the QCD interaction at a certain energy. The answer is that only specifically at the eigenenergies in the QCD eigenstates, whose spatial extension spans a confined region, do a quark and an antiquark exist and are confined. However, at all other energies different from those of the QCD quark–antiquark eigenenergies, states of a quark and an antiquark do not exists — they do not exist as bound states, nor do they exist as continuum states of an isolated quark and antiquark. In contradistinction, for isolatable particles such as an electron and a positron interacting in QED, states of an electron and a positron exist at all energies above the positronium ground state energy, either as bound e^+e^- states or as continuum states of an isolated electron and positron. Therefore, a quark and an antiquark can be described as being confined in a certain interaction, if there exist confined $q\bar{q}$ eigenstates at the eigenenergies when a quark and an antiquark interact in that interaction, in conjunction with the absence of continuum states of an isolated quark and antiquark at other energies.

We would like to study quark confinement in the lowest energy states of a system of quarks interacting in the QED interaction. Such a study will benefit from the study of quarks interacting in the QCD interaction and vice versa. For this reason, we include also the QCD interaction in our consideration when it is appropriate. In order for quark–antiquark states to be observable, they must be among the bound and confined eigenstates arising from the quark and the antiquark interacting

[1)] We use the term "quarks" to include also the antiquarks implicitly, if no ambiguity arises. The term "antiquark(s)" will be explicitly used, if ambiguities may arise.

non-pertubatively at the appropriate eigenenrgies. As bound state are involved, we shall therefore consider the QCD and QED interactions between the quark and the antiquark to be implicitly non-perturbative in nature, and limit our attention to those systems that can potentially be bound and confined at possible eigenenergies.

For the non-Abelian QCD interaction, the question of quark confinement in QCD can be inferred from the QCD potential between a static quark and a static antiquark. For example, the quark and the antiquark appear as static external probes represented by time-like world lines at fixed spatial separations in a Wilson loop, given in terms of the product of link variables. The area law of the Wilson loop gives a linear QCD interaction potential between the quark and the antiquark, which leads to QCD meson eigenstates at eigenenergies in the confining quark–antiquark potential and the absence of continuum states of an isolated quark and antiquark at other energies.

However, for quarks interacting in the QED interaction, the question of quark confinement in (3+1)D cannot be answered by just studying the static QED potential between a static quark and an antiquark as inferred from static lattice gauge calculations only, because there is an important Schwinger confinement mechanism[2)] associated with the interplay between gauge fields A^μ and dynamical quark currents j^μ [1–4] that may play an important role in the question of confinement as we shall examine in Section 3. In particular, if we consider quark confinement just from the viewpoint of the static QED potential between a static quark and an antiquark as inferred from static lattice gauge calculations, we will reach the conclusion that a static quark and an antiquark will be deconfined in compact QED in (3+1)D because the compact QED interaction[3)] belongs to the weak-coupling regime in lattice gauge calculations in (3+1)D [5–18], as we shall discuss in more detail in Section 6. However, a serious question arises because if a static quark and a static antiquark are deconfined in compact QED in (3+1)D, the isolated quark and antiquark will appear as fractional charges, because there exists no physical laws to forbid quarks and antiquarks to interact in QED alone below the pion mass gap m_π. In a contradicting manner, no such deconfined quarks and antiquarks in the form of isolated fractional charges have ever been observed in (3+1)D. The absence of fractional charges suggests that previous conclusion of deconfined static quark and antiquark in compact QED in (3+1)D may not be as definitive as it may appear to be. The Schwinger confinement mechanism may need to be included in future lattice gauge calculations. We may need to return to the basic description of quark confinement in terms of the existence of confining eigenstates at quark–antiquark eigenenergies when quarks are treated as dynamical fields in an Abelian QED gauge interaction, in conjunction with the absence of continuum states of an isolated quark and antiquark at other energies. We shall return to this question and discuss the relevant salient points in Section 6.

Out of scientific curiosity with encouraging suggestions from theories and experiments, we study whether quarks are confined when they interact in QED alone, without the QCD interaction. If we approximate light quarks as massless and we apply the Schwinger confinement mechanism [1, 2] to light quarks, we will reach the conclusion that a light quark and a light antiquark will be confined in QED in (1+1)D as in an open string [27–34]. From the work of Coleman, Jackiw, and Susskind on massive Schwinger model [3, 4], we can infer further that the Schwinger confinement mechanism persists in (1+1)D even for massive quarks. Could such a QED-confined one-dimensional $q\bar{q}$ open string in (1+1)D space-time be the idealization of a flux tube in the physical (3+1)D, with the quark and the antiquark at the two ends of the flux tube? If so, the confined $q\bar{q}$ states in (1+1)D will show up as neutral QED mesons in (3+1)D. Is it ever possible for a quark and an antiquark to be produced and to interact in QED alone so as to form a confined QED meson? Is there any experimental evidence to indicate the possible existence of the QED-confined $q\bar{q}$ meson or mesons?

Such questions have not been brought up until recently for obvious reasons. It is generally perceived that a quark and an antiquark interact with the QCD and the QED interactions simultaneously, with the QED interaction as a perturbation, and the occurrence of a stable and confined state of the quark and the antiquark interacting in the QED interaction alone, without the QCD interaction, may appear impossible. Furthermore,

[2)] The Schwinger confinement mechanism, also known as the Schwinger model or the Schwinger QED2 model, refers to the mechanism in which a massless charged fermion and its antifermion interacting in QED in (1+1)D are confined and bound into a neutral boson with a mass $m = g_{2D}/\sqrt{\pi}$, where g_{2D} is the magnitude of the dimensional coupling constant in (1+1)D [1, 2]. It differs from the Schwinger pair production mechanism which refers to the mechanism for the production of charge pairs in a strong electric field examined in [19]. For a pedagogical review of the Schwinger pair-production mechanism and the Schwinger confinement mechanism, see Chapter 5 and Chapter 6 of [20] respectively. Recent generalizations and extensions of the Schwinger model have been presented in [21–25]. Recent lattice gauge solution of the massive Schwinger model has been obtained in [26].

[3)] To study quark confinement in QED in lattice gauge calculations in (3+1)D, we need to consider only the compact QED because in non-compact QED a quark and an antiquark are always deconfined in lattice gauge calculations in (3+1)D [6]. For the Schwinger confinement mechanism in (1+1)D, the confinement mechanism occurs in the continuum limit, which is the same for both the compact QED or the non-compact QED. There is no need to specify the compact or non-compact nature of the QED interaction in the Schwinger confinement mechanism.

the common perception is that only the QCD interaction with its non-Abelian properties can confine a quark and an antiquark, whereas the QED interaction is Abelian. It has been argued that even if a quark and an antiquark can interact in the QED interaction alone, the QED interaction by itself cannot confine the quark and the antiquark, as in the case of an electron and a positron, so the quark and the antiquark cannot be confined even if they can interact with the QED interaction alone.

Experimentally, the occurrence of anomalous neutral bosons with masses in the region of many tens of MeV suggests a need to re-examine the above common perceptions with regard to the question of quark confinement in the QED interaction. Specifically, (i) the observation of the anomalous soft photons in high-energy hadron–hadron collisions [36–42] and e^+e^- annihilation collisions [42–45], (ii) the observation of the X17 particle at about 17 MeV [46–51], and (iii) the observation of the E38 particle at about 38 MeV [52, 53] point to the possible existence of anomalous neutral particles at energies of many tens of MeV [27–34]. These anomalous particles may apparently place them outside the known families of the Standard Model. However, if we wish to include only particles and interactions within the Standard Model, a consistent and viable picture of these anomalous particles emerges to describe them as composite particles of a quark and an antiquark interacting non-perturbatively in the QED interaction [27–34]. We would like to explain here how such a description of quark confinement in QED in (3+1)D emerges as a reasonable theoretical concept consistent with the experimental observations. The present review is also timely since it predicts an isoscalar $q\bar{q}$ composite particle with a mass of about 17 MeV that is a good candidate for the observed X17 particle, and the confirmation of the X17 particle is actively pursued by many laboratories as summarized in [54], including ATOMKI [55], Dubna [56], STAR [57], MEGII [58], TU Prague [59], NTOF [60], NA64 [61], INFN-Rome [62], NA48 [63], Mu3e [64], MAGIX/DarkMESA [65], JLAB PAC50 [66, 67], PADME [68], DarkLight [69, 70], LUXE [71], and Montreal TandemMon22.

This paper is organized as follows. In Section 2, we present examples of reactions in which a $q\bar{q}$ pair may be produced and may interact in QED alone. In Section 3, we apply the Schwinger confinement mechanism to quarks interacting in QED and show that a quark and an antiquark approximated as massless are confined in QED in (1+1)D. We discuss the effects of quark masses on the Schwinger confinement mechanism. We infer from the works of Coleman, Jackiw & Susskind that the Schwinger confinement mechanism persists even for massive quarks in (1+1)D. In Section 4, we make the quasi-Abelian approximation of the non-Abelian QCD dynamics to search for stable collective excitations in QCD. The quasi-Abelian approximation allows the generalization of the Schwinger mechanism from QED in (1+1)D to (QCD+QED) in (1+1)D. We obtain the open string model of QCD and QED mesons. We use the open string model of QCD and QED mesons in (1+1)D as a phenomenological model to study the masses of π^0, η, and η' in order to determine the QCD coupling constant and the flux tube radius. Extrapolation of the QCD open string model to the QED open string model with the QED fine-structure coupling constant, we predict the masses of the QED mesons. In Section 5, we discuss the decay modes of the QED mesons and examine recent experimental observations of anomalous particles in the mass region of many tens of MeV produced in low-energy pA, and high-energy e^+–e^-, hadron–hadron, and nucleus–nucleus collisions. We compare the masses of the experimental anomalous particles with the predicted QED meson masses. There is a reasonable agreement of the predicted QED meson masses with the observed experimental masses of the X17 and the E38 particles, placing the QED mesons as good candidates to describe these anomalous particles. In Section 6, we examine the question of quark confinement in QED from the viewpoint of lattice gauge calculations which indicate that quarks in compact QED in (3+1)D are not confined. We discuss the lattice gauge calculation results of deconfined quarks in compact QED in (3+1)D, which contradicts the experimental absence of fractional charges. It is therefore suggested that the Schwinger confinement mechanism may need to be included in future lattice gauge calculations for quarks in compact QED in (3+1)D. We propose a "stretch (2+1)D" model to study the importance of the Schwinger confinement mechanism by combining the Schwinger confinement mechanism of QED in (1+1)D with Polyakov's transverse confinement in (2+1)D. In Section 7, We discuss the implications of quark confinement in the QED interaction. Many new phenomena and molecular states may emerge if quarks are confined in the QED interaction. We present our conclusions and discussion in Section 8.

2 Could a $q\bar{q}$ pair be produced and interact non-perturbatively in QED alone?

The proposal of quark confinement in QED [27–34] involves the hypothesis that a quark and an antiquark could be produced below the QCD pion mass gap m_π and could interact non-perturbatively in QED to lead to QED collective excitation, whereas the collective excitations of the QCD interaction will not be excited as they require an excitation energy higher then the pion mass gap and the QCD interaction appears as a spectator interaction. From the static quark and antiquark viewpoint, the common perception is that a quark and an antiquark interact simultaneously in QCD and QED. However, from the dynamical viewpoint of the quantum field theory of quarks interacting in the QED and the QCD interaction, we envisage that quarks can exchange a virtual gluon to interact non-perturbatively in the

QCD interaction. They can also exchange a virtual photon to interact non-pertuabatively in the QED interaction. There is no theorem nor basic physical principle that forbids a quark and an antiquark to exchange a virtual photon and interact non-perturbative in the QED interaction alone. What is not forbidden is allowed, in accordance with Gell-Mann's Totalitarian Principle [73]. Therefore, it is theoretically permitted to explore the hypothesis that a quark and an antiquark could interact in QED alone.

Experimentally, we can consider the production of $q\bar{q}$ pairs in e^+ and e^- collisions in Fig. 1 as examples. The energy threshold for such a reaction is $m_q + m_{\bar{q}}$ which is about a few MeV [74]. At low collision energies, a single $q\bar{q}$ pair may be produced as shown in the diagrams in Figs. 1(a) and (b). As the collision energy increases, many $q\bar{q}$ pairs may be produced in high-energy collisions, as shown in Fig. 1(c):

$$e^+ + e^- \to \gamma \to q + \bar{q}, \tag{1a}$$

$$e^+ + e^- \to \gamma + \gamma \to q + \bar{q}, \tag{1b}$$

$$e^+ + e^- \to \gamma \ \text{ or } \ Z^0 \to (q\bar{q})^n. \tag{1c}$$

The incident e^+ and e^- pair is in a colorless color-singlet state in reactions (1a) and (1b). The produced $q + \bar{q}$ pair must combine with their interacting virtual gauge boson γ or g to result in a colorless color-singlet final state. The produced q resides in the color-triplet **3** representation, and the produced $\bar{q}$ in the anti-triplet $\mathbf{3}^*$ representation. They can combine to form the color-singlet **1** and the color-octet **8** configurations,

$$\mathbf{3} \otimes \mathbf{3}^* = \mathbf{1} \oplus \mathbf{8}. \tag{2}$$

The produced q and $\bar{q}$ in their coupled color-singlet configuration can interact non-perturbatively in the QED interactions and combine with a virtual photon γ to form a color-singlet $[(q\bar{q})^1\gamma^1]^1$ final state, where the superscripts denote color multiplet indices. Similarly, the produced q and $\bar{q}$ in their color-octet configuration can interact non-perturbatively in the QCD interactions and combine with a virtual gluon g to form a color-singlet $[(q\bar{q})^8 g^8]^1$ final state. A $q\bar{q}$ pair will be produced at the eigenenergy of a QCD-confined $[(q\bar{q})^8 g^8]^1$ eigenstate, as a QCD meson. In a similar way, a $q\bar{q}$ pair will be produced at the eigenenergy of a QED-confined $[(q\bar{q})^1\gamma^1]^1$ eigenstate as a QED meson, if there is such an eigenstate at that eigenenergy. At all other energies, no $q\bar{q}$ pair will be produced because a confined $q\bar{q}$ or a continuum state of a quark q and an antiquark $\bar{q}$ do not exist at these energies. Reactions involving the production of a $q\bar{q}$ pair contain the density of final-states factor, which is a delta-function at the eigenenergies of the confined $q\bar{q}$ eigenstates.

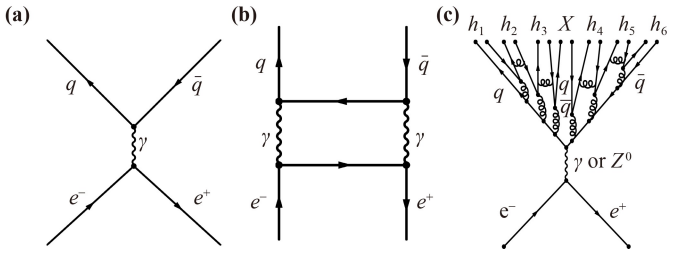

Fig. 1 **(a)** The production of a $q\bar{q}$ pair by the e^++e^- collision with a single intermediary virtual photon at low energies, **(b)** the production of a $q\bar{q}$ pair by the e^++e^- collision with two intermediary virtual photons at low energies, and **(c)** the production of many $q\bar{q}$ pairs by the e^++e^- collision at high energies.

We can examine the $e^+ + e^- \to q + \bar{q}$ reactions in Figs. 1(a) and (b) with a center-of-mass energy $\sqrt{s}(q\bar{q})$ in the range $(m_q + m_{\bar{q}}) < \sqrt{s}(q\bar{q}) < m_\pi$, where the sum of the rest masses of the light quark and light antiquark is of order a few MeV and $m_\pi \sim 135$ MeV [74]. If there is a confined $[(q\bar{q})^1\gamma^1]^1$ QED eigenstate in this energy range, then a confined $q\bar{q}$ pair can be produced as a QED meson. Such a QED meson can come only from the non-perturbative QED interaction but not from the non-perturbative QCD interaction, because the non-perturbative QCD interaction with a virtual gluon exchange would endow the $q\bar{q}$ pair as a composite $[(q\bar{q})^8 g^8]^1$ QCD meson with a center-of-mass energy $\sqrt{s}(q\bar{q})$ beyond this energy range, in a contradictory manner. It is therefore possible for a quark and an antiquark to be produced and interact non-pertubatively in the QED interaction to lead to a QED meson, if there exists a QED meson eigenstate in this energy range. At energies other than the QED meson eigenenergies, in this energy range below m_π, the $e^+ + e^-$ collisions will probe the dynamics of a quark and antiquark interacting in QED alone, without the QCD interaction. In this energy range, the absence of fractional charges in $e^+ + e^-$ collisions will indicate the absence of the continuum isolated quark and antiquark states when a quark and an antiquark interact in the QED interaction alone.

As the $e^+ + e^-$ collision energy increases, many $q\bar{q}$ pairs will be produced as shown in Fig. 1(c). At the Z^0 resonance energy in the DELPHI experiments [42–45], most of the produced $q\bar{q}$ pairs will materialize as $q\bar{q}$ QCD mesons labeled schematically as h_i in Fig. 1(c). However, there may be a small fraction of the $q\bar{q}$ pairs which will have invariant masses below the pion mass. If there is a confined $q\bar{q}$ QED meson state at the appropriate eigenenergy below m_π, then the $q\bar{q}$ pair will be produced as a QED meson, shown schematically as the X particle in Fig. 1(c). The decay of the QED mesons into e^+ and e^- pairs may be the source of the anomalous soft photons observed at DELPHI [42–45].

As an illustrative case for a $q\bar{q}$ pair to be produced and to interact in the QED interaction alone, we have examined the above reaction, e^++e^-→ q+$\bar{q}$ below the

pion mass energy — as good examples. There are actually other circumstances in which a $q\bar{q}$ pair can also be created with a total pair energy lower than the QCD pion mass gap in other reactions, and the produced $q\bar{q}$ pair can interact in the QED interaction alone without the QCD interaction. For example, in the proposed experiment at JLAB with the collision of an electron on a nuclear charge Z [66, 67], a single or many $q\bar{q}$ pairs may be produced by the bremsstrahlung-type reaction as shown in Fig. 2(a) or in the fusion of two virtual photons as shown in Fig. 2(b):

$$e + Z \to e' + Z' + q + \bar{q}. \tag{3}$$

In such a reaction, in addition to the production of QCD mesons which are composite QCD-confined $q\bar{q}$ bound states, a QED meson may also be produced (shown schematically as the X particle in Fig. 2), if there is a QED-confined $q\bar{q}$ meson state at the appropriate eigenenergy below m_π. The produced QED may be detected by its decay products of an e^+e^- pair, a pair of real photons, or a pair of virtual photons as two pairs of dileptons.

In another example as shown in Fig. 3(a), we show an excited state of ^{4}He nucleus, that has been prepared in a low-energy p+^{3}H proton fusion reaction. For example, the $J^\pi I = 0^-0$ excited state at 20.02 MeV of ^{4}He can be formed by placing a proton in the stretched-out p state interacting with the ^{3}H core in Fig. 3(a) [46–48]. The de-excitation of the 20.02 MeV $J^\pi I = 0^-0$ ^{4}He* excited state to the ^{4}He$_{\text{g.s.}}$ ground state can occur by the proton emitting a virtual gluon which fuses with the virtual gluon from the ^{3}H core, to lead to the production of a $q\bar{q}$ pair as shown in Fig. 3(a). Note that in Fig. 3(a), the projectile A and target ^{3}H triton (BCD) are initially colorless prior to the collision. After each emitting a gluon such that the fusion of the two gluons lead to the production of the colorless QED meson, the scattered projectil nucleon

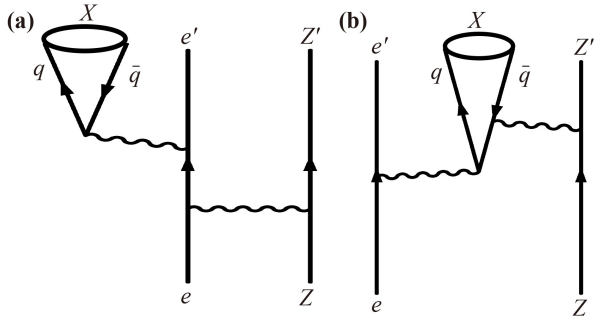

Fig. 2 In high-energy electron scattering off an atomic nuclei with charge Z, the bremsstrahlung-like reaction may lead to the emission of a photon, with the creation of a $q\bar{q}$ pair [66, 67]. A QED meson may be produced if the $\sqrt{s}$ of the emitted $q\bar{q}$ pair coincides with the eigenenergies of the QED meson, X, by a single photon emission as in **(a)**, or by the fusion of two photons, as in **(b)**.

A′ and the triton target (BCD′) are colored objects. The colored projectil nucleon A′ and the colored triton target (BCD′) can become colorless by exchanging a gluon and fusing into the colorless ground state of ^{4}He. Only by the exchanging a gluon and fusing into the ^{4}He ground state will the scattered proton A′ and ^{3}H′ lead to a colorless observable final state. Therefore, the emission of the QED meson is necessarily accompanied by the fusion of the proton and the triton core. It is interesting to note that there appears to be a similar requirement that the emission of the ABC resonance at ~310 MeV is accompanied by the fusion of the reacting nucleons [75–80], as will be discussed in Section 7.6.

Gluons reside in the color-octet **8** representation. In the fusion of gluons in the reaction $g + g \to q + \bar{q}$, the fusion gives rise to color multiplets as

$$\mathbf{8} \otimes \mathbf{8} = \mathbf{1} \oplus \mathbf{8} \oplus \mathbf{8} \oplus \mathbf{10} \oplus \mathbf{10} \oplus \mathbf{27}, \tag{4}$$

which contains the color-singlet component, **1**, among other color multiplets. There is thus a finite probability in which a color-singlet $q\bar{q}$ pair can be produced by gluon fusion. At very low energies in the de-excitation of the ^{4}He* nucleus, this gluon fusion process may lead to the production of a QED meson, if a QED meson eigenstate X exists at the appropriate energy, as labeled schematically in Fig. 3(a).

In high-energy hadron–hadron collisions at CERN [36–42] and nucleus–nucleus collisions at Dubna [52, 53], many $q\bar{q}$ pairs may be produced as depicted schematically in Fig. 3(b),

$$A + B \to A' + B' + (q\bar{q})^n. \tag{5}$$

The invariant masses of most of the produced $q\bar{q}$ pairs will exceed the pion mass, and they will materialize as QCD mesons and labeled as h_i in Fig. 2(b). However, there may remain a small fraction of the color-singlet $[q\bar{q}]^1$ pairs with an invariant masses below m_π. The $q\bar{q}$ pairs in this energy range below mass m_π allow the

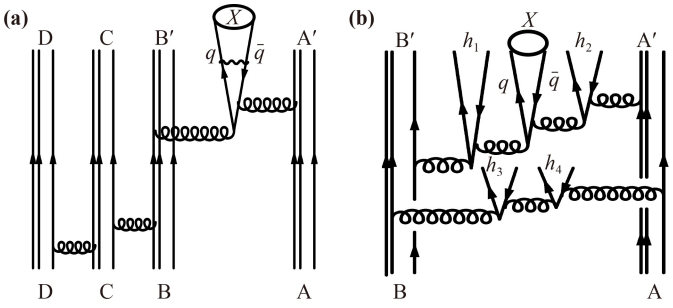

Fig. 3 **(a)** $q\bar{q}(X)$ production by the fusion of two virtual gluons in the de-excitation of a highly-excited ^{4}He*(ABCD) $\to^4$ He (ground state) (A′B′CD) + $q\bar{q}$(X) with the fusion of two virtual gluons between B and A. **(b)** $q\bar{q}(X)$ production in hadron $q\bar{q}$-hadron or a nucleus–nucleus collision by A + B $\to$ A′ + B′ + $(q\bar{q})^n \to$ A′ + B′ + $\sum_i h_i + q\bar{q}(X)$.

quark and the antiquark to interact in QED alone, without the QCD interaction, to lead to possible QED meson eigenstates labeled schematically as $q\bar{q}(X)$ in Fig. 3(b).

In other circumstances in the deconfinement-to-confinement phase transition of the quark–gluon plasma in high-energy heavy-ion collisions, a deconfined quarks and a deconfined antiquark in close spatial proximity can coalesce to become a $q\bar{q}$ pair with a pair energy below the pion mass, and they can interact in QED alone to lead to a possible QED meson, if there is QED-confined eigenstate in this energy range.

3 Quarks are confined in QED in (1+1)D

Having settled on the possibility for the production of a quark and an antiquark interacting in QED alone, we proceed to explore whether there can be confined $q\bar{q}$ eigenstates for quarks interacting in QED in (3+1)D. From the discussions in the Introduction, we are well advised to limit our attention only to those $q\bar{q}$ systems which potentially will be bound and confined. For this reason, we shall first examine the case of (1+1)D space-time and then proceed subsequently to the case of (3+1)D space-time.

Schwinger showed previously that a massless fermion and its antifermion interacting in an Abelian QED $U(1)$ gauge interaction with a coupling constant g_{2D} in (1+1)D are bound and confined as a neutral boson with a mass [1, 2],

$$m = \frac{g_{2D}}{\sqrt{\pi}}, \tag{6}$$

where the coupling constant g_{2D} has the dimension of a mass. We take the convention that the coupling constant g_{2D} to describe the interaction between a quark and an antiquark is positive for the QED and QCD interactions. We call this mechanism the Schwinger confinement mechanism[2)]. Such a Schwinger confinement mechanism occurs for massless fermions interacting in Abelian gauge interactions of all strengths of the coupling constant, including the interactions with a weak coupling strength (e.g., QED), as well as the interactions with a strong coupling strength (e.g., QCD). From the works of Coleman, Jackiw & Susskind [3, 4], we can infer further that the Schwinger confinement mechanism persists even for massive quarks in (1+1)D. It is in fact a general property for fermions and (quarks) of all masses interacting in the Abelian and quasi-Abelian gauge interaction with all coupling strengths in (1+1)D.

The masses of light quarks are about a few MeV [74], and they can be first approximated as massless. A light quark and its antiquark can be produced and can interact in a $U(1)$ Abelian QED gauge interaction alone, as discussed in the last section. Because they cannot be isolated, they reside predominantly in (1+1)D. The conditions for which the Schwinger confinement mechanism can be applicable are met by the light quark and its antiquark interacting in the QED interaction. We can therefore apply the Schwinger confinement mechanism to light quarks interacting in the QED interaction to infer that a light quark and its antiquark are bound and confined in QED in (1+1)D.

It is instructive to review here the Schwinger confinement mechanism how light quarks approximated as massless are confined in QED in (1+1)D. We shall subsequently discuss how the confinement property persists when quarks are massive. We envisages the vacuum of the interacting system as the lowest-energy state consisting of quarks filling up the (hidden) negative-energy Dirac sea and interacting with the QED interaction in (1+1)D space-time with coordinates $x = (x^0, x^1)$. The vacuum is defined as the state that contains no valence quarks as particles above the Dirac sea and no valence antiquarks as holes below the Dirac sea. We wish to describe in detail how an applied local QED disturbance in the form of $A^\mu(x)$ will generate self-consistently stable collective particle–hole excitations of the quark-QED system as in a quantum fluid. Subject to the applied disturbing gauge field $A^\mu(x)$ with a coupling constant g_{2D} in (1+1)D, the massless quark field $\psi(x)$ satisfies the Dirac equation,

$$\gamma_\mu(p^\mu - g_{2D}A^\mu)\psi = 0. \tag{7}$$

The applied gauge field $A^\mu(x)$ instructs the quark field $\psi(x)$ how to move. From the motion of the quark field $\psi(x)$, we can obtain the induced quark current $j^\mu(x) = \bar{\psi}(x)\gamma^\mu\psi(x)$. If we consider only the sets of states and quark currents that obey the gauge invariance by imposing the Schwinger modification factor to ensure the gauge invariance of the quark Green's function, the quark current $j^\mu(x)$ at the space-time point x induced by the applied $A^\mu(x)$ can be evaluated. After the singularities from the left and from the right cancel each other, the gauge-invariant induced quark current $j^\mu(x)$ is found to relate explicitly to the applied QED gauge field $A^\mu(x)$ by [1, 2, 20]

$$j^\mu(x) = -\frac{g_{2D}}{\pi}\left(A^\mu(x) - \partial^\mu\frac{1}{\partial_\eta\partial^\eta}\partial_\nu A^\nu(x)\right). \tag{8}$$

The derivation of the above important equality can be found in [2] and Chapter 6 of [20]. We can provide an intuitive understanding of the above relation between applied $A^\mu(x)$ and the induced $j^\mu(x)$ in the following way. The induced current $j^\mu(x)$ is a function of the applied gauge field $A^\mu(x)$, and $j^\mu(x)$ gains in strength as the applied strength of the gauge field $A^\mu(x)$ increases. So, the linear relation of Eq. (8) between $j^\mu(x)$ and $A^\mu(x)$ and its coupling constant g_{2D}, is a reasonable concept. The proportional property involving the coupling constant g_{2D} in Eq. (8) can also inferred by dimensional

analysis and the negative sign from simple intuitive physics arguments[4]. However, $j^\mu(x)$ is a gauge-independent quantity, whereas $A^\mu(x)$ is a gauge-dependent quantity. The right-hand side must be made gauge-independent and gauge invariant. The additional term on the right-hand side of the above relation consists of a linear function of $A^\mu(x)$ and a unique functional combination of partial derivatives that ensures the gauge-independence and gauge-invariance between $j^\mu(x)$ and $A^\mu(x)$. The gauge invariance of the relationship between $j^\mu(x)$ and $A^\mu(x)$ can be easily demonstrated directly upon a change of the gauge in $(A^\mu)'(x) \to A^\mu(x) - \partial^\mu\Lambda(x)$, for any local function of $\Lambda(x)$ in Eq. (8).

The induced gauge-invariant quark current $j^\mu(x)$ in turn generates a new gauge fields $\tilde{A}^\mu(x)$ through the Maxwell equation,

$$\begin{aligned}\partial_\mu F^{\mu\nu}(x) =&\partial_\mu\{\partial^\mu\tilde{A}^\nu(x) - \partial^\nu\tilde{A}^\mu(x)\}\\ =&g_{2D}j^\nu(x) = g_{2D}\bar{\psi}(x)\gamma^\nu\psi(x).\end{aligned} \tag{9}$$

A stable collective particle–hole excitation of the quark system occurs, when the initial applied $A^\mu(x)$ gives rise to the induced quark current j^μ which in turn leads to the new gauge field $\tilde{A}^\mu(x)$ self-consistently. We impose this self-consistency condition of the gauge field, $A^\mu(x) = \tilde{A}^\mu(x)$, by substituting the relation (8) into the Maxwell equation (9). We get both $j^\mu(x)$ and $A^\mu(x)$ satisfy the Klein–Gordon equation:

$$\begin{aligned}&\partial_\nu\partial^\nu A^\mu(x) + \frac{g_{2D}^2}{\pi}A^\mu(x) = 0,\\ &\text{and}\quad \partial_\nu\partial^\nu j^\mu(x) + \frac{g_{2D}^2}{\pi}j^\mu(x) = 0,\end{aligned} \tag{10}$$

for a bound and confined boson with a mass $m = g_{2D}/\sqrt{\pi}$ as given by Eq. (6). Hence, massless quarks in an Abelian QED U(1) gauge in (1+1)D are bound and confined as a neutral boson with a mass [1, 2]. In reaching the above Klein–Gordon equations for A^μ and j^μ for a bound boson, the second term on the right-hand side of Eq. (8) plays a crucial role, and such a term arises from the gauge invariance of the current. From this viewpoint, the confinement of the fermion–antifermion pair or the quark-antiquark into a boson owes crucially to the dynamics originating from the gauge invariance of the current, as emphasized by Schwinger [1, 2].

Light quarks have small but non-zero rest masses. From the Particle Group Tables, we have $m_u = 2.16^{+0.49}_{-0.26}$ MeV, and $m_d = 4.67^{+0.48}_{-0.17}$ MeV [74]. It is necessary to examine the effects of quark rest masses on the property of quark confinement because quarks are not exactly massless. How good is the massless approximation for light quarks in QCD and in QED in (1+1)D? Do the quark masses affect the quark confinement property of the Schwinger mechanism in (1+1)D?

Coleman, Jackiw & Susskind [3, 4] studied how the fermion masses affect the Schwinger confinement mechanism in (1+1)D. They showed that the Schwinger confinement mechanism persists even for massive fermions. Therefore, when we apply the results of Coleman, Jackiw, and Susskind for fermions to quarks, we reach the conclusion that a quark and its antiquark of the same flavor are always confined in QED in (1+1)D, no matter whether they have a small or large quark mass. As the Schwinger confinement mechanism occurs for all strength of the coupling constant, we can infer that a quark and an antiquark are confined as a neutral $q\bar{q}$ boson in QED in (1+1)D for all flavors of quarks, whatever their masses or the strengths of the coupling constant.

While the confinement of a quark–antiquark pair is quite a general result in (1+1)D for quarks with different flavors and coupling strengths of the gauge interaction, the effect of the quark masses and coupling constants manifest themselves in the spectral properties, boson properties, and the number of bound states of the confined bosons, depending on the comparison between the strength of the coupling constant g_{2D} and the quark mass m_q.

In the Schwinger confinement mechanism in (1+1)D, the coupling constant g_{2D} has the dimension of a mass and the coupling constant g_{2D} can be compared directly with the quark mass m_q. A quark of mass m_q interacting in a gauge interaction with a gauge coupling constant g_{2D} in (1+1)D belongs to the strong 2D-coupling regime if $g_{2D} \gg m_q$, and it belongs to the weak 2D-coupling regime if $g_{2D} \ll m_q$ [4]. We have added the label "2D" to the coupling regime to refer to the coupling regime in the Schwinger confinement mechanism in (1+1)D.

Coleman calculated the spectra of the quark systems in both the strong and the weak 2D-coupling regimes in [4]. In the strong 2D-coupling regime, quark systems always contain at least a stable meson, $m = g_{2D}/\sqrt{\pi} = m_{\text{meson}}$. It displays the properties of a meson with a weak-strength interaction between mesons. There will be a weakly bound collection of n-meson states of mass $\sim nm$ plus perturbation contributions that depend on the quark mass m_q. The spectra can be obtained by non-relativistic reasoning. In the weak 2D-coupling regime, quarks display the theory of a weak Coulomb interaction and the spectrum can be calculated by the mass-perturbation theory. Coleman also calculated the number of stable particles for the weak 2D-coupling

[4] From the Dirac equation (7), the quantities $g_{2D}A^0$ and p^0 have the same dimension. The quantity p^0 has dimension 1/length (in high energy units and conventions with $\hbar = 1$, $c = 1$) which is also the dimension of the particle density j^0 in (1+1)D. Hence, from dimensional analysis, $g_{2D}A^\mu$ has the same dimension as j^μ to establish the proportional relation of Eq. (8). We can infer the sign of their relation by introducing a positive Coulomb field $A^0(x^1)$ from a positive charge source at x^1, which will induce locally a negative charge density $j^0(x^1)$. Hence, the sign of their proportional relation has a negative sign on the right-hand side of Eq. (8).

regime and generalized the quark system to two flavors [4]. Coleman's results are useful for future studies of the spectral and boson properties of the QED-confined and QCD-confined $q\bar{q}$ bosons in (1+1)D which may find applications in the physical (3+1)D.

It is important not to confuse the strong and weak 2D-coupling regimes in the Schwinger confinement mechanism in (1+1)D with the strong and weak coupling regimes in quark confinement in static quark lattice gauge calculations in (3+1)D. In lattice gauge calculations in (3+1)D, a static quark and a static antiquark belong to the strong coupling regime with confined quarks for $g^2_{\rm 4D}/(4\pi) \gg \alpha_{\rm crit}$, and they belong to the weak coupling regime with deconfined quarks if $g^2_{\rm 4D}/(4\pi) \ll \alpha_{\rm crit}$ [5–18], where $\alpha_{\rm crit} = 0.988989481$ [17, 18]. For quarks interacting in the QED interaction for which $\alpha^{\rm QED} = (g^{\rm QED}_{\rm 4D})^2/(4\pi) = 1/137$, and $\alpha^{\rm QED} < \alpha_{\rm crit}$, we can conclude that a static quark and a static antiquark in QED interactions belongs to the deconfined weak-coupling regime in (3+1)D static quarks lattice gauge calculations. So, in (3+1)D a static quark and a static quark are not confined in compact QED lattice gauge calculations. In contrast, in the Schwinger confinement mechanism for QED in (1+1)D, a quark and an antiquark are always confined, whatever the magnitude of the coupling constant.

In the Schwinger confinement mechanism, it is instructive to compare the strength of coupling constant relative to the quark masses for quarks interacting with its antiquark in the QED interaction in the physical (3+1)D space-time. We can carry out similar comparison when we approximate non-Abelian QCD interaction as a quasi-Abelian interaction, as described in the next Section. The QED and QCD coupling constants, $g_{\rm 4D}$, are known in the physical (3+1)D world, and we need to know their corresponding (1+1)D coupling constant, $g_{\rm 2D}$, when we approximate a flux tube with a radius R_T as a string without a structure. We showed previously [27, 30, 31, 81, 82] that in such an idealization, $g^\lambda_{\rm 2D}$ in (1+1)D is related to $g^\lambda_{\rm 4D}$ in (3+1)D by

$$g^\lambda_{\rm 2D} = \left(\frac{1}{\sqrt{\pi} R_T}\right) g^\lambda_{\rm 4D} = \frac{\sqrt{4\alpha_\lambda}}{R_T}, \qquad \lambda = \begin{cases} 0 & \text{QED} \\ 1 & \text{QCD} \end{cases}, \tag{11}$$

where R_T is the radius of the flux tube, $\alpha_\lambda = (g^\lambda_{\rm 4D})^2/4\pi$, and λ is the label for the interaction. The qualitative consistency of such a relationship can be checked by dimensional analysis. By such a "dimensional transmutation" relation, the information on the structure of the flux tube radius R_T in (3+1)D is stored in the coupling constant $g_{\rm 2D}$ for its subsequent dynamics in (1+1)D.

For the QCD interaction, the value of R_T for a QCD open string has been found to be $R_T = 0.4$ fm, and $\alpha_{\rm QCD} = 0.67$ from the masses of the π^0, η, and η' [30], and $R_T = 0.35$ fm from the average transverse momentum of produced hadrons in pp collisions [27] in the open-string description. We have therefore

$$g^{\rm QCD}_{\rm 2D} = 807.5 \text{ to } 922.84 \text{ MeV}. \tag{12}$$

Thus, as far as Schwinger confinement mechanism in (1+1)D is concerned, $g^{\rm QCD}_{\rm 2D} \gg m_u, m_d, m_s$ and u, d, and s quarks interacting in the QCD interaction belongs to the strong 2D-coupling regime, whereas $g^{\rm QCD}_{\rm 2D} \ll m_c, m_b, m_t$ and c, b, and t quarks interacting in QCD belong to the weak 2D-coupling regime.

We do not know the flux tube radius R_T for the QED interaction. The meager knowledge from the possible QED meson spectrum and the anomalous soft photons suggests the flux tube may be an intrinsic property of a quark that may be independent or weakly dependent on the interactions, as such an assumption gives a reasonable description of the X17, E38, and anomalous soft photon masses [30], subject to future amendments as more experimental data become available. So, for the QED interaction with $\alpha_{\rm QED} = 1/137$ and we get for $R_T \sim 0.35$ to 0.4 fm,

$$g^{\rm QED}_{\rm 2D} \sim 84.28 \text{ to } 96.32 \text{ MeV}, \tag{13}$$

indicating $g^{\rm QED}_{\rm 2D} \gg m_u, m_d$. Light u and d quarks interacting in QED belong to the strong 2D-coupling regime whereas $g^{\rm QED}_{\rm 2D} \sim m_s$ and $g^{\rm QED}_{\rm 2D} \ll m_c, m_b$, and m_t, the s quark has a mass comparable to the $g^{\rm QED}_{\rm 2D}$. The c, b, and t quarks interacting in QED belongs to the weak 2D-coupling regime. Consequently, with light quarks interacting in QED belonging to the strong 2D-coupling regime, $g^{\rm QED}_{\rm 2D} \gg m_q$, the quarks mass will only be a perturbation in the light-quark QED meson spectrum.

The QED-confined meson states in (1+1)D can be viewed in two equivalent ways [27, 30, 31]. It can be depicted effectively as a QED-confined one-dimensional open string, with a quark and an antiquark confined at the two ends of the open string subject to an effective linear two-body confining interaction. A more basic and physically correct picture depicts the boson as the manifestation of a collective particle–hole excitation from the Dirac sea involving the coupled self-consistent responses of quark current j^μ and the gauge field A^μ. The quark confinement arises because the quark current j^μ and the gauge field A^μ depend on each other self-consistently and such a self-consistency leads to a stable and self-sustainable space-time variations of both the current j^μ and the gauge field A^μ. Specifically, through the Dirac equation for quarks, a space-time variation of the gauge field A^μ leads to a space-time variation in the quark current j^μ, which in turn determines the space-time variation of the gauge field A^μ through the Maxwell equation [1, 2, 20]. As a consequence of such self-consistent dependencies, a quantized and locally-confined space-time collective variations of the quark current j^μ and the QED gauge field A^μ can sustain themselves indefinitely at the lowest eigenenergy of the QED-confined $q\bar{q}$ state in a collective

motion as a one-dimensional open string with a mass, when the decay channels for the confined collective state are turned off for such an examination [27, 30]. From such a viewpoint, the Schwinger confinement mechanism is a many-body phenomenon containing dynamical quark effects beyond the potential interaction between a static quark and a static antiquark alone.

4 Generalizing the Schwinger confinement mechanism in (1+1)D from quarks in QED to quarks in (QCD+QED)

4.1 Question of the compactification of QCD and QED from (3+1)D to (1+1)D

From the works of Schwinger, Coleman, Jackiw, and Susskind [1–4], it can be inferred that the Schwinger confinement mechanism applies generally to all Abelian gauge theories in (1+1)D with fermions and quarks of all masses and coupling strengths. Even though QCD is a non-Abelian gauge theory, if the non-Abelian QCD can be approximated as an Abelian or quasi-Abelian gauge theory in (1+1)D, then the Schwinger confinement mechanism will apply also to quarks in QCD dynamics. Indeed, many features of the QCD mesons (such as quark confinement, meson states, and meson production), mimick those of the Schwinger model for the Abelian gauge theory in (1+1)D, as noted early on by Bjorken, Casher, Kogut, and Susskind [83, 84]. Such generic string feature in hadrons was first recognized even earlier by Nambu [85, 86] and Goto [87]. They indicated that in matters of confinement, quark–antiquark bound states and hadron production, an Abelian approximation of the non-Abelian QCD theory is a reasonable concept. Various nonlocal maximally Abelian projection methods to approximate the non-Abelian QCD by an approximate Abelian gauge theory have been suggested by 't Hooft [88], Belvedere *et al*. [89], Sekeido *et al*. [90], and Suzuki *et al*. [91]. Suganuma and Ohata [92] investigated Abelian projected QCD in the maximally Abelian gauge, and found a strong correlation between the local chiral condensate and magnetic fields in both idealized Abelian gauge systems and Abelian projected QCD.

Before we embark on the study of the dynamics of QCD and QED in the lower-dimension (1+1)D space-time, it is necessary to know how the dynamics of the lowest states in QCD and QED can be compactified from (3+1)D to (1+1)D. For the QCD dynamics in (3+1)D, 't Hooft showed that in a gauge theory with an $SU(N_{\rm color})$ gauge group approximated as a $U(N_{\rm color})$ gauge group in the large $N_{\rm color}$ limit, planar Feynman diagrams with quarks at the edges dominate, and the QCD dynamics in (3+1)D can be well approximated as QCD dynamics in (1+1)D [93, 94]. Numerical lattice calculations for a quark and antiquark system supports such concepts as they exhibits a flux tube structure [95–100]. Thus, the compactification of QCD in (3+1)D to QCD in (1+1)D is a reasonable concept.

For a quark and an antiquark interacting in the QED interaction in (3+1)D, however, the compactification from (3+1)D to (1+1)D is much more complicated and must be examined carefully. It has been known for a long time since the advent of Wilson's lattice gauge theory that a static fermion and a static antifermion in (3+1)D in compact QED interaction has a strong-coupling confined phase and a weak-coupling deconfined phase [7]. The same conclusion was reached subsequently by Kogut, Susskind, Mandelstam, Polyakov, Banks, Jaffe, Drell, Peskin, Guth, Kondo and many others [5–16]. The transition from the confined phase to the deconfined phases occurs at the coupling constant $\alpha_{\rm crit} = g^2_{\rm crit}/(4\pi) = 0.988\ 989\ 481$ [17, 18]. The magnitude of the QED coupling constant, the fine-structure constant $\alpha_c = 1/137$, places the QED interaction between a quark and an antiquark as belonging to the weak-coupling deconfined regime. Therefore, a static quark and a static antiquark are deconfined in lattice gauge calculations in compact QED in (3+1)D. However, no such fractional charges have ever been observed, even though there exists no physical law to forbid a quark and an antiquark to interact in the QED interaction alone. On the other hand, according to Schwinger, Coleman, Jackiw, and Susskind [1–4], there is a confined QED regime in (1+1)D, and from the work of Polyakov, there is in addition a confined regime for quarks in (2+1)D in compact QED [5], for all gauge coupling interaction strengths. To study the importance of the Schwinger confinement mechanism on quark confinement in QED in (3+1)D, we can combine Polyakov's transverse confinement of quarks in compact QED in (2+1)D with the longitudinal confinement of Schwinger's dynamical quarks in (1+1)D QED in our investigation on the compactification in (3+1)D, as is carried out in [34]. We construct a stretch (2+1)D model to study the importance of the Schwinger confinement mechanism in (3+1)D [33, 34]. We find there that the Polyakov's transverse confinement can effectively maintain a flux tube structure and the Schwinger longitudinal confinement can lead the compactification from $q\bar{q}$ in (3+1)D in QED to $q\bar{q}$ in (1+1)D as reviewed in Section 6. In view of the observation that quarks cannot be isolated and can be considered to reside predominantly in (1+1)D space-time, we can proceed to consider the compactification as a working hypothesis and examine its consequences as in [30], while we await the theoretical resolution on the question of QED compactification from (3+1)D to (1+1)D.

4.2 QCD and QED dynamics and bosonization in (1+1)D

Because of the three-color nature of the quarks, the quark current $j^\mu(x)$ and the gauge field $A^\mu(x)$ are 3×3

color matrices with 9 matrix elements at space-time point $x^\mu = (x^0, x^1)$ in (1+1)D space-time. The 9 matrix elements in the color space can be separated naturally into color-singlet and color-octet subgroups of generators. Specifically, quarks reside in the **3** representation and antiquarks reside in the $\mathbf{3}^*$ representation, and they form a direct product of $\mathbf{3}\otimes\mathbf{3}^* = \mathbf{1}\oplus\mathbf{8}$, with a color-singlet **1** subgroup and a color-octet **8** subgroup. The quark current j^μ and the QED and QCD gauge field A^μ are 3×3 color matrices which can be expanded in terms of the nine generators of the $U(3)$ group,

$$j^\mu = \sum_{i=0}^{8} j_i^\mu t^i, \quad A^\mu = \sum_{i=0}^{8} A_i^\mu t^i, \quad t^0 = \frac{1}{\sqrt{6}}\begin{pmatrix} 1 & 0 & 0 \\ 0 & 1 & 0 \\ 0 & 0 & 1 \end{pmatrix}, \tag{14}$$

where t^0 is the generator of the $U(1)$ color-singlet subgroup and $t^1, t^2, \cdots, t^8$ are the eight generators of the $SU(3)$ color-octet subgroup, with $A^\mu_{\rm QED}(x) = A^\mu_0(x)t^0$ and $A^\mu_{\rm QCD}(x) = \sum_{a=1}^{8} A^\mu_a(x)t^a$. We use the convention of summation over repeated indices, but the summation symbol and indices are occasionally written out explicitly to avoid ambiguities. The current j^μ and gauge field A^μ also possess the additional flavor label f and the interaction label λ. For brevity of notations, the indices a, f, and λ in various quantities are often implicitly understood except when they are needed. The coupling constants g^a_f in (1+1)D are given explicitly by

$$g^0_u = -Q_u\, g^{\rm QED}_{\rm 2D}, \quad g^0_d = -Q_d\, g^{\rm QED}_{\rm 2D} \qquad \text{for QED}, \tag{15a}$$

$$g^{\{1,..,8\}}_{\{u,d,s\}} = Q^{\rm QCD}_{\{u,d,s\}}\, g^{\rm QCD}_{\rm 2D} \qquad \text{for QCD}, \tag{15b}$$

where we have introduced the charge numbers

$$\begin{aligned} &Q^{\rm QED}_u = 2/3, Q^{\rm QED}_d = -1/3, Q^{\rm QED}_s = -1/3, \\ &Q^{\rm QCD}_u = Q^{\rm QCD}_d = Q^{\rm QCD}_s = 1, \\ &Q^{\{\rm QCD,QED\}}_{\bar q} = -Q^{\{\rm QCD,QED\}}_q. \end{aligned} \tag{16}$$

The Lagrangian density for the system is [101]

$$\mathcal{L} = \bar\psi(\mathrm{i}\not{D})\psi - \frac{1}{4}F_{\mu\nu}F^{\mu\nu} - m\bar\psi\psi, \tag{17a}$$

$$\mathrm{i}\not{D} = \gamma^\mu(\mathrm{i}\partial_\mu + gA_\mu), \tag{17b}$$

where for the non-Abelian QCD dynamics,

$$F_{\mu\nu} = \partial_\mu A_\nu - \partial_\nu A_\mu - \mathrm{i}g[A_\mu, A_\nu], \quad F_{\mu\nu} = F^a_{\mu\nu}t^a, \tag{18}$$

and the equation of motion for the gauge field A_μ is

$$\begin{aligned} &D_\mu F^{\mu\nu} = \partial_\mu F^{\mu\nu} - \mathrm{i}g[A_\mu, F^{\mu\nu}] = gj^\nu, \\ &j^\nu = j^{\nu\,a}t^a, \quad j^{\nu\,a} = 2\ \mathrm{tr}\ \bar\psi_f\gamma^\nu t^a\psi_f. \end{aligned} \tag{19}$$

We wish to search for bound states arising from the QED and QCD interactions in (1+1)D by the method of bosonization [3, 4, 84, 102, 106, 107, 109–114, 117], which consists of introducing boson fields ϕ^a to describe an element u of the $U(3)$ group and showing subsequently that these boson fields lead to stable bosons with finite or zero masses. As in any method of bosonization, the method will succeed for systems that contain stable and bound boson states with relatively weak residual interactions between the bosons. Thus, not all the degrees of freedom available to the bosonization technique will lead to good boson states with these desirable properties.

An element of the $U(1)$ subgroup of the $U(3)$ group can be represented by the boson field ϕ^0

$$u = \exp(\mathrm{i}2\sqrt{\pi}\phi^0 t^0). \tag{20}$$

Such a bosonization poses no problem as it is an Abelian subgroup. It will lead to a stable boson as in the Schwinger confinement mechanism.

On the other hand, the $U(3)$ gauge interactions under consideration contain the non-Abelian color $SU(3)$ interactions. Consequently the bosonization of the color degrees of freedom should be carried out according to the method of non-Abelian bosonization which preserves the gauge group symmetry [106]. While we use non-Abelian bosonization for the $U(3)$ gauge interactions, we shall follow Coleman to treat the flavor degrees of freedom as independent degrees of freedom [3, 4]. This involves keeping the flavor labels in the bosonization without using the flavor group symmetry.

In the non-Abelian bosonization, the current $j_\pm$ in the light-cone coordinates, $x^\pm = (x^0 \pm x^3)/\sqrt{2}$, is bosonized as [106]

$$j_+ = \ (\mathrm{i}/2\pi)u^{-1}(\partial_+ u), \tag{21a}$$

$$j_- = -(\mathrm{i}/2\pi)(\partial_- u)u^{-1}. \tag{21b}$$

To carry out the bosonization of the color $SU(3)$ subgroup, we need to introduce boson fields ϕ^a, with $a = 1, \cdots, 8$, to describe an element u of $SU(3)$ with the eight t^a generators which provide eight degrees of freedom as

$$u = \exp\left(\mathrm{i}2\sqrt{\pi}\sum_{a=1}^{8}\phi^a t^a\right). \tag{22}$$

However, the QCD $SU(3)$ gauge field and quark current dynamics in QCD will be coupled in the color-octet space in the eight t^a directions. Such couplings in the non-Abelian degrees of freedom will lead to color excitations, the majority of which will not lead to stable collective excitations. A general variation of the element $\delta u/\delta x^\pm$ will lead to quantities that in general do not commute with u and u^{-1}, resulting in $j_\pm$ currents in Eqs. (21) that are complicated non-linear admixtures of the boson fields ϕ^a. It will be difficult to look for stable boson states with these currents.

We can guide ourselves to a situation that has a greater chance of finding stable bosons by examining the

bosonization problem from a different viewpoint. We can introduce a unit generator vector τ^1 randomly in the eight-dimensional $SU(3)$ generator space,

$$\tau^1 = \sum_{i=1}^{8} n_a t^a, \quad \text{with } n_a = \text{tr}\{\tau^1 t^a\}/2$$
$$\text{and } \sqrt{n_1^1 + n_2^2 + \cdots + n_8^2} = 1. \tag{23}$$

We can describe an $SU(3)$ group element u by an amplitude ϕ^1 and the unit vector τ^1. To look for stable boson states, we wish to restrict our considerations in the color-octet subspace with a fixed orientation of τ^1 but allowing the amplitude ϕ^1 boson field to vary. The boson field ϕ^1 describes one degree of freedom, and the direction cosines $\{n^a, a = 1, \cdots, 8\}$ of the unit vector τ^1 describe the other seven degrees of freedom. A variation of the amplitude ϕ^1 in u while keeping the unit vector orientation fixed will lead to a variation of $\delta u/\delta x^{\pm}$ that will commute with u and u^{-1} in the bosonization formula (21), as in the case with an Abelian group element. Such a quasi-Abelian approximation will lead to simple currents and stable QCD bosons with well defined masses, which will need to be consistent with experimental QCD meson data. On the other hand, a variation of $\delta u/\delta x^{\pm}$ in any of the other seven orientation angles of the unit vector τ^1 will lead to $\delta u/\delta x^{\pm}$ quantities along other t^a directions with $a = \{1, \cdots, 8\}$. These variations of $\delta u/\delta x^{\pm}$ will not in general commute with u or u^{-1}. They will lead to $j_{\pm}$ currents that are complicated non-linear functions of the eight degrees of freedom. We are therefore well advised to search for stable bosons by varying only the amplitude of the ϕ^1 field, keeping the orientation of the unit vector fixed, and forgoing the other seven orientation degrees of freedom. For the $U(3)$ group, there is in addition the group element $u = \exp\{\text{i}2\sqrt{\pi}\phi^0 t^0\}$ from the QED $U(1)$ subgroup. Combining both $U(1)$ and $SU(3)$ subgroups, we can represent an element u of the $U(3)$ group by ϕ^0 from QED and ϕ^1 from QCD as [27]

$$u = \exp(\text{i}2\sqrt{\pi}\phi^0\tau^0 + \text{i}2\sqrt{\pi}\phi^1\tau^1), \tag{24}$$

where we have re-labeled t^0 as τ^0 such that

$$2\text{tr}(\tau^\lambda \tau^{\lambda'}) = \delta^{\lambda\lambda'}, \quad \text{with } \lambda, \lambda' = 0, 1. \tag{25}$$

The superscripts in the above equation is the interaction label with $\lambda = \{0, 1\}$ for QED and QCD, respectively. When we write out the flavor index explicitly, we have

$$u_f = \exp\{\text{i}2\sqrt{\pi}\phi_f^0\tau^0 + \text{i}2\sqrt{\pi}\phi_f^1\tau^1\}. \tag{26}$$

From (21a) and (21b), we obtain

$$j_{f\pm} = \mp\frac{1}{\sqrt{\pi}}\left[(\partial_\pm\phi_f^0)\tau^0 + (\partial_\pm\phi_f^1)\tau^1\right]$$
$$\text{when all } Q_f^\lambda = 1, \tag{27a}$$

$$= \mp\frac{1}{\sqrt{\pi}}\left[Q_f^0(\partial_\pm\phi_f^0)\tau^0 + Q_f^1(\partial_\pm\phi_f^1)\tau^1\right]$$
$$\text{when we include charge number } Q_f^\lambda. \tag{27b}$$

The Maxwell equation in light-cone coordinates is

$$\partial_\mu\partial^\mu A^\pm - \partial_\pm\partial_\mu A^\mu = g j^\pm. \tag{28}$$

We shall use the Lorenz gauge

$$\partial_\mu A^\mu = 0, \tag{29}$$

then the solution of the gauge field is

$$A^\pm = \frac{g}{2\partial_+\partial_-} j^\pm. \tag{30}$$

Interaction energy H_{int} is

$$\begin{aligned} H_{\text{int}} =& \frac{g}{2}\int \text{d}x^+\text{d}x^-\ 2\,\text{tr}\,(j\cdot A) \\ =& \frac{g}{2}\int \text{d}x^+\text{d}x^-\ 2\,\text{tr}\,(j^+A^- + j^-A^+) \\ =& \frac{g}{2}\int \text{d}x^+\text{d}x^-\ 2\,\text{tr}\left(j^+\frac{g}{2\partial_+\partial_-}j^- + j^-\frac{g}{2\partial_+\partial_-}j^+\right). \end{aligned} \tag{31}$$

We integrate by parts, include the charge numbers and the interaction dependency of the coupling constant, $g_{2\text{D}}^\lambda = g^\lambda$, and we obtain the contribution to the Hamiltonian density from the confining interaction between the constituents, $H_{\text{int}} = \int \text{d}x^+\text{d}x^-\mathcal{H}_{\text{int}}(\phi_f^\lambda)$,

$$\begin{aligned} &\mathcal{H}_{\text{int}}(\phi_f^\lambda) \\ &= \frac{1}{2}\left[\frac{(g_{2\text{D}}^0)^2}{\pi}(\sum_f^{N_f} Q_f^0\phi_f^0)^2 + \frac{(g_{2\text{D}}^1)^2}{\pi}(\sum_f^{N_f} Q_f^1\phi_f^1)^2\right], \end{aligned} \tag{32}$$

which matches the results of [4, 114].

For the mass bi-linear term, we follow Coleman [4] and Witten [106] and bosonized it as

$$\begin{aligned} m_f :\bar\psi_f\psi_f: \to& (-\frac{e^\gamma}{2\pi})\mu m_f\ 2\text{tr}\left(\frac{u_f + u_f^{-1}}{2}\right), \\ =& (-\frac{e^\gamma}{2\pi})\mu m_f\ 2\text{tr}\cos\left(2\sqrt{\pi}\phi_f^0\tau^0 + 2\sqrt{\pi}\phi_f^1\tau^1\right), \end{aligned} \tag{33}$$

where $\gamma = 0.5772$ is the Euler constant, and μ is a mass scale that arises from the bosonization of the scalar density $\bar\psi\psi$. It is proportional to the quark condensate $\langle 0|\bar\psi\psi|0\rangle$ and is interaction-dependent [4]. In the QCD case, we shall see later that through the Gell–Mann–Oakes–Renner relation, μ is related to the quark condensate $\langle 0|\bar q q|0\rangle$ by Eq. (57).

When we sum over flavors, we get the contribution to the Hamiltonian density from quark masses,

$$H_{\rm m}=\int {\rm d}x^+{\rm d}x^-\mathcal{H}_{\rm m}(\phi_f^\lambda), \tag{34}$$

where

$$\mathcal{H}_{\rm m}(\phi_f^\lambda)=e^\gamma\mu\sum_f m_f\left[(\phi_f^0)^2+(\phi_f^1)^2+...\right]$$
when μ is independent of interaction, (35a)

$$=e^\gamma\sum_f m_f\left[\mu^0(\phi_f^0)^2+\mu^1(\phi_f^1)^2+...\right]$$
when μ depends on interaction. (35b)

Finally, for the kinematic term, we bosonize it as [106, 107]

$$:\bar\psi{\rm i}\partial\!\!\!/\psi:\to\ \frac{1}{8\pi}\left\{2\,{\rm tr}\left[\partial_\mu u)\ (\partial^\mu u^{-1})\right]\right\}+n\Gamma, \tag{36}$$

where $n\Gamma$ is the Wess-Zumino term which vanishes for u of (24) containing commuting elements τ^0 and τ^1. We get the kinematic contribution

$$H_{\rm kin}=\int {\rm d}x^0{\rm d}x^1\mathcal{H}_{\rm kin}$$
$$=\int {\rm d}x^0{\rm d}x^1\sum\nolimits_f\frac{1}{8\pi}\left\{2\,{\rm tr}\left[(\partial_\mu u_f)\ (\partial^\mu u_f^{-1})\right]\right\}, \tag{37}$$

where

$$\mathcal{H}_{\rm kin}(\phi_f^\lambda)=\frac{1}{2}\sum\nolimits_f\left[\partial_\mu\phi_f^0\partial^\mu\phi_f^0+\partial_\mu\phi_f^1\partial^\mu\phi_f^1\right]$$
$$=\frac{1}{2}\sum\nolimits_\lambda\sum\nolimits_f\left[(\Pi_f^\lambda)^2+(\partial_x\phi_f^\lambda)^2\right], \tag{38}$$

and Π_f^λ is the momentum conjugate to ϕ_f^λ. The total Hamiltonian density in terms of ϕ_f^λ is

$$\mathcal{H}(\phi_f^\lambda)=\mathcal{H}_{\rm kin}(\phi_f^\lambda)+\mathcal{H}_{\rm int}(\phi_f^\lambda)+\mathcal{H}_{\rm m}(\phi_f^\lambda), \tag{39}$$

where $\mathcal{H}_{\rm kin}(\phi_f^\lambda)$, $\mathcal{H}_{\rm int}(\phi_f^\lambda)$, $\mathcal{H}_{\rm m}(\phi_f^\lambda)$ are given by Eqs. (38), (32), and (35b) respectively.

4.3 Orthogonal transformation to $q\bar q$ flavor eigenstates

We consider $q\bar q$ systems with dynamical flavor symmetry that lead to flavor eigenstates as a linear combination of states with different flavor amplitudes. Such eigenstates arise from additional considerations of isospin invariance, $SU(3)$ flavor symmetry, and configuration mixing. As a result of such considerations, the physical $q\bar q$ composite eigenstates i in the interaction type λ, Φ_i^λ, can be quite generally related to various flavor components ϕ_f by a linear orthogonal transformation as

$$\Phi_i^\lambda=\sum_f D_{if}^\lambda\phi_f^\lambda. \tag{40}$$

The orthogonal transformation matrix D_{if}^λ obeys $(D^\lambda)^{-1}=(D^\lambda)^\dagger$ with $((D^\lambda)^\dagger)_{fi}=D_{if}^\lambda$. The inverse transformation is

$$\phi_f^\lambda=\sum_i D_{if}^\lambda\Phi_i^\lambda. \tag{41}$$

Upon substituting the above equation into (39), we obtain the total Hamiltonian density in terms of the physical flavor state Φ_i^λ as

$$\mathcal{H}(\Phi_f^\lambda)=[\mathcal{H}_{\rm kin}(\Phi_i^\lambda)+\mathcal{H}_{\rm int}(\Phi_i^\lambda)+\mathcal{H}_{\rm m}(\Phi_i^\lambda)], \tag{42}$$

where $\mathcal{H}_{\rm kin}(\Phi_i^\lambda)=\frac{1}{2}\sum_\lambda\sum_i\left(\partial_\mu\Phi_i^\lambda\partial^\mu\Phi_i^\lambda\right)$
$$=\frac{1}{2}\sum_\lambda\sum_i\left[(\Pi_i^\lambda)^2+(\partial_x\Phi_i^\lambda)^2\right], \tag{43a}$$

$$\mathcal{H}_{\rm int}(\Phi_i^\lambda)=\frac{1}{2}\left[\sum_\lambda\frac{(g_{\rm 2D}^\lambda)^2}{\pi}(\sum_f Q_f^\lambda\sum_i D_{if}^\lambda\Phi_i^\lambda)^2\right], \tag{43b}$$

$$\mathcal{H}_{\rm m}(\Phi_i^\lambda)=e^\gamma\sum_f m_f\left[\sum_\lambda\mu^\lambda(\sum_i D_{if}^\lambda\Phi_i^\lambda)^2\right]. \tag{43c}$$

We can get the boson mass m_i^λ of the physical state Φ_i^λ by expanding the potential energy term, $\mathcal{H}_{\rm int}(\Phi_i^\lambda)+\mathcal{H}_{\rm m}(\Phi_i^\lambda)$, about the potential minimum located at $\Phi_i^\lambda=0$, up to the second power in $(\Phi_i^\lambda)^2$, as

$$\mathcal{H}(\Phi_i^\lambda)$$
$$=\sum_\lambda\sum_i\left[\frac{1}{2}(\Pi_i^\lambda)^2+\frac{1}{2}(\partial_x\Phi_i^\lambda)^2+\frac{1}{2}(m_i^\lambda)^2(\Phi_i^\lambda)^2\right]+..., \tag{44}$$

where

$$(m_i^\lambda)^2$$
$$=\left[\frac{\partial^2}{\partial(\Phi_i^\lambda)^2}[\mathcal{H}_{\rm int}(\{\Phi_i^\lambda\})+\mathcal{H}_{\rm m}(\{\Phi_i^\lambda\})]\right]_{\Phi_0^\lambda,\Phi_1^\lambda=0}. \tag{45}$$

From Eqs. (43b) and (43c), we find the squared mass $(m_i^\lambda)^2$ for the state Φ_i^λ of interaction λ to be

$$(m_i^\lambda)^2=\frac{(g_{\rm 2D}^\lambda)^2}{\pi}\left(\sum_f^{N_f}D_{if}^\lambda Q_f^\lambda\right)^2+e^\gamma\sum_f^{N_f}m_f\mu^\lambda(D_{if}^\lambda)^2. \tag{46}$$

This mass formula includes the mixing of the configurations, and is applicable to the open string model in QCD and QED.

The two terms on the right-hand side of (46) receive contributions from different physical sources. The first

term, the "massless quark limit" arises from the confining interaction between the quark and the antiquark. A comparison of this first term with the mass formula for a single unit charge in Eq. (6), $m^2 = g_{2D}^2/\pi$, suggests that in the state i with constituents q and $\bar{q}$ interacting in the λ-type interaction with flavor mixing, the $q\bar{q}$ composite particle behaves as if it consists effectively of a quark constituent q with an effective charge $\tilde{Q}_q^\lambda(i)$ given by

$$\tilde{Q}_q^\lambda(i) = \sum_f^{N_f} D_{if}^\lambda Q_f^\lambda, \tag{47}$$

confined with an antiquark constituent $\bar{q}$ of the opposite effective charge

$$\tilde{Q}_{\bar{q}}^\lambda(i) = -\tilde{Q}_q^\lambda(i). \tag{48}$$

For brevity of notation of the quark effective charge, the label (i) for the composite particle are often implicitly understood such that $\tilde{Q}_q^\lambda \equiv \tilde{Q}_q^\lambda(i)$ and $\tilde{Q}_{\bar{q}}^\lambda \equiv \tilde{Q}_{\bar{q}}^\lambda(i)$, if no ambiguity arises. The quark constituent in a $q\bar{q}$ meson possesses both an effective color charge number $\tilde{Q}_q^1$ for the QCD interaction and an effective electric charge $\tilde{Q}_q^0$ for the QED interaction. We shall discuss the dependence of the quark–antiquark potential on the effective charges in Section 4.7.

The second term arises from quark masses and the quark condensate, $\sum_f m_f \langle \bar{\psi}_f \psi_f \rangle$. It can be called the "quark mass term", or the "quark condensate term" because it depends on both. If one labels the square root of the first term in (46) as the confining interaction mass and the square root of the second term as the condensate mass, then the hadron mass obeys a Pythagoras theorem with the hadron mass as the hypotenuse and the confining interaction mass and the quark condensate mass as two sides of a right triangle.

Under the quasi-Abelian approximation of the non-Abelian QCD dynamics, the Schwinger confinement mechanism leads naturally to the (1+1)D open-string description of neutral confined bosons for both QCD and QED, with masses that depend on the magnitudes of the gauge field coupling constants g_{2D}^λ as given in Eq. (46). For the QCD interaction, we mentioned earlier that such a one-dimensional open-string solution of the lowest energy hadron states was suggested early on by the dual-resonance model [122], the Nambu and Goto meson string model [85–87], the 't Hooft's two-dimensional meson model [93, 94], the classical yo–yo string model [123], Polyakov's quantum bosonic string [124], and the Lund model [125–128]. The open-string description of hadrons was supported theoretically for QCD by lattice gauge calculations in (3+1)D in which the structure of a flux tube shows up explicitly [95–100]. The open-string description for $q\bar{q}$ QCD systems in high-energy hadron–hadron and e^+–e^- annihilation collisions provided the foundation for the (1+1)D inside–outside cascade model for hadron production of Bjorken, Casher, Kogut, and Susskind [83, 84], the yo–yo string model [123], the generalized Abelian Model [89], the projected Abelian model [88], the Abelian dominance model [90, 91], and the Lund model in high-energy collisions [125–128]. The flux tube description of hadrons receives experimental support from the limiting average transverse momentum and the rapidity plateau of produced hadrons [81, 83, 84, 129–131], in high-energy e^+–e^- annihilations [132–136] and pp collisions [137].

While a confined open string in (1+1)D as the idealization of a stable quark–antiquark system in (3+1)D is well known in QCD, not so well-known is the analogous confined open string quark–antiquark system in (1+1)D with a lower boson mass in QED, when we apply the Schwinger confinement mechanism for massless fermions to light quarks in QED in (1+1)D, as discussed in Section 3 [27–30]. We have asked earlier in the introduction whether the confined quark–antiquark one-dimensional open string in QED in (1+1)D could be a reasonable idealization of a stable QED $q\bar{q}$ meson in (3+1)D, just as the confined quark–antiquark Nambu–Goto open string in QCD in (1+1)D can be the idealization of a stable QCD $(q\bar{q})$ meson in (3+1)D.

From the viewpoint of phenomenology, we note that no fractionally-charged particles have ever been observed. Thus, quarks cannot be isolated. The non-isolation of quarks is consistent with the hypothesis that the open string $q\bar{q}$ boson solution in (1+1)D is an idealization of a confining flux tube between the quark and the antiquark in (3+1)D. On such a hypothesis, the open string description of a QED-confined $q\bar{q}$ boson is a reasonable concept that can be the basis of a phenomenological description of QED mesons whose validity needs to be constantly confronted with experiments. We can therefore study the question of quark confinement in QED from the phenomenological point of view. It is also necessary to examine the question of quark confinement in QED from the lattice gauge calculations viewpoints in (3+1)D, to be taken up in Section 6.

4.4 Relation between the coupling constants in (3+1)D and (1+1)D

In the phenomenological open string model for QCD and QED mesons, we need an important relationship to ensure that the boson masses calculated in the lower (1+1)D can properly represent the physical boson masses in (3+1)D. The one-dimensional $q\bar{q}$ open string in (1+1)D can be considered as an idealization of a flux tube with a transverse radius R_T in the physical world of (3+1)D. The flux tube in (3+1)D has a structure with a transverse radius R_T, but the coupling constant g_{4D} is dimensionless. In contrast, the open string in (1+1)D does not have a structure, but the coupling constant

g_{2D} has the dimension of a mass. We proved previously that the (1+1)D open string can be considered an idealization of a flux tube with a transverse radius R_T in the physical meson in (3+1)D, if the coupling constants g_{2D} in (1+1)D and g_{4D} in (3+1)D are related by [27, 30, 31, 81, 82]

$$(g_{2D})^2 = \left(\frac{1}{\pi R_T^2}\right)(g_{4D})^2 = \frac{4\alpha_{4D}}{R_T^2}, \tag{49}$$

whose qualitative consistency can be checked by dimensional analysis. Thus, when the dynamics in the higher dimensional 3+1 space-time is approximated as dynamics in the lower (1+1)D, information on the flux tube structure is stored in the multiplicative conversion factor $(1/\pi R_T^2)$ in the above equation that relates the physical coupling constant square $(g_{4D})^2$ in (3+1)D to the new coupling constant square $(g_{2D})^2$ in (1+1)D, as we discussed earlier in Section 3. As a consequence, there is no loss of the relevant physical information. The boson mass m determined in (1+1)D is the physical mass in (3+1)D, when we relate the coupling constant g_{2D} in (1+1)D to the physical coupling constant g_{4D} in (3+1)D and the flux tube radius R_T by Eq. (49). Consequently, the masses of the QED and QCD mesons in (3+1)D in the open-string description are approximately

$$m^2_{QCD} = \frac{(g^{QCD}_{4D})^2}{\pi} = \frac{4\alpha_{QCD}}{\pi R_T^2},$$
$$m^2_{QED} == \frac{(g^{QED}_{4D})^2}{\pi} = \frac{4\alpha_{QED}}{\pi R_T^2}. \tag{50}$$

With $\alpha^{QED}_{4D} = \alpha_{QED} = 1/137$, $\alpha^{QCD}_{4D} = \alpha_s \sim 0.68$ from hadron spectroscopy [27, 30] and $R_T \sim 0.4$ fm from lattice QCD calculations [97] and $\langle p_T^2\rangle$ of produced hadrons in high-energy e^+e^- annihilations [134], we estimate the masses of the open string QCD and QCD mesons to be

$$m^{QCD} \sim 458 \text{ MeV}, \quad \text{and} \quad m^{QED} \sim 48 \text{ MeV}. \tag{51}$$

The above mass scales provide an encouraging guide for the present task of a quantitative description of the QCD and QED mesons, using QCD and QED gauge field theories in (1+ 1)D. The QED mesons reside in the region of many hundred of MeV whereas the QED mesons in the region of many tens of MeV.

To get a better determination of the QCD and QED meson masses, it is necessary to take into account the flavor mixtures D^λ_{ij} and the quark color and electric charges $Q^\lambda_{\{u,d,s\}}$, the quark masses m_f, and the chiral condensate, as discussed in [30].

4.5 Open string model description of QCD mesons

We consider $q\bar{q}$ systems with dynamical flavor symmetry with physical flavor eigenstates Φ^λ_i as a linear combination of states with different amplitudes of $|q_f\bar{q}_f\rangle$ for quark–antiquark pairs of different flavor f, $\Phi^\lambda_i = \sum_f D^\lambda_{if}|q_f\bar{q}_f\rangle = \sum_f D^\lambda_{if}\phi_f$. Such eigenstates arise from additional considerations of flavor $SU(2)$ isospin invariance, $SU(3)$ flavor symmetry, and configuration mixing. As a result of such considerations in flavor symmetry and configuration mixing, the physical eigenstates Φ^λ_i can be quite generally related to various flavor components $\phi^\lambda_f = |q^\lambda_f\bar{q}^\lambda_f\rangle$ by a linear orthogonal transformation as $\Phi^\lambda_i = \sum_f D^\lambda_{if}\phi^\lambda_f$ of Eq. (40) leading to the meson mass formula in the open string model in Eq. (46).

We study first the QCD case with the label $\lambda = 1$, which is often implicitly understood in this subsection. Equation (51) indicates that the mass scale $m^{QCD} \sim 458$ MeV $\gg m_u, m_d, m_s$. It is necessary to include u, d, and s quarks with $N_f = 3$ in the analysis of open strings QCD mesons.

It is generally known that QCD has an approximate $SU(3)_L \times SU(3)_R$ chiral symmetry and also an approximate flavor $U(3)\times U(3)$ symmetry. If the axial symmetry is realized as the Goldstone mode as a result of the spontaneous chiral symmetry breaking, then one would naively expect the singlet isoscalar η' particle to have a mass comparable to the pion mass. Experimentally, there is the $U_A(1)$ anomaly [103–105, 120, 121] in which the η' mass of 957.8 MeV is so much higher than the π mass. On the basis of the Schwinger confinement mechanism [1, 2], Kogut, Susskind, and Sinclair [103–105] suggested that such a $U_A(1)$ anomaly arises from the long-range confinement between the quark and the antiquark, as the η' acquires a large mass from the long-range confining interaction between a quark and an antiquark. The long range gauge interaction affects not only η' mass but also the other pseudoscalar π^0, and η masses, and there are furthermore the effects of quark rest masses, the quark condensate, and the configuration mixing between η and η'. When these effects are properly taken into account, the pseudoscalar particles π^0, η, and η' can indeed be adequately described as open string QCD mesons.

We denote the flavor component states ϕ_i, with $\phi_1 = |u\bar{u}\rangle$, $\phi_2 = |d\bar{d}\rangle$, and $\phi_3 = |s\bar{s}\rangle$, and assume the standard quark model description of physical states Φ_j with $|\pi^0\rangle = \Phi_1$, $|\eta\rangle = \Phi_2$, and $|\eta'\rangle = \Phi_3$ in terms of flavor octet and flavor singlet states. The physical states of $|\pi^0\rangle$, $|\eta\rangle$, and $|\eta'\rangle$ can be represented in terms of the flavor states ϕ_1, ϕ_2 and ϕ_3 by

$$|\pi^0\rangle = \Phi_1 = \frac{\phi_1 - \phi_2}{\sqrt{2}}, \tag{52a}$$

$$|\eta\rangle = \Phi_2 = |\eta_8\rangle\cos\theta_P - |\eta_1\rangle\sin\theta_P, \tag{52b}$$

$$|\eta'\rangle = \Phi_3 = |\eta_8\rangle\sin\theta_P + |\eta_1\rangle\cos\theta_P, \tag{52c}$$

where the mixing of the $|\eta\rangle$ and $|\eta'\rangle$ is represented by a mixing angle θ_P, and the flavor-octet state $|\eta_8\rangle$ and the

flavor-singlet state $|\eta_1\rangle$ are

$$|\eta_8\rangle = \frac{\phi_1+\phi_2-2\phi_3}{\sqrt{6}}, \tag{52d}$$

$$|\eta_1\rangle = \frac{\sqrt{2}(\phi_1+\phi_2+\phi_3)}{\sqrt{6}}. \tag{52e}$$

The physical states $\Phi_i = \sum_f D_{if}\phi_f$ and the flavor component states ϕ_f, are then related by

$$\begin{pmatrix}\Phi_1\\ \Phi_2\\ \Phi_3\end{pmatrix} = \begin{pmatrix} \frac{1}{\sqrt{2}} & -\frac{1}{\sqrt{2}} & 0 \\ \frac{1}{\sqrt{6}}(\cos\theta_P-\sqrt{2}\sin\theta_P) & \frac{1}{\sqrt{6}}(\cos\theta_P-\sqrt{2}\sin\theta_P) & \frac{1}{\sqrt{6}}(-2\cos\theta_P-\sqrt{2}\sin\theta_P) \\ \frac{1}{\sqrt{6}}(\sin\theta_P+\sqrt{2}\cos\theta_P) & \frac{1}{\sqrt{6}}(\sin\theta_P+\sqrt{2}\cos\theta_P) & \frac{1}{\sqrt{6}}(-2\sin\theta_P+\sqrt{2}\cos\theta_P) \end{pmatrix} \begin{pmatrix}\phi_1\\ \phi_2\\ \phi_3\end{pmatrix},$$

with the inverse relation $\phi_f = \sum_{i=1}^3 D_{if}\Phi_i$,

$$\begin{pmatrix}\phi_1\\ \phi_2\\ \phi_3\end{pmatrix} = \begin{pmatrix} \frac{1}{\sqrt{2}} & \frac{1}{\sqrt{6}}(\cos\theta_P-\sqrt{2}\sin\theta_P) & \frac{1}{\sqrt{6}}\{\sin\theta_P+\sqrt{2}\cos\theta_P\} \\ -\frac{1}{\sqrt{2}} & \frac{1}{\sqrt{6}}(\cos\theta_P-\sqrt{2}\sin\theta_P) & \frac{1}{\sqrt{6}}\{\sin\theta_P+\sqrt{2}\cos\theta_P\} \\ 0 & \frac{1}{\sqrt{6}}(-2\cos\theta_P-\sqrt{2}\sin\theta_P) & \frac{1}{\sqrt{6}}\{-2\sin\theta_P+\sqrt{2}\cos\theta_P\} \end{pmatrix} \begin{pmatrix}\Phi_1\\ \Phi_2\\ \Phi_3\end{pmatrix}. \tag{53}$$

The mass formula (46) gives

$$\begin{aligned}(m_i^{\rm QCD})^2 =& \frac{(g_{\rm 2D}^{\rm QCD})^2}{\pi}\left(\sum_{f=1}^{N_f} D_{if}^{\rm QCD}Q_f^{\rm QCD}\right)^2 \\ &+\sum_{f=1}^{N_f} m_f (D_{if}^{\rm QCD})^2 e^\gamma \mu^{\rm QCD}, \\ \frac{(g_{\rm 2D}^{\rm QCD})^2}{\pi} =& \frac{4\alpha_s}{\pi R_T^2},\end{aligned} \tag{54}$$

yielding an effective color charge $\tilde{Q}_q^{\rm QCD} = \sum_{f=1}^3 D_{if}^{\rm QCD}Q_f^{\rm QCD}$.

With color charge $Q_{\{u,s,d\}}^{\rm QCD} = 1$, the pion state $|\pi^0\rangle = \Phi_1$ has an effective charge $\tilde{Q}_q^{\rm QCD}(\pi^0)$ given by $\sum_{f=1}^3 D_{1f}^{\rm QCD}Q_f^{\rm QCD} = 1/\sqrt{2}-1/\sqrt{2} = 0$. Consequently the first term in the mass formula (54), the "massless quark limit" term, gives a zero effective color charge, $\tilde{Q}_q^{\rm QCD}(\pi^0) = 0$, and a value of zero for the pion mass. The only contribution to the pion mass comes from the second "quark condensate" term in (54) where $(D_{if}^{\rm QCD})^2 = 1/2$. The mass formula (54) for the pion then gives

$$m_\pi^2 = (m_u+m_d)\frac{e^\gamma\mu^{\rm QCD}}{2}, \tag{55}$$

which is in the same form as the Gell-Mann–Oakes–Renner relation [139],

$$m_\pi^2 = (m_u+m_d)\frac{|\langle 0|\bar{q}q|0\rangle|}{F_\pi^2}, \tag{56}$$

where $|\langle 0|\bar{q}q|0\rangle|$ is the light u and d quark–antiquark condensate and F_π is the pion decay constant. Consequently, we can infer that the unknown mass scale $\mu^{\rm QCD}$ in the bosonization formula for QCD has indeed the physical meaning of the quark condensate. We can therefore identify $\mu^{\rm QCD}$ in the bosonization mass formula (54) for QCD as

$$\frac{e^\gamma\mu^{\rm QCD}}{2} = \frac{|\langle 0|\bar{q}q|0\rangle|}{F_\pi^2}. \tag{57}$$

By such an identification and calibrating the pion mass to be the experimental mass m_π, the mass formula (54) for the pseudoscalar QCD mesons can be re-written as [30]

$$\begin{aligned}(m_i^{\rm QCD})^2 =& \frac{(g_{\rm 2D}^{\rm QCD})^2}{\pi}\left(\sum_{f=1}^{N_f} D_{if}^{\rm QCD}\right)^2 + m_\pi^2\sum_{f=1}^{N_f}\frac{m_f}{m_{ud}}(D_{if}^{\rm QCD})^2, \\ \frac{(g_{\rm 2D}^{\rm QCD})^2}{\pi} =& \frac{4\alpha_s}{\pi R_T^2},\end{aligned} \tag{58}$$

where $m_{ud} = (m_u+m_d)/2$.

We are ready to test whether the QCD mesons π^0, η and η' can be appropriately described as open string states in the 1+1 dimensional bosonization model. For these QCD neutral mesons, there is a wealth of information on the matrix $D_{if}^{\rm QCD}$ that describes the composition of the physical states in terms of the flavor components, as represented by the mixing angle θ_P between the flavor octet and flavor singlet components of the $SU(3)$ wave functions in η and η' in (52b) and (52c). The ratio of the strange quark mass to the light u and d quark masses that is needed in the above mass formula is also known. From the tabulation in PDG [74], we find $\theta_P = -24.5^{\rm o}$

and $m_s/m_{ud} = 27.3^{+0.7}_{-1.3}$. The only free parameters left in the mass formula (58) are the strong interaction coupling constant α_s and the flux tube radius R_T.

For the value of α_s, previous works on the non-perturbative potential models use a value of α_s of the order of 0.4–0.6 in hadron spectroscopy studies [140–144]. However, these potential models contain a linear confining interaction, in addition to the one-gluon exchange interaction involving α_s. In contrast, the present simplified 1+1 dimensional treatment uses only a single attractive gauge interaction, involving α_s and playing dual roles. We should be prepared to allow for a larger value of the strong coupling constant α_s in our case. We find that $\alpha_s = 0.68$ gives a reasonable description of the masses of the mesons considered, and we can take the difference between this α_s value and the α_s value of 0.6 used for the lowest meson masses in earlier hadron spectroscopy studies [140–144] as a measure of the degree of uncertainties in α_s, resulting in $\alpha_s = 0.68 \pm 0.08$.

For the value of R_T, lattice gauge calculations with dynamical fermions give a flux tube root-mean-square-radius $R_T = 0.411$ fm for a quark–antiquark separation of 0.95 fm [97]. The experimental value of $\langle p_T^2 \rangle$ of produced hadrons ranges from 0.2 to 0.3 GeV^2 for e^+–e^- annihilations at $\sqrt{s}$ from 29 GeV to 90 GeV [134], corresponding to a flux tube radius $R_T = \hbar/\sqrt{\langle p_T^2 \rangle}$ of 0.36 to 0.44 fm. It is reasonable to consider flux tube radius parameter to be $R_T = 0.4 \pm 0.04$ fm. This set of parameters of $\alpha_s = 0.68 \pm 0.08$ and $R_T = 0.40 \pm 0.04$ fm give an adequate description of the π^0, η and η' masses as shown in Table 1.

From our comparison of the experimental and theoretical masses in Table 1, we find that by using the method of bosonization and including the confining interaction and the quark condensate, the mass formula (58) in the 1+1 dimensional open string model can indeed describe the masses of π^0, η, and η', approximately within the limits of the uncertainties of the theory. The formulation can be used to extrapolate to the unknown region of open string $q\bar{q}$ QED mesons.

In order to infer the importance of the second quark condensate term relative to the massless quark limit arising from the confining interaction in (58), we tabulate in Table 1 the results of the hadron mass values obtained in the massless quark limit. We observe that for the pion mass, the massless quark limit is zero, and the pion mass arises only from the second quark condensate term. The importance of the quark condensate diminishes as the hadron masses increases to η and η'.

4.6 Open string model description of QED mesons

Having confirmed the approximate validity of the (1+1) D open string description of neutral QCD mesons which exist in (3+1)D, we proceed to extrapolate to the unknown region of the open string $q\bar{q}$ QED mesons in (3+1)D. In such a discussion involving the QED interaction in this subsection, the interaction label superscript is implicitly $\lambda = 0$ for QED unless noted otherwise. The mass scale in (51) gives $m^{\rm QED} \sim 48$ MeV $\gg m_u, m_d$, but $m^{\rm QED}$ is less than m_s. In the treatment of QED mesons, it is only necessary to include u and d quarks and anti-quarks, with $N_f = 2$. It is also necessary to include the fractional quark electric charges $Q_f^{\rm QED}$.

We denote the flavor $q\bar{q}$ component states $\phi_1 = |u\bar{u}\rangle$,

Table 1 Comparison of experimental and theoretical masses of neutral, $I_3 = 0$, and $S = 0$ QCD and QED mesons obtained with the semi-empirical mass formula (58) for QCD mesons and (64) for QED mesons, with $\alpha_s = 0.68 \pm 0.08$, $R_T = 0.40 \pm 0.04$ fm, and $\alpha_{\rm QED} = 1/137$.

		$J^\pi I$	Experimental mass (MeV)	Semi-empirical mass formula (MeV)	Meson mass in massless quark limit (MeV)
QCD meson	π^0	0^-1	134.9768±0.0005	134.9‡	0
	η	0^-0	547.862±0.017	498.4±39.8	329.7±57.5
	η'	0^-0	957.78±0.06	948.2±99.6	723.4±126.3
QED meson	isoscalar	0^-0		17.9±1.5	11.2±1.3
	isovector	0^-1		36.4±3.8	33.6±3.8
Possible QED meson candidates	X17	(1^+)	16.70±0.35±0.5†		
	X17	(0^-)	16.84±0.16±0.20#		
	X17	(1^-)	16.86±0.17±0.20□		
	E38		37.38±0.71⊕		
	E38		40.89±0.91⊖		
	E38		39.71±0.71⊗		

‡ Calibration mass
† A. Krasznahorkay, *et al.*, *Phys. Rev. Lett.* 116, 042501 (2016), ^{8}Be* decay
# A. Krasznahorkay, *et al.*, arXiv: 1910.10459, ^{4}He* decay
□ A. Krasznahorkay, *et al.*, arXiv: 2209.10795, ^{12}C* decay
⊕ K. Abraamyan, *et al.*, *EPJ Web Conf.* 204, 08004 (2019), dCu→$\gamma\gamma X$
⊖ K. Abraamyan, *et al.*, *EPJ Web Conf.* 204, 08004 (2019), pCu→$\gamma\gamma X$
⊗ K. Abraamyan, *et al.*, *EPJ Web Conf.* 204, 08004 (2019), dC→$\gamma\gamma X$

$\phi_2 = |d\bar{d}\rangle$, and construct the physical isoscalar $I = 0$ $|\Phi_1^{\rm QED}\rangle$ and the isovector $(I = 1, I_3 = 0)$ $|\Phi_2^{\rm QED}\rangle$ states as

$$\begin{aligned} &|\text{(isoscalar)}I = 0,\ I_3 = 0\rangle = \Phi_1 = (\phi_1 + \phi_2)/\sqrt{2}, \\ &|\text{(isovector)}I = 1,\ I_3 = 0\rangle = \Phi_2 = (\phi_1 - \phi_2)/\sqrt{2}. \end{aligned} \tag{59}$$

They are related by $\Phi_i^{\rm QED} = \sum_f D_{if}^{\rm QED}\phi_f$ and $\phi_i = \sum_f D_{if}^{\rm QED}\Phi_i$,

$$\begin{aligned} \begin{pmatrix}\Phi_1\\ \Phi_2\end{pmatrix} &= \begin{pmatrix}\frac{1}{\sqrt{2}} & +\frac{1}{\sqrt{2}}\\ \frac{1}{\sqrt{2}} & -\frac{1}{\sqrt{2}}\end{pmatrix}\begin{pmatrix}\phi_1\\ \phi_2\end{pmatrix}, \\ \begin{pmatrix}\phi_1\\ \Phi_1\end{pmatrix} &= \begin{pmatrix}\frac{1}{\sqrt{2}} & +\frac{1}{\sqrt{2}}\\ \frac{1}{\sqrt{2}} & -\frac{1}{\sqrt{2}}\end{pmatrix}\begin{pmatrix}\Phi_1\\ \Phi_1\end{pmatrix}. \end{aligned} \tag{60}$$

The mass formula (58) for the mass of the physical QED meson Φ_i becomes

$$\begin{aligned} &(m_I^{\rm QED})^2 = \frac{(g_{\rm 2D}^{\rm QED})^2}{\pi}\left[\frac{Q_u^{\rm QED} + (-1)^I Q_d^{\rm QED}}{\sqrt{2}}\right]^2 + m_{ud}e^\gamma\mu^{\rm QED}, \\ &\text{with}\ \ \frac{(g_{\rm 2D}^{\rm QED})^2}{\pi} = \frac{4\alpha_{_{\rm QED}}}{\pi R_T^2}, \end{aligned} \tag{61}$$

where the mass scale $\mu^{\rm QED}$ for QED mesons is not known. From the results for QCD mesons in (54)–(56), we expect an analogous relationship relating the mass scale $\mu^{\rm QED}$ and the quark condensate for QED mesons,

$$e^\gamma\mu^{\rm QED} \propto |\langle 0|\bar{q}q|0\rangle|_{_{\rm QED}}, \tag{62}$$

where $|\langle 0|\bar{q}q|0\rangle|_{_{\rm QED}}$ is the quark condensate in the presence of QED gauge interactions between the quark and the antiquark.

The chiral condensate depends on the interaction type λ, specifically, on the coupling constant. We note that the chiral current anomaly in the chiral current depends in (3+1)D on the coupling constant as $e^2 = (g_{_{\rm 4D}}^{\rm QED})^2$ as given in Eq. (19.108) of [101]

$$\partial_\mu j^{\mu 53} = -\frac{e^2}{32\pi}\epsilon^{\alpha\beta\gamma\delta}F_{\alpha\beta}F_{\gamma\delta}, \tag{63}$$

which shows that the degree of non-conservation of the chiral current is proportional to e^2. It is therefore reasonable to infer that the chiral condensate term in Eqs. (58) and (61) depends on the coupling constant as $(g_{_{\rm 4D}}^\lambda)^2$ or α_λ. Hence, we have a general mass formula for the mass m_I^λ of a neutral QCD and QED meson I in the λ-type interaction given by [30]

$$\begin{aligned} &(m_I^\lambda)^2 = \frac{(g_{\rm 2D}^\lambda)^2}{\pi}\left(\sum_{f=1}^{N_f} D_{If}^\lambda Q_f^\lambda\right)^2 + m_\pi^2\frac{\alpha_\lambda}{\alpha_{_{\rm QCD}}}\frac{\sum_f^{N_f}(D_{If}^\lambda)^2 m_f}{m_{ud}}, \\ &\frac{(g_{\rm 2D}^\lambda)^2}{\pi} = \frac{4\alpha_\lambda}{\pi R_T^2}, \quad \lambda = \begin{cases}0 & \text{QED}\\ 1 & \text{QCD}\end{cases}. \end{aligned} \tag{64}$$

Here, the first term is the massless quark limit arising from the confining interaction between the quark and the antiquark, with $Q_u = 2/3$, $Q_d = -1/3$, and $\alpha_{_{\rm QED}} = 1/137$. The second term arises from the quark masses and the quark condensate in the presence of the QED interaction.

In applying the above mass formula for QED mesons, we extrapolate from the QCD sector to the QED sector by using those R_T and α_s parameters that describe well the π^0, η and η' QCD mesons. We do not know the flux tube radius R_T for the QED interaction. The meager knowledge from the possible QED meson spectrum and the anomalous soft photons suggests that the assumption of an intrinsic quark flux tube radius R_T appears to be a reasonable concept as it gives a good description of the X17, E38, and anomalous soft photon masses as described in [30], subject to future amendments as more data become available. So, for the QED interaction with $\alpha_{\rm QED} = 1/137$ and we use the same R_T as used in the QCD mesons.

We list the theoretical masses of the neutral, $I_3 = 0$, QED mesons obtained by Eq. (64) in Table 1. We find an $I = 0$ isoscalar QED meson at $m_{\rm isoscalar}^{\rm QED} = 17.9\pm 1.5$ MeV and an $(I = 1, I_3 = 0)$ isovector QED meson at $m_{\rm isovector}^{\rm QED} = 36.4\pm 3.8$ MeV. As the $I^G(J^{PC})$ quantum numbers of the QCD mesons are known, we can infer the quantum numbers of the corresponding QED mesons with the same I and S by analogy. Such an inference by analogy provides a useful tool to determine the quantum numbers and some electromagnetic decay properties of QED mesons. Using such a tool, we find that the isoscalar QED meson has quantum numbers $I^G(J^{PC}) = 1^-(0^{-+})$ and the isovector $I_3 = 0$ QED meson has quantum numbers $I^G(J^{PC}) = 0^+(0^{-+})$. Within the theoretical and experimental uncertainties, the matching of the $I(J^\pi)$ quantum numbers and the mass may make the isoscalar QED meson a good candidate for the X17 particle and the isovector QED meson for the E38 particle. It will be of great interest to confirm or refute the existence these hypothetical particles by independent experimental investigations, as a test of the QED meson concepts.

In order to show the effects of the second quark condensate term relative to the massless quark limit in (64), we tabulate in Table 1 the results of the QED meson masses values obtained in the massless quark limit. One observes that the mass of the isoscalar QED meson with the quark condensate is 17.9 ± 1.5 MeV but it is reduced to 11.2 ± 1.3 MeV in the massless quark

limit without the quark condensate.

4.7 Effective charge numbers and quark space-time classical trajectories

With the solutions of the phenomenological QCD and QED open string models well at hand, it is illuminating to examine in some detail the effective charge numbers for the QCD and QED mesons. The effective charges are useful concepts as they present a simple and physical way to study the dynamics and the interaction of the constituents in these mesons in the presence of flavor symmetry and flavor mixing. The dynamics occur in such a way that even though quarks of different charges in different flavors are involved, they can be equivalently described as having a quark constituent interacting with its antiquark constituent with an opposite effective charge. With the introduction of effective charge, the flavor dynamics is subsumed and greatly simplified. We list the effective color and electric charges of π^0, η and η' in Table 2. For other hadrons when there is no flavor mixing, there is no need to introduce effective charges, and their color and electric quark charges are those given by the standard quark model.

It is interesting to note that for the isovector π^0 with isospin $I=1, I_3=0$, the effective quark color charge $\tilde{Q}_q^{\rm QCD}$ is zero and thus, π^0 is a Goldstone boson whose mass would be zero if the mass comes only from the confining interaction. That is, the contribution to the pion mass arising from the confining interaction is zero because the effective charge that will respond to the confining force is zero. The mass for π^0 arises only from the quark condensate, the second term of Eq. (64), corresponding to the variational response of the quark condensate due to the variation of the boson field as indicated by Eq. (45). As noted by Georgi [25], the case of quarks with two flavors with a zero effective color charge is a remarkable occurrence, because it leads to a confined boson with a zero mass from the confining potential and is an example of an "unparticle" system without a mass scale or length scale, a case with conformal symmetry. There appears to be an automatic fine-tuning in the two-flavor Schwinger model [24]. The π^0 in QCD is however not massless and does not become an unparticle on account of the quark condensate in the second term of Eq. (64), which depends on the quark rest masses and the strength of the coupling constant. It is the forces associated with the presence of the condensate and its variation with respect to the boson field that gives the second term and the mass of the pion [Eq. (45)].

It would be intuitively illuminating to see how the effective charges in Table 2 are related to the dynamics of quark constituents for the case with two flavors. The effective charge $\tilde{Q}_i^\lambda$ for the quark constituent q interacting with its antiquark constituent $\bar{q}$ in particle i with isospin I interacting in the interaction of type λ is

$$\tilde{Q}_q^\lambda(i)=\sum_f^{N_f} D_{if}^\lambda Q_f^\lambda=\frac{Q_u^\lambda+(-1)^I Q_d^\lambda}{\sqrt{2}}, \tag{65}$$

for which we have $Q_u^{\rm QCD}=Q_d^{\rm QCD}=1$, and $Q_u^{\rm QED}=2/3$, and $Q_d^{\rm QED}=-1/3$. As indicated in Table 2, the effective color charge $\tilde{Q}_q^{\rm QCD}(\pi^0)=0$, the effective electric charges $\tilde{Q}_q^{\rm QED}({\rm isoscalar})=1/(3\sqrt{2})$ and $\tilde{Q}_q^{\rm QED}({\rm isovector})=1/\sqrt{2}$. We can examine and study the space-time dynamics of the up and down quarks. Treating the quarks as massless and studying the classical trajectories of the constituents in the yo–yo model in (1+1)D [123], we describe the quark trajectories as described in Chapter 7 of [20]. We show in Fig. 4(a) the yo–yo trajectories of the up and down quarks in the flavor singlet $I=0$ state, and in Fig. 4(b) the flavor triplet $I=1, I_3=0$ state. We observe that in the isoscalar $I=0$ case, the classical trajectories of the quark motion is in phase, and the charges of the two quarks add together and in the isovector $I=1$ case, the classical trajectories are out of phase and the two charges subtract from each other. On the other hand, the color charges are of the same sign in QCD, but they are of different magnitudes and signs in QED. Therefore, there is a complete cancellation of the color-charges for the case of QCD isovector case, but an additive reinforcement in the QCD isoscalar case. Thus, the quark effective color charge for π^0 is zero, $\tilde{Q}_q^{\rm QCD}(\pi^0)=0$. On the other hand, for the case of electric charges in QED, because the up quark and the down quark have different magnitudes of electric charges with opposite signs, the effective electric charge of QED meson is less than the effective electric charge of the isovector QED meson. The factor of $1/\sqrt{2}$ comes from the wave functions,

Table 2 The effective color charge $\tilde{Q}_q^{\rm QCD}(i)$ and the effective electric charge $\tilde{Q}_q^{\rm QED}(i)$ of the quark constituent in the QCD or QED meson i, in the presence of flavor mixing. The mixing angle $\theta_p=-24.5^{\rm o}$ is from Ref. [74].

	Particle i	$J^\pi I$	$\tilde{Q}_q^{\rm QCD}(i)$	$\tilde{Q}_q^{\rm QCD}(i)$ $\theta_p=-24.5^{\rm o}$	$\tilde{Q}_q^{\rm QED}(i)$	$\tilde{Q}_q^{\rm QED}(i)$ $\theta_p=-24.5^{\rm o}$
QCD meson	π^0	0^-1	0	0	$1/\sqrt{2}$	0.7071
	η	0^-0	$-\sqrt{3}\sin\theta_p$	0.7182	$3\cos\theta_p/\sqrt{6}$	1.1144
	η'	0^-0	$\sqrt{3}\cos\theta_p$	1.576	$\sin\theta_p/\sqrt{6}$	–0.1693
QED meson	isoscalar (X17)	0^-0			$1/(3\sqrt{2})$	
	isovector (E38)	0^-1			$1/\sqrt{2}$	

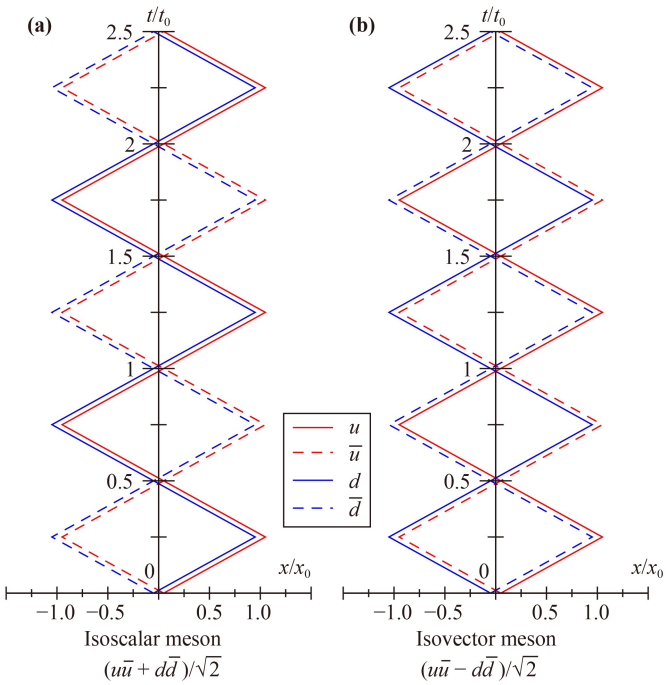

Fig. 4 **(a)** Classical space-time trajectories of massless quarks in the yo–yo motion of a meson with two flavors in the isospin singlet state with $I=0, I_3=0$. The motion of the u and d quarks are in phase, and the quark charges effectively add together. **(b)** Classical space-time trajectories of massless quarks in yo–yo motion of a meson with two flavors in the isospin triplet state with $I=1, I_3=0$. The motion of the u and d quarks are out of phase, and the quark charges effectively subtract from each other.

resulting in the effective electric charges $\tilde{Q}_q^{\rm QED}(\text{isoscalar}) = 1/(3\sqrt{2})$ for the $I=0$ QED meson and $\tilde{Q}_q^{\rm QED}(\text{isovector}) = 1/\sqrt{2}$ for the $(I, I_3) = (1, 0)$ QED meson.

5 Experimental evidence for the possible existence of the QED mesons

5.1 Different modes of QED meson decays

We have discussed in Section 2 the mechanism of the production of $q\bar{q}$ pairs in many low- and high-energy e^+–e^-, hadron–hadron, and nucleus–nucleus collisions. A $q\bar{q}$ pair will be produced and materialize as a QED or QCD meson final state, when the center-of-mass energy $\sqrt{s}(q\bar{q})$ of the pair coincides with the eigenenergy of a confined QED or QCD meson. In the energy range $(m_q + m_{\bar{q}}) < \sqrt{s}(q\bar{q}) < m_\pi$, a $q\bar{q}$ will be produced and materialize as a QED meson when $\sqrt{s}(q\bar{q})$ coincides with the eigenenergy of a confined QED meson. At energies different from the eigenenergies of QCD and QED mesons, no $q\bar{q}$ pair will be produced, because quarks cannot be isolated.

Methods for the detection of various QCD mesons are well known and we do not need to belabor them again. On the other hand, a QED meson can be detected by its decay products from which its invariant mass can be measured. It is necessary to know its decay modes.

In (1+1)D, a QED meson with massless quarks cannot decay as the quark and the antiquark execute yo–yo motion along the string. The exchange photon in (1+1) D between the quark and the antiquark constituent leads to longitudinal confinement, and there are no free transverse photons. The open string in one dimension is however only an idealization of a flux tube. In the physical (3+1)D, the structure of the flux tube and the transverse photons must be taken into account. In (3+1)D space-time, the quark and the antiquark at different transverse coordinates in the flux tube traveling from opposing longitudinal directions in a QED meson can make a turn to the transverse direction by which the quark and the antiquark can meet and annihilate, leading to the emission of two real transverse photons $\gamma_1\gamma_2$ as depicted in the Feynman diagram Fig. 5(a). A QED meson can decay into two virtual photons $\gamma_1^*\gamma_2^*$ each of which subsequently decays into an e^+e^- pair as $(e^+e^-)(e^+e^-)$ shown in Fig. 5(b). The coupling of the transverse photons to an electron pair leads further to the decay of the QED meson into an electron-positron pair e^+e^- as shown in Fig. 5(c). The mass of a QED meson can be obtained by measuring the invariant mass of its decay products.

5.2 The observation of the anomalous soft photons

In exclusive high-energy K^+p [36, 37], π^+p [37], π^-p [38–40], pp collisions [41], and e^+e^- annihilations [42–45] at the Z^0 resonance at $\sqrt{s} = 91.1876$ GeV [42–45], a large number of hadrons are produced. Photons are also produced and are detected as converted e^+e^- pairs in these reactions. In these exclusive measurements in which the secondary photons from hadron decays can be tracked and separated out from the direct photons, attention can be focused on the produced direct photons and their correlation with the hadron products.

Upon choosing the longitudinal axis as the incident hadron axis in hadron–hadron collisions, or the jet axis of one of the jets in e^+–e^- annihilations, the associated

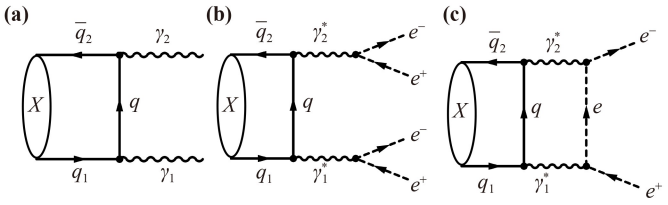

Fig. 5 **(a)** A QED meson X can decay into two real photons $X \to \gamma_1 + \gamma_2$, **(b)** it can decay into two virtual photons each of which subsequently decays into an (e^+e^-) pair, $X \to \gamma_1^* + \gamma_2^* \to (e^+e^-) + (e^+e^-)$, and **(c)** it can decay into a single (e^+e^-) pair, $X \to \gamma_1^* + \gamma_2^* \to e^+e^-$.

direct photons can be further classified as direct soft photons and direct hard photons. The (direct) soft photons are those with a transverse momentum p_T less than about 60 MeV/c, while the (direct) hard photons are those with p_T greater than about 60 MeV/c. The bremsstrahlung process with the production of both soft and hard photons, but no hadrons, has been studied in e^+–e^- elastic scattering and in $e^+ + e^- \to \mu^+ + \mu^-$ reactions as a purely electroweak processes, and such bremsstrahlung process has been found to agree well with QED considerations [44].

Experimental measurements of the (direct) soft photons associated with hadron production is a interesting problem because it involves the soft photon production in QED, the hadron production in QCD, and the interplay between QCD and QED particle production processes. Exclusive measurements of the soft photon production over a period of many decades since 1984 consistently exhibit the anomalous soft photon anomaly as we shall describe in detail below.

5.3 The Low Theorem

Because the Low Theorem [145] plays an important role in quantifying the anomalous soft photon anomaly, it is worthwhile to review its theoretical foundation and its contents.

We consider the process $p_1 + p_2 \to p_3 + p_4 + k$ where p_i represents a hadron and its momentum, and k represents a photon and its momentum. For the simplest case with neutral p_2 and p_4, and charged p_1 and p_3 hadrons, the Feynman diagrams are shown in Fig. 6. The amplitude for the production of a photon with a polarization ϵ is

$$\begin{aligned} &M(p_1p_2;p_3p_4k)\\ &= M_0(p_1p_2;p_3p_4)\left(\frac{e_1p_1\cdot\epsilon}{(p_1-k)^2}+\frac{e_3p_3\cdot\epsilon}{(p_3+k)^2}\right)\\ &= M_0(p_1p_2;p_3p_4)\left(\sum_i^{\text{All charged particles}}\frac{\eta_i e_i p_i\cdot\epsilon}{2p_i\cdot k}\right), \end{aligned} \tag{66}$$

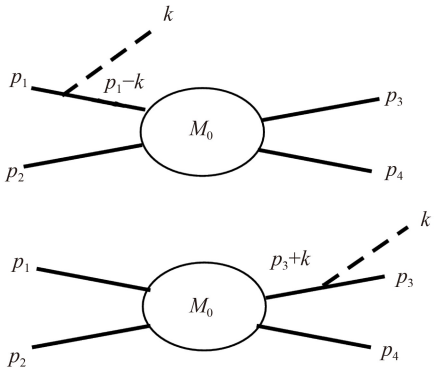

Fig. 6 Feynman diagrams for $p_1+p_2\to p_3+p_4+k$.

where e_i is the charge of p_i, and η_i is +1 for an outgoing hadron and –1 for an incoming hadron respectively. In obtaining the above equation, we have assumed soft photons with small k values so that the production amplitude satisfies

$$\begin{aligned} M_0(p_1-kp_2;\ p_3p_4) \sim& M_0(p_1p_2;\ p_3+kp_4)\\ \sim& M_0(p_1p_2;\ p_3p_4). \end{aligned} \tag{67}$$

This is a reasonable assumption in high energy processes in which $|\boldsymbol{p_1}|$ and $|\boldsymbol{p_3}|$ in the C.M. frame are much greater than the transverse momentum of the soft photon, k_T. The amplitude M_0 with the production of a soft photon is then approximately independent of k and can be adequately represented by $M_0(p_1p_2;p_3p_4)$, the Feynman amplitude for the production of only hadrons.

We can generalize the above Eq. (66) to the process $p_1 + p_2 \to p_3 + p_4 + ... + p_N + k$ where p_i is a hadron and k is a soft photon. The Feynman amplitude is

$$\begin{aligned} &M(p_1p_2;p_3p_4...p_Nk)\\ =&M_0(p_1p_2;p_3p_4...p_N)\left(\sum_i^{\text{All charged particles}}\frac{\eta_i e_i p_i\cdot\epsilon}{2p_i\cdot k}\right), \end{aligned} \tag{68}$$

From the relation between Feynman amplitudes and cross sections, the above equation gives [145]

$$\begin{aligned} \frac{\mathrm{d}N_\gamma}{\mathrm{d}^3k} =& \frac{\alpha}{2\pi k_0}\int \mathrm{d}^3p_1\mathrm{d}^3p_2\mathrm{d}^3p_3\cdots\mathrm{d}^3p_N\\ &\cdot\sum_{i,j=1}^{N}\eta_i\eta_j e_i e_j\frac{-(p_i\cdot p_j)}{(p_i\cdot k)(p_j\cdot k)}\frac{\mathrm{d}N_{\text{hadrons}}}{\mathrm{d}^3p_1\mathrm{d}^3p_2\mathrm{d}^3p_3\cdots\mathrm{d}^3p_N}, \end{aligned} \tag{69}$$

where the sum over i and j include all incoming and outgoing primary charged particles. In exclusive measurements, the distribution of all participating incoming and outgoing charged particles are track and detected, the quantity $\mathrm{d}N_{\text{hadrons}}/\mathrm{d}^3p_1\mathrm{d}^3p_2\mathrm{d}^3p_3\cdots\mathrm{d}^3p_N$ is measured, and the sum in Eq. (69) can be carried out. Thus, the spectrum of soft photons arising from QED bremsstrahlung can be calculated from exclusive measurements on the spectrum of the produced hadrons.

5.4 Experimental measurements of anomalous soft photon in hadron production

In which part of the photon spectrum are soft photons expected to be important? Upon choosing the beam direction as the longitudinal axis, Eq. (69) indicates that the contributions are greatest when the transverse momentum of the photon, $k_T \propto p_i\cdot k$, is small, as pointed out by Gribov [146]. Hence, it is of great interest to measure the yield of soft photons with small transverse momenta.

Many high-energy experiments were carried out to

obtain the spectra of soft photons with transverse momenta of the order of many tens of MeV/c, with the soft photons detected as converted e^+e^- pairs. The soft photon spectra were then compared with what would be expected from electromagnetic bremsstrahlung of the hadrons as given by Eq. (69).

Anomalous soft photon production in excess of QED bremsstrahlung predictions by a factor of 4.0±0.8 in association with hadron production was first observed in 1984 by the WA27 Collaboration at CERN using the BEBC bubble chamber in $K^+ + p$ collisions at $p_{\rm lab}(K^+) =$ 70 GeV [36]. For over several decades since that time, in many exclusive measurements in high-energy K^+p [37], π^+p [37], π^-p [38–40], pp collisions [41], and e^+e^- annihilations [42–45], it has been consistently and repeatedly observed that whenever hadrons are produced, anomalous soft photons in the form of excess e^+e^- pairs, about 4 to 8 times of the bremsstrahlung expectations, are proportionally produced, and when hadrons are not produced, these anomalous soft photons are also not produced as shown in Fig. 7 [44]. The transverse momenta of these excess e^+e^- pairs lie in the range of a few MeV/c to many tens of MeV/c, corresponding to a mass scale of the e^+e^- pair from a few MeV to many tens of MeV (Fig. 8). The anomalous soft photon measurements are summarized well by Perepelitsa in [42] in Table 3.

These experimental measurements indicate that low-k_T soft photons are produced in excess of what is expected from the QED electromagnetic bremsstrahlung process. In particular, in DELPHI measurements in high-energy e^+–e^- annihilations in Z^0 hadronic decay, the ratio of the soft photon yield to the bremsstrahlung yield associated with hadron production is about 4 [45], whereas the ratio of soft photon yield to the bremsstrahlung yield in the corresponding $e^+ + e^- \to \mu^+ + \mu^-$ reaction is about 1 [43]. This indicates clearly that anomalous soft photons are present only when hadrons are produced. The QCD hadron production is accompanied by an additional soft photon source appearing as excess e^+e^- pairs. The anomalous soft photons provide an interesting window to examine non-perturbative aspects of QCD and QED particle production processes.

5.5 DELPHI measurements of anomalous soft photon in high-energy e$^+$–e$^-$ annihilations

DELPHI carried out a series of quantitative measurements to study the anomalous soft photons in the hadronic decay of the Z^0 resonance at $\sqrt{s} = 91.19$ GeV at CERN. In addition to measuring the overall ratio of soft photon production, the DELPHI Collaboration measured the soft photon yields in different regions of the phase space in coincidence with various hadron production variables. They provide a wealth of information on the characteristics of the anomalous soft photons in association with hadron production [43–45]. The main features of the observations from the DELPHI Collaboration can be summarized as follows:

1) Anomalous soft photons in the form of excess e^+e^- pairs are produced in association with hadron production at high energies. They are absent when there is no hadron production as demonstrated in Ref. [44] and in Fig. 7(c). The anomalous soft photon yield is proportional to the hadron yield as shown in Fig. 7(c).

2) The anomalous soft photon yield increases approximately linearly with the number of produced neutral or charged particles, but, the anomalous soft photon yields increases much faster with increasing neutral particle multiplicity than with charged particle multiplicity, as

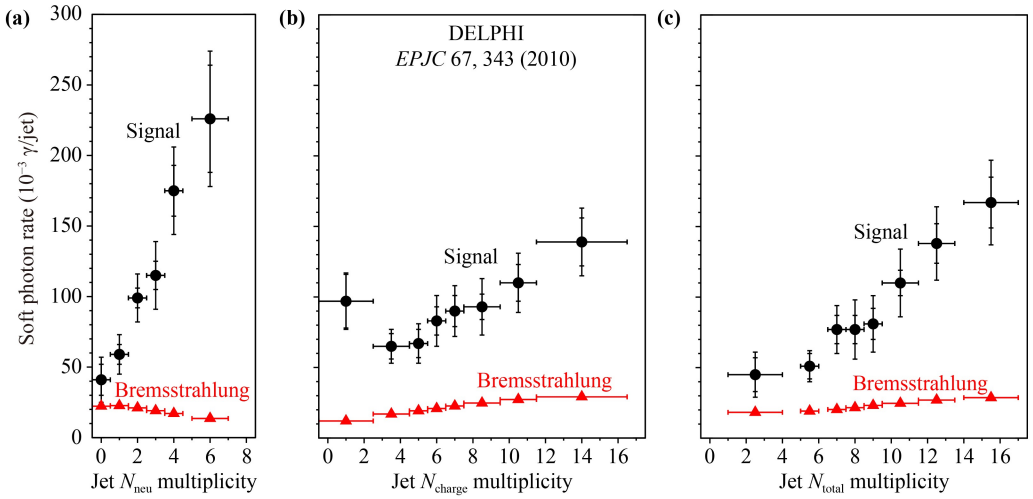

Fig. 7 Number of soft photons N_γ in units of ($10^{-3}\gamma$/jet), shown as solid circular points, as a function of **(a)** neutral hadron multiplicity $N_{\rm neu}$, **(b)** charged hadron multiplicities, $N_{\rm charge}$, and **(c)** the total hadron multiplicity, $N_{\rm total}$, from the DELPHI Collaboration [45]. The number of soft photons from the bremsstrahlung process is shown as triangular data points.

shown in Figs. 7(a) and (b).

3) The transverse momenta of the anomalous soft photons are in the region of many tens of MeV/c, as shown in Fig. 8(b).

5.6 Models of anomalous soft photons

Many different model have been proposed to explain the anomalous soft photon production in association with hadron production. As the transverse momenta of the anomalous photons are of order of many tens of MeV, Van Hove and Lichard suggested that there is a source of these low-energy photons in the form of a glob of cold quark–gluon system of low temperature with $T \sim 10$ to 30 MeV at the end of parton virtuality evolution in hadron production [147–149]. In such a cold quark–gluon plasma, soft photons may be produced by $q + \bar{q} \to \gamma + g$ or $g + q \to \gamma + q$, and will acquire the characteristic temperature of the cold quark–gluon plasma.

Kokoulina *et al.* [150, 151] followed similar idea of a cold quark–gluon plasma as the source of soft photon production. Collaborative evidence of a cold quark–gluon plasma with $T \sim 10$ to 30 MeV from other sources however remain lacking.

Barshay proposed that pions propagate in pion condensate and they emit soft photons during the propagation. Rate of soft photon emission depends on the square of pion multiplicity [152]. The concept of a pion condensation in high-energy e^+–e^- annihilations in Z^0 hadronic decay has however not been well established.

Shuryak suggested that soft photons are produced by pions reflecting from a boundary under random collisions. Hard reflections lead to no effect, but soft pion collisions on wall leads to large enhancement in soft photon yield [153].

Balek, Pisutova & Pisut [154] presented a review of

Table 3 The ratio of the soft photon yield associated with hadron production to the bremsstrahlung yield in high-energy hadron–hadron collisions and e^+–e^- annihilations, compiled by Perepelitsa [42].

Experiment	Collision energy	Photon k_T	Photon/Brem ratio
K^+p, CERN, WA27, BEBC (1984)	70 GeV/c	$k_T < 60$ MeV/c	4.0 ± 0.8
K^+p, CERN, NA22, EHS (1993)	250 GeV/c	$k_T < 40$ MeV/c	6.4 ± 1.6
π^+p, CERN, NA22, EHS (1997)	250 GeV/c	$k_T < 40$ MeV/c	6.9 ± 1.3
π^-p, CERN, WA83, OMEGA (1997)	280 GeV/c	$k_T < 10$ MeV/c	7.9 ± 1.4
π^+p, CERN, WA91, OMEGA (2002)	280 GeV/c	$k_T < 20$ MeV/c	5.3 ± 0.9
pp, CERN, WA102, OMEGA (2002)	450 GeV/c	$k_T < 20$ MeV/c	4.1 ± 0.8
e^+e^-→hadrons, CERN, DELPHI with hadron production (2010)	~91 GeV (CM)	$k_T < 60$ MeV/c	4.0
e^+e^-→$\mu^+\mu^-$, CERN, DELPHI with no hadron production (2008)	~91 GeV (CM)	$k_T < 60$ MeV/c	1.0

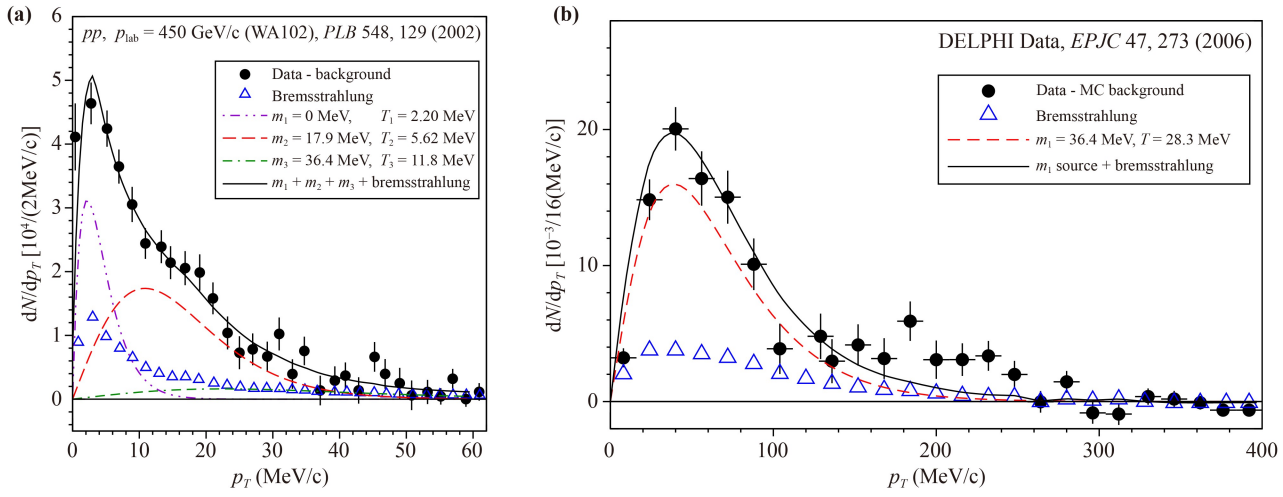

Fig. 8 **(a)** Anomalous soft photon dN/dp_T data from pp collisions at $p_{lab} = 450$ GeV/c obtained by Belogianni *et al.* [41]. **(b)** Anomalous soft photon dN/dp_T data from the DELPHI Collaboration for e^+e^- annihilation at the Z_0 mass of 91.18 GeV [43]. The solid circular points represent the experimental data after subtracting the experimental background, and triangle points represent the deduced bremsstrahlung contributions. The component yields from different masses of the thermal model are shown as separate curves. The total theoretical yields from the different masses and the QED bremsstrahlung contribution are shown as the solid curves.

the data analysis, the corrections to the Low Theorem, and the proposed models up to 1989.

Czyz and Florkowski [155] proposed that soft photons are produced by classical bremsstrahlung, with parton trajectories following string breaking in a string fragmentation. They suggested that photon emissions along the flux tube agree with the Low limit whereas photon emissions perpendicular to the flux tube are enhanced over the Low limit.

Nachtmann *et al.* [156–158] suggested that soft photons produced by synchrotron radiation from quarks in the stochastic QCD vacuum. Hatta and Ueda suggested that soft photons are produced in ADS/CFT supersymmetric Yang–Mills theory [159]. Darinian *et al.* [160] suggested that they arose from the Unruh radiation of quarks. Simonov *et al.* [161–164] suggested that soft photons arose from closed quark–antiquark loop. Kharzeev and Loshaj [165] suggested that the soft photon arise from the continuous spectrum from the induced currents in the Dirac sea.

5.7 QED-confined $q\bar{q}$ meson description of the anomalous soft photons

We would like to focus our attention on an open-string description of QED-confined $q\bar{q}$ meson as the source of the anomalous soft photons because it has the prospect of linking many different anomalies together in a consistent framework. As the anomalous soft photons arise from excess electron–positron pairs, the parent particles of the anomalous soft photons must be neutral objects. The results from DELPHI and Fig. 7 indicate that they are proportionally produced only as hadrons are produced, and their rate of production in association with neutral hadrons is much greater than the production rate in association with a charged hadron. The simultaneous and correlated production alongside with hadrons suggest that the neutral parent particle of the anomalous soft photons is likely to contain some elements of the hadron sector, such as a light quark and a light antiquark of the same flavor. The elements of the hadron sector comprise of u, d, c, s, b, t quarks, antiquarks, and gluons. The mass scale of the anomalous soft photons excludes all but the u and d quarks and antiquarks as possible constituents.

The quark and antiquark constituents carry color and electric charges and they interact mutually with the QCD and QED interactions. A parent particle of the anomalous soft photons cannot arise from the quark–antiquark pair interacting with the QCD interaction non-perturbatively, because such an interaction will endow the pair with a mass much greater than the mass scale of the anomalous soft photons. We are left with the possibility of the quark and the antiquark interacting with the QED interaction. We note that light u and d quarks have small masses, they reside predominantly in (1+1)D, and they interact in the QED interaction. They fit the requirements for which the Schwinger confinement mechanism [1, 2] is applicable. We can therefore apply the Schwinger confinement mechanism to quarks to conclude that a light quark q and its antiquark $\bar{q}$ will be confined as a $q\bar{q}$ boson in the Abelian $U(1)$ QED gauge interaction in (1+1)D, as in an open string, with a mass proportional to the coupling constant of the interaction. From the work of Coleman, Jackiw & Susskind [3, 4], we can infer further that the Schwinger confinement mechanism persists even for massive quarks in (1+1)D. Such a possibility of confined $q\bar{q}$ is further reinforced by the special nature of a confining gauge interaction, for which the greater the coupling constant of the attractive confining interaction, the greater will be the mass of the composite particle it generates [see Eq. (6)], in contrast to a non-confining interaction in which the effect is just the opposite[5)]. Relative to the QCD interaction, the QED interaction will bring the quantized mass of a $q\bar{q}$ pair to the lower mass range of the anomalous soft photons, as Eq. (51) indicates. It was therefore proposed in [27–29] that a quark and an antiquark in a $q\bar{q}$ system interacting with the QED interaction may lead to new open string bound states (QED-meson states) with a mass of many tens of MeV. These QED mesons may be produced simultaneously with the QCD mesons in the string fragmentation process in high-energy collisions [36–45], and the excess e^+e^- pairs may arise from the decays of these QED mesons.

The phenomenological open string description of the QCD and QED mesons in the last section indicates that π^0, η, and η' particles can be adequately described as open string $q\bar{q}$ QCD mesons. By extrapolating into the $q\bar{q}$ QED sector in which a quark and an antiquark interact with the QED interaction, we find an open string isoscalar $I(J^\pi) = 0(0^-)$ QED meson state at 17.9±1.5 MeV and an isovector $(I(J^\pi) = 1(0^-), I_3 = 0)$ QED meson state at 36.4 ± 3.8 MeV as listed in Table 1. We can make an approximate consistency check on these extrapolated masses using the transverse momentum distributions of the anomalous soft photons.

5.8 Transverse momentum distributions of anomalous soft photons

The WA102 Collaboration [41] and the DELPHI Collaboration [45] measured the transverse momentum distributions of the anomalous soft photons which provide

[5)] For the confining QED interaction in (1+1)D in the Schwinger mechanism, $m = g_{2D}/\sqrt{\pi}$, the mass m increases with an increase in the coupling constant g_{2D}, say, from the QED to the QCD interaction. In contrast, in a non-confining QED interaction between an electron and a positron, the mass of a positronium is $m_{\text{positronium}} = 2m_e - m_e\alpha_c^2/(4n^2)$, for which the mass of the positronium decreases as the coupling constant α_c increases.

valuable information on the masses of the parent bosons of the anomalous soft photons. They are exclusive measurements in which the momenta of all participating charged particles are measured. The knowledge of the momenta of all initial and final charged particles allows an accurate determination of the QED bremsstrahlung dN/dp_T distributions shown as triangular points in Fig. 8. As shown in Fig. 8, the observed yields of soft photons exceed the bremsstrahlung contributions substantially in both pp collisions in Fig. 8(a) and e^+e^- annihilations in Fig. 8(b). The solid circular points in Fig. 8 show the experimental dN/dp_T data of soft photons after subtracting the experimental background. Figure 8(a) gives the WA102 data for pp collisions at $p_{\rm lab} = 450$ GeV/c from Belogianni *et al.* [41], and Fig. 8(b) is the DELPHI results for e^+e^- annihilation at the Z_0 mass of 91.18 GeV [43].

We would like to inquire how the production of the QED mesons may be consistent with the transverse momentum distribution of the anomalous soft photons. For such an investigation, we rely on the thermal model which describes well the transverse momentum distributions in the production of hadrons of different masses in high-energy pp collisions [166–169]. We assume that the thermal model can be extended from the production of QCD mesons to the production of QED mesons whose decay products are assumed to appear as anomalous soft photons. In such a thermal model, the transverse momentum distribution of the produced QED mesons is related to the produced QED meson mass m by [166]

$$\frac{dN}{p_T dp_T} = Ae^{-\sqrt{m^2+p_T^2}/T}. \tag{70}$$

The contribution to the total dN/dp_T from each boson of mass m is proportional to $p_T e^{-\sqrt{m^2+p_T^2}/T}$ which is zero at $p_T = 0$ and has a peak at the location p_T given by

$$p_T^2 = \frac{1}{2}(T^2 + \sqrt{T^4 + 4T^2m^2}). \tag{71}$$

If $m = 0$, then dN/dp_T peaks at $p_T = T$. If m is much greater than T, then dN/dp_T peaks at $p_T \sim \sqrt{mT}$. Hence, for each contributing boson mass component, the thermal model gives a distribution that starts at zero at $p_T = 0$ and reaches a peak of dN/dp_T and decreases from the peak. The total dN/dp_T is a sum of contributions from different QED mesons and boson components,

$$\frac{dN}{p_T dp_T} = \sum_i A_i e^{-\sqrt{m_i^2+p_T^2}/T_i}. \tag{72}$$

There can be as many contributing bosons as the number of underlying peaks in the dN/dp_T spectrum. While different decompositions of the spectrum into different masses (and peaks) are possible, the structure of the dN/dp_T data appears to require many components in Fig. 8(a) and only a single component in Fig. 8(b). In the thermal model analysis of the pp data in Fig. 8(a), we note that there appears to be a boson component of real photons with $m_1 = 0$. Because of the m_iT_i ambiguity[6] associated with the product of the meson mass m_i and the temperature T_i, we are content with only a consistency analysis. We assume that QED isoscalar and isovector mesons with masses as given by Table 1 are produced in the collision, and their subsequent decay into e^+e^- pairs give rise to the excess e^+e^- pairs observed as anomalous soft photons. Allowing other parameters to vary, the thermal model fit in Fig. 8(a) is obtained with parameters $A_1 = 3.85 \times 10^4/(2\ \text{MeV/c})$, $T_1 = 2.20$ MeV, $A_2 = 6.65 \times 10^4/(2\ \text{MeV/c})$, $T_2 = 5.62$ MeV, $A_3 = 0.266 \times 10^4/(2\ \text{MeV/c})$, and $T_3 = 11.8$ MeV, where the different components also shown as separate curves. Adding the contributions from the three components onto the bremsstrahlung contributions yields the total dN/dp_T shown as the solid curve. The comparison in Fig. 8(a) indicates that the pp data are consistent with a photon component and a boson component with a mass around 17 MeV. The magnitude of the $m_3 = 36.4$ MeV component is of the same order as the bremsstrahlung contribution or the noise level, and is rather uncertain in Fig. 8(a). In Fig. 8(b), the addition of the single component with $A_1 = 2.7 \times 10^{-3}/(16\ \text{MeV/c})$, $m_1 = 36.4$ MeV, and $T_1 = 28.3$ MeV onto the bremsstrahlung contributions gives a consistent description of the soft photon data in e^+e^- annihilations shown as the solid curve.

The component with $m_1 = 0$ in Fig. 8(a) may be associated with the decay of the QED mesons into two photons. If so, it will be of interest to measure the $\gamma\gamma$ invariant mass to look for diphoton resonances, as carried out in [52, 53, 203–206]. The $m_2 = 17.9$ MeV components in Fig. 8(a) and the $m_3 = 36.4$ MeV component in Fig. 8(b) may be associated with the predicted isoscalar and isovector QED mesons of Table 1. If so, a measurement on the invariant masses of the m_2 and m_3 components will be of great interest to confirm the existence of these QED mesons. The recent reports of the observation of a hypothetical E38 boson at 38 MeV and the structures in the $\gamma\gamma$ invariant masses at 10–15 MeV and 38 MeV [52, 53, 203–206] provide encouraging impetus for further studies.

In a recent study, D'yachencho and collaborators re-analyzed the transverse momentum distributions of anomalous soft photons of the WA102 Collaboration [41] and the momentum distribution of the reaction of $p + C \to 2\gamma + X$ [52] and reached similar conclusions on possible production of neutral X17 and E38 bosons in these reactions [170, 171].

5.9 Observation of the anomalous X17 particle in $^3\text{H}(p,e^+e^-)^4\text{He}_{\text{g.s.}}$ and $^7\text{Li}(p,e^+e^-)^8\text{Be}_{\text{g.s.}}$

The anomalous soft photons discussed in the last subsec-

[6] In fitting the thermal model, the m_iT_i ambiguity gives different values of m_i for different values of T_i without changing significantly the overall quality of the fitting.

tion are produced in highly-relativistic reactions in which the produced particles travel with velocities close to the speed of light with a transverse momentum p_T of the order of many tens of MeV/c. Hence the parent particles of the anomalous soft photon that decay into electron–positron pairs would have a rest mass of order $m \sim p_T/(\text{speed of light})$, or many tens of MeV/c^2. They indicate possible existence of neutral particles in the mass regions of many tens of MeV. The extraction the anomalous particle masses from the p_T spectrum in the thermal model analysis has high degrees of uncertainty. The particle masses can be better ascertained by direct measurements. Independent of the anomalous soft photons, two other methods have been employed in the search of light neutral bosons. One uses the decay of the neutral boson into an e^+e^- pair [46–51, 172–175, 202], and the other uses the decay into two real photons [52, 53, 196, 197].

In search of possible candidate particles for the axion [198], de Boer and collaborators initiated a program to study the e^+e^- spectrum in low-energy proton fusion of light nuclei [172–175]. The E1 e^+e^- decay of the 17.2 MeV state in ^{12}C, and the M1 e^+e^- decay of the 17.6 MeV state in ^{8}Be to their respective ground states were examined to look for short-lived neutral bosons with masses between 5 and 15 MeV/c^2. Whereas for the E1 decay at large correlation angles exhibits no deviation from internal pair conversion, the M1 angular correlation in the decay of the excited 1^+ state of ^{8}Be at 18.15 MeV surprisingly deviates from internal pair conversion at the 4.5σ level [172–174]. In collaboration with ATOMKI, the group reported a neutral particle at 12 ± 2.5 MeV in the decay of the excited 1^+ isovector 17.64 state of ^{8}Be [175].

Krasznarhokay and collaborators [175] at ATOMKI has been continuing the search for a neutral boson with an improved e^+e^- spectrometer. In a subsequent experiment in the reaction of $p+^7\text{Li} \rightarrow e^+ + e^- + ^8\text{Be}_{\text{ground state}}$ at proton energies about 1 MeV, the 18.15 MeV $J^\pi I = 1^+0$ excited $^8\text{Be}^*$ state was observed to decay to the ^{8}Be ground state by the emission of a hypothetical neutral "X17" boson with a mass of $16.70 \pm 0.35(\text{stat}) \pm 0.5(\text{syst})$ MeV [46]. The ATOMKI observation of such an X17 boson has generated a great deal of interest. Even though a neutral isoscalar QED-confined $q\bar{q}$ state was predicted earlier to have a mass of 12.8 MeV in Table 1 of [27][7)], the observed neutral boson with a mass of 17 MeV led to many speculations inside and outside the known families of particles of the Standard Model [27, 30, 176–195].

Supporting experimental evidence for the X17 particle in the decay of the excited 18.05 MeV $J^\pi I = 0^-0$ state of ^{4}He [47, 48] and the decay of the excited 17.23 MeV $J^\pi I = 1^-1$ state of ^{12}C [51] have been reported by the ATOMKI Collaboration. Earlier observations of similar e^+e^- pairs with invariant masses between 3 to 20 MeV in the collision of nuclei with emulsion detectors have been reported [199–202]. There are furthermore possible $\gamma\gamma$ invariant mass structures at an energy around 10 to 15 MeV and 38 MeV in pp, and π^-p reactions in COMPASS experiments [203–207, 210, 211]. Different theoretical interpretations, astrophysical implications, and experimental searches have been presented, including the fifth force of Nature, the extension of the Standard Model, the QCD axion, dark matter, the QED mesons, 12-quark-state and many others [27, 30, 176–181, 186–195]. As reviewed in the Proceedings to the X17 Workshop [54], the confirmation of the X17 particle is actively pursued by many laboratories, including ATOMKI [55], Dubna [56], STAR [57], MEGII [58], TU Prague [59], NTOF [60], NA64 [61], INFN-Rome [62], NA48 [63], Mu3e [64], MAGIX/DarkMESA [65], JLAB PAC50 [66, 67], PADME [68], DarkLight [69, 70], and LUXE [71].

In the ATOMKI experiments, proton beams at a laboratory energy of 0.5 to 2.5 MeV were used to fuse with ^{3}H, ^{7}Li, and ^{11}B target nuclei to form excited states of ^{4}He, ^{8}Be, and ^{12}C, respectively [46–51]. The target nuclei have been so chosen that the ground states of the product nuclei by proton fusion are closed-shell nuclei. Specifically, the ^{4}He ground state in the reaction of $^3\text{H}(p, e^+e^-)^4\text{He}_{\text{g.s.}}$ is a spherical closed-shell nucleus. The ^{8}Be ground state in the reaction of $^7\text{Li}(p, e^+e^-)^8\text{Be}_{\text{g.s.}}$ is an prolate close-shell nucleus with a longitudinal to transverse radius ratio of about 2:1. The ^{12}C ground state in the reaction of $^{11}\text{B}(p, e^+e^-)^{12}\text{C}_{\text{g.s.}}$ is an oblate closed-shell nucleus with a longitudinal to transverse radius ratio of about 1:2 [212]. There is consequently a large single-particle energy gap between particle states above the closed shell and the hole states at the top of the Fermi surface below the closed shell. The captured proton in the product nucleus in the proton fusion reaction populates proton single-particle states above the large closed-shell energy gap, with the proton hole single-particle states of the triton core ^{3}H much below at the top of the Fermi surface. The transition of the proton from the proton particle states above the closed-shell energy gap to the proton hole state at the top of the Fermi surface to reach the closed-shell ^{4}He ground state in the reaction will release the large closed-shell-gap energy that is of order about 17–20 MeV, as shown in Figs. 9(a) and (b). Such a large closed-shell-energy gap may be sufficient to produce a neutral boson, if there would exist such a stable neutral boson particle with the proper energy, quantum numbers, and other conditions appropriate for its production.

The picture is simplest for the $p+^3\text{H} \rightarrow ^4\text{He}^* \rightarrow (e^+ + e^-) + ^4\text{He}_{\text{g.s.}}$ reaction for which the ground state of the product ^{4}He nucleus is spherical. The captured proton in the

[7)] The prediction of the mass of 12.8 MeV for the isoscalar QED meson in Table 1 of [27] was calculated in the massless quark limit. When the correction of the non-zero quark mass has been taken into account, the predicted mass of the isoscalar QED meson increases to 17.9 MeV [30].

lowest few excited ^{4}He* state must occupy a p-shell proton single-particle state that is significantly stretched outside the triton ^{3}H core with a proton and two neutrons in the lower occupied s-states. In the collision of the incident proton on the target ^{3}H nucleus, there is the fusion barrier which comprises of the Coulomb and centrifugal barrier for a single-particle with an angular momentum l,

$$E_l = \frac{Z_p Z_T\, e^2}{R} + \frac{l(l+1)\hbar^2}{2\mu R^2}, \tag{73}$$

where $R = r_0(A_p^{1/3} + A_T^{1/3})$, $\mu = [(A_p A_T)/(A_p + A_T)]m_{\text{nucleon}}$, (Z_p, A_p), and (Z_T, A_T) are the projectile and target charge and atomic numbers, respectively. For $r_0 = 1.3$ fm, the p+^{3}H→^{4}He* fusion barrier for $l = 1$ is about 6 MeV which places the low energy beam of around 1 MeV to lie below the fusion barrier for the $l = 1$ partial waves.

The capture of a proton of E_{lab} will lead to an excited ^{4}He* nucleus at an excitation of $E_x = [A_T/(A_T+1)]E_{\text{lab}} + Q$ where the Q value for the p+^{3}H→^{4}He* reaction is 19.815 MeV. The ATOMKI experimental proton energies of $E_{\text{lab}} = \{510, 610, \text{and } 900\}$ keV in [48] in Fig. 10(a), correspond to the ^{4}He* excitation energies of $E_x = \{20.20, 20.27, 20.49\}$ MeV. We can compare these excitation energies E_x with the energy levels of ^{4}He* states in Fig. 9(a) [216], where the lowest states are likely pocket resonances in the potential pocket [214], as evidenced by their narrow proton widths: The $J^\pi I = 0^+0$ state at 20.21 MeV has a proton width of 0.64 MeV while the $J^\pi I = 0^-0$ state at 21.02 MeV has a proton width of 0.50 MeV.

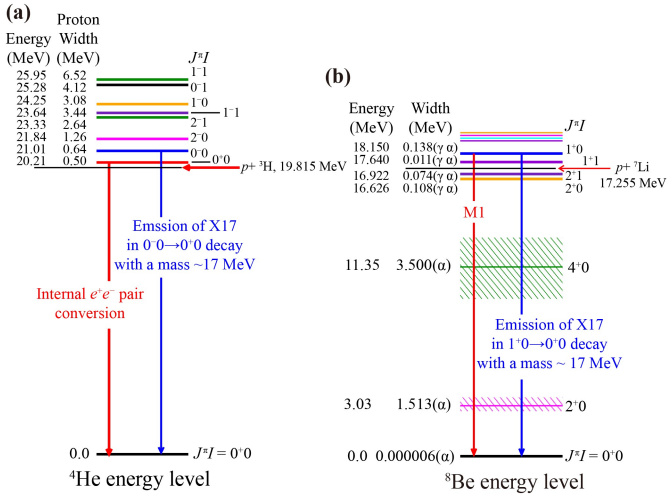

Fig. 9 **(a)** The energy levels and widths of ^{4}He states showing the transition in the decay of the 21.01 MeV $J^\pi I = 0^-0$ ^{4}He excited state to the ^{4}He ground state with the emission of the X17 particle at ~17 MeV, as interpreted in [47]. **(b)** The energy levels and widths of ^{8}Be states showing the transition in the decay of the excited 18.15 MeV $J^\pi I = 1^+0$ state to the ^{8}Be ground state with the emission of the X17 particle, as interpreted in Ref. [46].

Depending on the collision energy, there will be probabilities for capturing into the pocket resonances inside the potential pocket with various proton capture widths. These resonances will subsequently decay to the ground state by internal conversion with the emission of an e^+e^- pair. For example, capturing to the 0^+0 resonance state at 20.21 MeV will decay to the ground state by internal conversion with the emission of an e^+e^- pair, as indicated in Fig. 9(a). There is also a finite probability for the direct non-resonant $l = 1$ capture into a continuum state which tunnels through the Coulomb and centrifugal barrier to the interior region and subsequently decays into the ground state, with the emission an e^+e^- pair by the E1 electromagnetic radiation. The range of the collision energies in the ATOMKI experiment lead to the population of both the $J^\pi I = 0^+0$ state at 20.21 MeV and the $J^\pi I = 0^-0$ state at 21.02 MeV. The de-excitation of the $J^\pi I = 0^+0$ state at 20.21 MeV can be accounted for by the internal pair conversion from $0^+0 \to 0^+0$ final state. The solid curves in Fig. 10(a) represent the sum of (i) the $0^+0 \to 0^+0$ internal conversion contribution and (ii) the E1 non-resonant capture contribution to e^+e^- [47]. As one observes in Fig. 10(a), there appears an excess of the e^+e^- counts at large correlation angles. The excess e^+e^- yield can be described as arising from the decay of the $J^\pi I = 0^-0$ excited state of ^{4}He* at 21.02 MeV to the ^{4}He ground state with the emission of a neutral "X17" boson with a mass of 16.94±0.12 MeV as indicated in Fig. 10(b) [48]. In such an interpretation, the reaction for the production of the X17 state is

$$^4\text{He}^*(21.02\text{ MeV}, J^\pi I = 0^-0) \to$$
$$\text{X17} + {}^4\text{He (ground state , } J^\pi I = 0^+0), \tag{74}$$

which implies that the quantum numbers of the emitted X17 particle is $J^\pi I = 0^-0$.

In another experiment in the reaction of ^{7}Li+$p \to$ ^{8}Be*→ $(e^+ + e^-)$+^{8}Be$_{\text{g.s.}}$ at ATOMKI [46, 47] at a proton beam energy of a few MeV, the 18.15 MeV $J^\pi I = 1^+0$ state of ^{8}Be* was populated together with its neighboring states. From the nuclear reaction viewpoints, the captured proton populates single-particle states in the deformed Nilsson single-particle p-shell states. The fusion barrier for $l = 1$ partial waves lies at about 4.5 MeV if the target nucleus were spherical. Even though the fusion barrier will be modified because of the target deformation [213], the fusion barrier for $l = 1$ would likely place the low energy beam of around 1 to 2 MeV to be below the fusion barrier for $l = 1$ partial waves, as evidenced by their narrow resonance widths. The capture of a proton of E_{lab} will lead to an excited ^{8}Be* nucleus at an excitation energy of $E_x = [A_T/(A_T+1)]E_{\text{lab}} + Q$ where the Q value for the p+ ^{7}Li→^{8}Be* reaction is 17.255 MeV. The proton fusion experiments at ATOMKI with energies $E_{\text{lab}} = \{0.800, 1.04, 1.10, 1.20\}$ MeV in p+^{7}Li→^{8}Be* in [46] correspond to

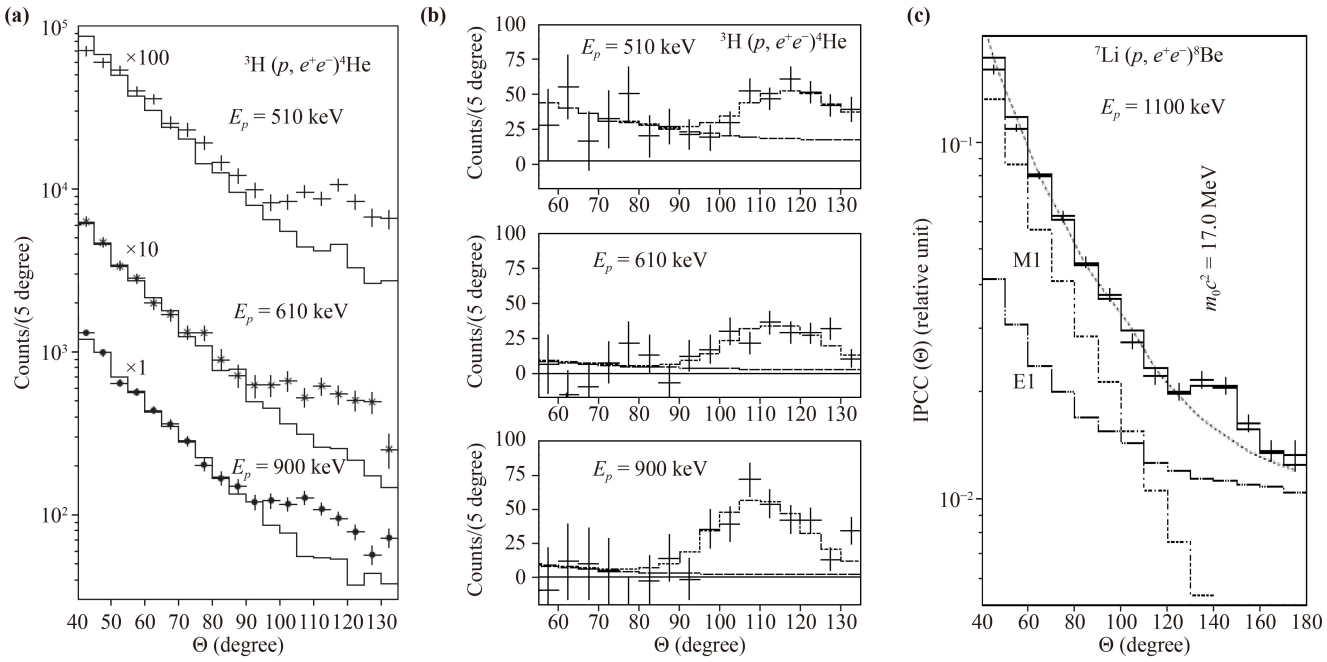

Fig. 10 **(a)** ATOMKI experimental e^+ and e^- angular correlations at different proton energies in the reaction of ^{4}He(p, e^+e^-)^{4}He$_{g.s.}$ [47, 48]. The solid curves are contributions from known sources of the e^+e^- cross sections from the decay of the 20.21 MeV 0^+0 ^{4}He* excited state to 0^+0 (ground state) and the E1 decay from non-resonant capture into an excited ^{4}He continuum state, displaying an excess of e^+e^- production at large correlation angles [47, 48]. **(b)** The data of an excess e^+e^- production at large correlation angles can be described by the de-excitation of the 21.02 MeV 0^+0 ^{4}He* state to the ground state with the emission of a hypothetical X17 particle with a mass of 16.94 MeV, as described by the solid histograms [47, 48]. **(c)** Similar e^+e^- excess occurs in the reaction of ^{7}Li(p, e^+e^-)^{8}Be$_{g.s.}$ [49]. The data of excess e^+e^- production at large correlation angles can be described as arising from the decay of the excited 18.15 MeV $J^\pi I$=1^+0 state of ^{8}Be to the ground state with the emission of the X17 particle at ~17 MeV (solid histogram) [49].

the production of an excited ^{8}Be* nucleus at E_x ={17.955,18.165,18.2175,18.305} MeV, respectively.

We can compare these excitation energies E_x with the energy levels of ^{8}Be* states in Fig. 9(b) [217]. Of particular interest are the 17.640 MeV $J^\pi I$ =1^+1 isovector state with a total width of 0.011 MeV decaying by γ and α emissions, and the 18.150 MeV $J^\pi I$ =1^+0 isoscalar state with a total width of 0.138 MeV decaying by γ and α emissions. Depending on the collision energy, there will be probabilities for capturing into the pocket resonance states inside the potential pocket with various proton capture widths. These resonances will subsequently decay into the ground state by internal conversion with the emission of an e^+e^- pair. There will also be a finite probability for the non-resonant $l = 1$ capture into a continuum state which tunnels through the Coulomb and centrifugal barrier and decays to the ground state with an e^+e^- pair by an E1 electromagnetic radiation. The $J^\pi I = 1^+0$ state at 18.15 MeV can make a transition to the 0^+0 final ground state by the M1 e^+e^- internal pair conversion. The dotted curve in Fig. 10(c) represents the sum of (i) the M1 e^+e^- internal conversion contribution and (ii) the E1 non-resonant capture contribution to e^+e^- [49]. As one observes in Fig. 10(c), there appears an excess of the e^+e^- counts at large correlation angles around $\theta \sim 140^o$. The excess e^+e^- yield can be described by the solid curve as arising from the decay of $J^\pi I$ = 1^+0 excited state of ^{8}Be* at 18.15 MeV to the ^{8}Be ground state with the emission of a neutral "X17" boson with a mass of 17.11±0.12 MeV [49].

The approximate equality of the masses of the hypothetical neutral boson in ^{4}He* and ^{8}Be* decays suggests that they are likely to be the same particle, the X17 particle with $J^\pi I = 0^-0$, emitted in the decay of the excited 0^-0 state at 21.02 MeV of ^{4}He*, in the $l = 1$ partial wave from the excited 1^+0 state at 18.05 MeV of ^{8}Be*. From Wheeler's molecular viewpoints of the nuclei structure of light nuclei [215], the ground state of ^{8}Be is likely to be in the form of two α clusters because of the strong binding of the alpha particle. So, in the excited 18.05 MeV $J^\pi I$ =0^-0 excited ^{8}Be* system, the emission would likely come from one of the two α clusters of ^{8}Be* and the emitting cluster has a non-zero angular momentum relative to the ^{8}Be* nucleus center of mass. From this viewpoint, it is reasonable to assign the quantum numbers of the X17 to be $J^\pi I = 0^-0$ from the ^{8}Be* decay, the same as those from the ^{4}He* decay.

Recently, a question was raised concerning the background subtraction of the e^+e^- signals from the M1 and E1 contributions in the analysis of the anomalous X17 particle in the ^{7}Li+p→Be* decay [46]. Hayes *et al.* [238]

re-examined the angular correlations in the e^+e^- decay of those excited states in ^{8}Be in the ATOMKI experiment. In the range of ATOMKI proton energies, the ratio of the E1 and M1 contributions to the e^+e^- production was found to be a sensitive function of energy. They questioned the earlier assumption in [46] of an energy-independent admixture of the E1 and M1 contributions for the e^+e^- production. They found that the existence of a "bump" in the measured angular distribution depended strongly on the assumed M1/E1 ratio and the measured large-angle contributions to the e^+e^- angular distribution to be lower than expectation. They cast doubts on the evidence for the existence of the anomaly in the present analysis.

However, there was another recent measurement of the angular correlation of e^+e^- pairs produced in the ^{7}Li$(p,\gamma)^8$Be$_{g.s}$ reaction at the sharp $E_p = 441$ keV resonance and 650 keV, 800 keV and 1100 keV proton beam energies [50]. The spectra measured at the resonance could be understood through the M1 internal pair creation process, but in the case of the off-resonance regions (direct proton capture) significant anomalies were observed in the e^+e^- angular correlations supporting the X17 hypothetical particle creation and decay. Clearly, many more measurements in search of the X17 particles and many theoretical analyses need to be carried out to clarify the situation.

5.10 Observation of the anomalous X17 particle in ^{11}B$(p,e^+e^-)^{12}$C$_{\rm g.s.}$

Subsequent to the observation of the X17 particle, it was suggested that the electromagnetic E1 decay of the excited $J^\pi I = 1^-1$ ^{12}C* state at 17.23 MeV to the ground state should be studied in order to determine whether the X17 particle has a vector or axial-vector characteristics [218]. ATOMKI measurements with proton energies between 1.5 to 2.5 MeV showed that the X17 particle was generated predominantly by the E1 radiation. It was concluded in [51] that the association of the observation of the X17 particle with the decay of the 17.23 MeV $J^\pi I = 1^-1$ ^{12}C* state supports the vector character of the X17 particle, as suggested by Feng and collaborators [51]. In such an interpretation, the reaction for the production of the X17 state is

$$\begin{aligned} &^{12}\mathrm{C}^*\ (17.23\ \mathrm{MeV}, J^\pi I = 1^-1) \\ &\rightarrow \mathrm{X17} + ^{12}\mathrm{C}(\mathrm{ground\ state}, J^\pi I = 0^+0), \end{aligned} \tag{75}$$

which implies that the quantum numbers of the emitted X17 particle is $J^\pi I = 1^-1$.

In the fusion of p with ^{11}B target nucleus, the captured proton populates a Nilsson oblate orbital originating from the spherical p-shell states. The Coulomb and centrifugal barrier for a spherical $l = 1$ partial waves would lie at about 4.3 MeV. Even though the fusion barrier will be modified because of the target deformation, the collision energy of $E_{\rm lab}$ from 1.5 to 2.5 MeV are much below the fusion barrier. So most of the lowest ^{12}C* excited states populated by the proton fusion reaction are likely pocket resonances in the potential pocket with small proton decay widths. The capture of a proton of $E_{\rm lab}$ will lead to an excited ^{12}C* nucleus at an excitation of $E_x = [A_T/(A_T+1)]E_{\rm lab} + Q$ where the Q value for the $p+$ ^{11}B$\rightarrow^{12}$C* reaction is 15.957 MeV [221]. The proton-^{11}B fusion experiments at ATOMKI with energies of $E_{\rm lab} =$ {1.5,1.70,1.88, 2.10, 2.5} MeV in [51] correspond to the production of an excited ^{12}C at energies of $E_x =$ $\{17.33, 17.52, 17.68, 17.88, 18.25\}$ MeV, respectively. They can be compared with the energy levels and their widths of ^{12}C* states listed in [221]. One observes that there are five ^{12}C* excited states which will be populated within the experimental range of proton energies of the ATOMKI experiments. Three of these states, the 17.23 MeV 1^-1 state, the 18.15 MeV 1^+0 state, and the 18.35 MeV 3^-1 state emits gamma radiation which will contribute to the e^+e^- internal conversion.

The interpretation of the X17 as possessing the $J^\pi I = 1^-1$ isovector characteristics as presented in [51] is subject to serious questions. First of all, such an interpretation of the X17 as an isovector $J^\pi I = 1^-1$ particle differs from the $J^\pi I = 0^-0$ isoscalar interpretation of the X17 particle as suggested earlier in ^{4}He* and ^{8}Be* decays [46, 47]. The observed boson or bosons in the two measurements have about the same mass, and are likely the same particle. If there is only a single neutral boson with a mass of about 17 MeV, then one of the two assignments of the $J^\pi I$ quantum numbers of the neutral X17 particle may be incorrect. Secondly, the large number of states in the neighborhood of the 17.23 MeV 1^+1 ^{12}C state [221] that are populated within the experimental range of proton energies of the ATOMKI experiments make it clear that it may be necessary to take into account the possibility that the X17 may arise from other states. Of particular interest is the 18.16 MeV 1^+0 state with a width of 0.24 MeV, which decays by γ and p emissions. This 18.16 MeV 1^+0 ^{12}C state may be the analogue of the 18.15 MeV 1^+0 ^{8}Be state because they have the same quantum numbers, excitation energies, decay widths, decay channels, and they may represent a proton populating a p orbital away from a triton core in one of the α particles in the picture of Wheeler's alpha-particle model. The X17 particle observed in the ^{11}Li$(p,e^+e^-)^{12}$C$_{\rm g.s.}$ reaction in [51] may arise also from the decay of the 18.15 MeV 1^+0 state in ^{11}Li$(p,e^+e^-)^{12}$C$_{\rm g.s.}$ collisions. If the transition from the 18.15 MeV $J^\pi I = 0^-0$ to the ground state contributes dominantly to the X17 production instead of the transition from the 17.23 MeV $J^\pi I = 1^-1$ state as suggested in [51], the X17 data of ^{4}He* decay, the ^{8}Be* decay and the ^{12}C* decay will be consistent with each other, whereas the $J^\pi I = 1^-1$ interpretation of ^{12}C contradicts the $J^\pi I = 0^-0$ interpretation of ^{4}He and ^{8}Be.

In order to discriminate the two possible assignments of $J^\pi I = 1^-1$ or 0^-0, we can suggest the search for two-

photon decay of the X17 particle. Such a decay is possible if the X17 is a $J^\pi I = 0^-0$ particle. However, because of the Landau–Yang theorem [222, 223], the decay of a 1^- state into two photons is impossible. If X17 is found to decay into two photons, then the X17 can only be a 0^-0 particle and not a 1^-1 particle.

Another way to study the $^{12}C^*$ system and the X17 particle is to excite a ^{12}C target ground state by direct photon excitation to various states, such as the 1^-1 at 17.23 MeV by E1 excitation and the 1^+0 at 18.15 MeV by M1 excitation. After the nucleus excited to these specific states, their decay by the emission of an X17 particle or an internal conversion photon in the form of e^+e^- can be examined.

There is one more way to study the X17 particle and its quantum number assignments, if the X17 indeed has the $J^\pi I = 1^-1$ property as proposed by [51, 218]. Because the strength of the giant dipole state of ^{12}C resides at 25 MeV and not at 17.23 MeV and the 17.23 represents only a very small fraction of the giant dipole strength [219, 220], the X17 particles would be copious produced at $E_x = 25$ MeV, and such a copious X17 production would allow the study of the X17 properties, if the X17 indeed has the $J^\pi I = 1^-1$ property.

5.11 The observation of the E38 particle

Abraamyan and collaborators at Dubna have been using the two-photon decay of a neutral boson to study the resonance structure, the dynamics, and the interaction of the lightest hadrons near their thresholds. Their experiments have been carried out by using the proton, deuteron, and other light-ion beams of the Nucleotron at JINR, Dubna on fixed internal fixed targets of C, Cu, and other nuclei, with the production of hadrons and photons. Their PHONTON2 photon detector consists of two arms placed at 26° and 28° degrees from the beam direction, with each arm equipped with 32 lead-glass photon detectors as shown in Fig. 11(a). The photon detectors measure the energies and the emission angles of the photons. From the energies and the opening angle θ_{12} of two photons γ_1 and γ_2 in coincidence, the invariant mass of the pair, $M_{\gamma_1\gamma_2} = E_{\gamma 1}E_{\gamma 2}(1-\cos\theta_{12})$, can be evaluated and the invariant mass distribution determined. Neutral bosons with large invariant masses can be searched by selecting photon pairs with large opening angles from different arms. On the other hand, by selecting photon pairs from the same arm with small opening angles, it is possible to study neutral bosons with small invariant masses such as those below the pion mass gap m_π, if they ever could be stable. Thus, the PHOTON2 detector can be used to probe the possible existence of neutral bosons over a large dynamical range. Previously, along with the detection of the π^0 and η mesons, the Dubna Collaboration uncovered a new resonance structure at $M_{\gamma\gamma} = 360$ MeV (the R360 resonance) [196]. The resonance was subsequently confirmed by repeated measurements [197] with higher statistics. We shall explore a possible model for R360 in Section 7.6 in terms of a molecular state of two pions and two E38 QED mesons.

In 2011, van Beveren and Rupp studied $e^+e^-\to\pi^+\pi^-$ [233], $p\bar{p}\to J/\psi\pi^+\pi^-$ [234], and $e^+e^-\to\Upsilon\pi^+\pi^-$ cross sections and observed that the deviation of the cross section from a global fit oscillates with a period of 73 to 79 MeV [224, 225]. An analysis of the invariant mass distribution of $M_{\Upsilon(1S)}$ as determined from $e^+e^-\to\Upsilon(2^3S_1)\to\pi^+\pi^-\to\pi^+\pi^-\mu^+\mu^-$ and the invariant mass distribution of $M_{\Upsilon(1S)}$ as determined from $\Upsilon(2^3S_1)\to\mu^+\mu^-$ [226] suggested a shift of the excitation function by 38 MeV. Van Beveren and Rupp [224, 225] therefore speculated on the possible existence of a light boson with a mass of 38 MeV. Their examination of the two photon spectrum of the COMPASS Collaboration data [205] also suggested a possible resonance at 38 MeV. There ensued a debate on the background subtraction of the COMPASS data and the reliability of the identification of the E38 resonance using the raw COMPASS data [203–207, 210, 211].

Stimulated by the possibility of a light neutral boson with a mass of about 38 MeV, the Dubna Collaboration undertook a search for the E38 particle using the two-photon decay. The search was carried out in the d(2.0 GeV/n)+C, d(3.0 GeV/n)+Cu and p(4.6 GeV)+C reactions with internal targets at the JINR Nuclotron. It was reported in Version 1 of Ref. [52] that the invariant masses of the two-photon distribution in these reactions exhibit a resonance structure at around 38 MeV. Unaware of the earlier theoretical prediction of an isoscalar $J^\pi I = 0^-0$ QED-confined $q\bar{q}$ state at 38.4 MeV in Table 1 of [27] that could be a good candidate for such a particle, Version 2 of Ref. [52] stated, however, "due to non-ordinariness of the obtained results (standing out of The Standard Model) and at the request of co-authors, the first version of the article is withdrawn for further verification and more detailed description of the experiment and data analysis." Subsequent repeated checking of the results of their analysis over a period of many years confirmed their findings, and the updated results were then reported in [53].

In the latest Dubna experiment, the two-photon invariant masses spectra were studied in nuclear reactions of dC, dCu, and pC at 2.75, 3.83, and 5.5 GeV/c per nucleon, respectively. In different momentum windows, photon pairs in the same event from the PHOTON2 detector are selected and their invariant masses calculated to construct the invariant mass distribution shown as the solid curves in Fig. 11(b). The corresponding combinatorial backgrounds are obtained in the event-mixing method by calculating the invariant masses of two photons from two different events, shown as the shade regions in Fig. 11(b). The difference between the correlated

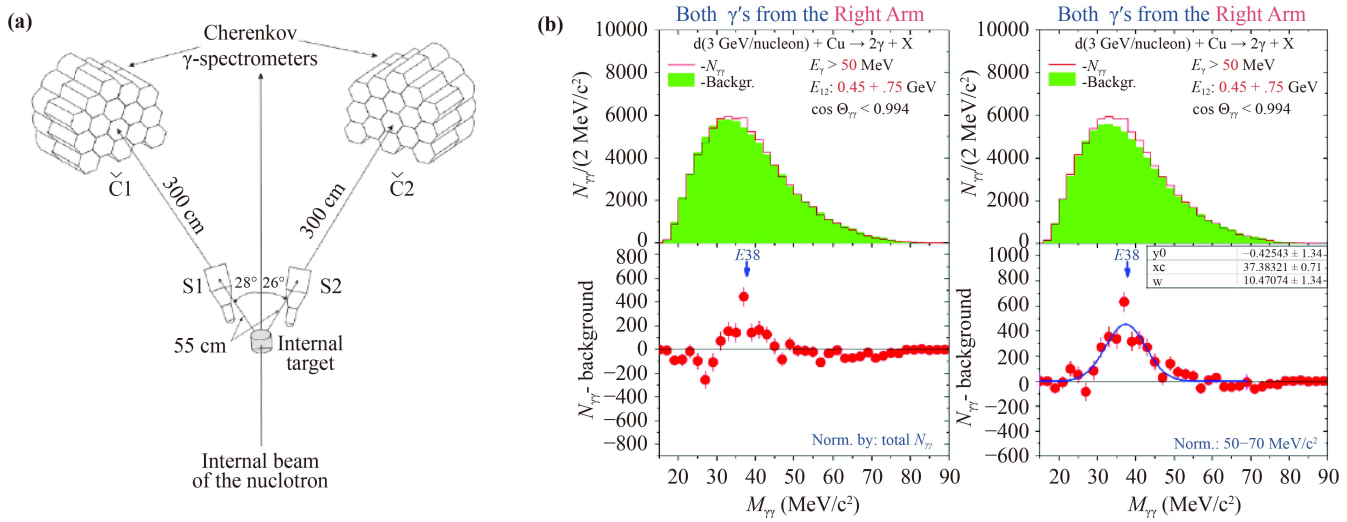

Fig. 11 **(a)** Dubna PHOTON2 detector arrangement to study the two-photon decay of reaction products in the collision of proton and light ions on fixed internal targets. **(b)** The invariant mass distribution of photon pairs from the same event is shown as the solid curves with the invariant mass distribution of photon pairs from the mixed events shown as the shaded regions. The signal of the invariant mass of the correlated pair after subtracting the mixed-event gubernatorial background shows a resonance structure at 38 MeV.

invariant mass distribution and the mixed-event invariant mass distribution gives the signal invariant mass distribution, as shown in the lower panels of Fig. 11(b) for different phase space windows. The resonance structure in Fig. 11(b) indicate a neutral boson, the E38 particle, at about 38 MeV [53]. Signals from other phase space windows show a similar resonance structure.

The observation of E38 at Dubna completes an important piece of the anomalous particle puzzle as the isoscalar X17 and the isovector E38 come in a pair, and they are orthogonal linear combinations of the $|u\bar{u}\rangle$ and $|d\bar{d}\rangle$ components. The agreement of their masses with those predicted by the phenomenological open-string model of QED-confined $q\bar{q}$ model of Section 4 lends support to the description that a quark and an antiquark can be confined and bound as stable QED-confined mesons interacting in the Abelian $U(1)$ QED interaction.

5.12 Anomalous particle production mechanisms

It is necessary to understand the mechanisms how the anomalous particles may be produced in order to fully support the interpretation on their production as QED mesons. For the low-energy production of the X17 particle in the decays of the excited states of ^{4}He* and ^{8}Be* at ATOMKI [46, 48], we envisage the scenario as described in Section 2 that the excited states of ^{8}Be(1^+18.15 MeV) and ^{4}He(0^-20.02 MeV) are formed by pulling a proton out of one of the alpha-particles of the $(\alpha)^n$-nucleus core and by placing the proton on an orbital that is considerably outside the corresponding tritium core as shown in Fig. 3(a). The stretched string-like interaction between the proton and the tritium core polarizes the vacuum so much that the proton may emit a virtual gluon which fuses with the virtual gluon from the ^{3}H core to lead to the production of a color-singlet $q\bar{q}$ pair by the reaction $g + g \to q + \bar{q}$ as shown in Fig. 3(a). At the appropriate $\sqrt{s}(q\bar{q})$ eigenenergy, the QED interaction between the q and the $\bar{q}$ may result in the formation of the QED-confined $q\bar{q}$ bound state X17 [27, 30], which subsequently decays into e^+–e^-.

For the production of E38 in high-energy nucleus–nucleus collisions at Dubna Collaboration [52, 53], and the anomalous soft photons in the high-energy hadron–hadron collisions at CERN [36–42], we envisage the production of many $q\bar{q}$ pairs as described in Fig. 3(b) of Section 2. In such high-energy processes, many $q\bar{q}$ pairs are produced. Even though most of the produced $q\bar{q}$ will materialize as QCD mesons, some of the $q\bar{q}$ pairs may materialize as QED mesons, as the E38 particle that decays into diphotons at Dubna [53] and as the X17 particle and the E38 particle that decay into the anomalous soft photons in the WA102 experiment [41].

In the other process for the production of the anomalous soft photons in high-energy e^+e^- annihilation at Z^0 mass at DELPHI, we envisage the production $q\bar{q}$ pairs as described in Fig. 1(c) of Section 2 in which the e^+e^- annihilation process leads to the production of a large number of $q\bar{q}$ pairs. While most produced $q\bar{q}$ pairs will lead to hadron production, there may however be $q\bar{q}$ pairs with $(m_q + m_{\bar{q}}) < \sqrt{s}(q\bar{q}) < m_\pi$ for which the QED interaction between the quark and the antiquark may lead to the production of the X17 and E38 particles at the appropriate energies and the anomalous particles subsequently decay into e^+e^- pairs.

6 Questions on quark confinement in compact QED in (3+1)D from lattice gauge calculations

6.1 Lattice gauge calculations prediction of deconfined static quark and antiquark in compact QED in (3+1)D

We mentioned in Section 4 that in lattice gauge theory a static fermion and a static antifermion in (3+1)D in compact QED interaction has a strong-coupling confined phase and a weak-coupling deconfined phase, as shown by Wilson, Kogut, Susskind, Mandelstam, Polyakov, Banks, Jaffe, Drell, Peskin, Guth, Kondo and many others [5–16]. The transition from the confined phase to the deconfined phases occurs at the coupling constant $\alpha_{\text{crit}} = g^2_{\text{crit}}/(4\pi) = 0.988989481$ [17, 18]. The magnitude of the QED coupling constant as given by the fine-structure constant $\alpha_c = 1/137$ is less than α_{crit}. That is, the QED interaction between a quark and an antiquark belongs to the weak-coupling deconfined regime. Therefore, a static quark and a static antiquark are deconfined in lattice gauge calculations in compact QED in (3+1)D.

The deconfined static quark and static antiquark in the lattice gauge results in (3+1)D poses a serious question. There are experimental circumstances in which a quark and an antiquark can be produced and they can interact in QED alone, without the QCD interaction, as we discussed in Section 2. For example, we can study the reactions $e^+ + e^- \to \gamma^* \to q + \bar{q}$ and $e^+ + e^- \to \gamma^* \gamma^* \to q + \bar{q}$ with a center-of mass energy range $(m_q + m_{\bar{q}}) < \sqrt{s}(q\bar{q}) < m_\pi$, where the sum of the rest masses of the quark and the antiquark is of order a few MeV and $m_\pi \sim 135$ MeV [74]. The incident $e^+ + e^-$ pair is in a colorless color-singlet state, and thus the produced q and $\bar{q}$ pair and the quanta mediating their interactions must also combine together into a color-singlet final state. In this energy range below the collective QCD excitation mass gap of m_π, there is insufficient energy to excite a collective QCD excitation to produce a QCD meson. A q and $\bar{q}$ can be produced and interact in the QED interaction alone. In the color-singlet $(q\bar{q})^1$ configuration, the produced q and $\bar{q}$ can interact with the colorless Abelian $U(1)$ QED interaction to form a color-singlet $[(q\bar{q})^1\gamma^1]^1$ final state, if there is a QED meson eigenstate at this eigenenergy. At energies other than the QED meson eigenenergies in this energy range below m_π, the $e^+ + e^-$ collision will probe the dynamics of a quark and antiquark interacting in QED alone, without the QCD interaction. The absence of fractional charges in collisions in this energy range in $e^+ + e^-$ collisions indicates the absence of the continuum states of an isolated quark and an antiquark in the interaction of a quark and an antiquark in the QED interaction.

On the other hand, the solution of deconfined static quark and static antiquark in the lattice gauge calculations in QED in (3+1)D predicts that the q and $\bar{q}$ produced in $e^+ + e^-$ collisions in the range of energy below the QCD collective excitation mass gap m_π will not be confined and would appear as fraction charges, when the quark interact with the antiquark in QED alone in (3+1)D. However, no such fractional charges have ever been observed. Furthermore, the phenomenological open-string QCD and QED meson model with the hypothesis of a confined $q\bar{q}$ pair in QED in (3+1)D leads to QED meson and QCD meson spectra in agreement with experimental data, as discussed in Section 5. There is a confined regime in (1+1)D QED for dynamical massless quarks in the Schwinger confinement mechanism [1, 2], and there is also a confined regime for quarks in compact QED in (2+1)D [5, 6] in Polyakov's transverse confinement, for all gauge coupling interaction strengths. They indicate that the present-day lattice gauge calculations for compact QED in (3+1)D may not be complete and definitive, because the important Schwinger dynamical quark effects associated with light quarks has not been included. Future lattice gauge calculations with dynamical quarks in compact QED interactions in (3+1)D will be of great interest in clarifying the question of quark confinement in QED.

6.2 Compact and non-compact $U(1)$ QED gauge interactions in lattice gauge calcualtions

Whatever the theoretical predictions on the confinement of quarks in QED in (3+1)D may be, in the final analysis, the question whether a $q\bar{q}$ pair is confined in QED in (3+1)D can only be settled by experiment. In the meantime, in the presence of the two opposing theoretical conclusions on quark confinement in QED in (3+1)D and the agreement of the experimental spectrum of the anomalous particles with the QED meson predictions, it is possible that the two conclusions can still be consistent with each other, if the confinement conclusions arise from the inclusion of the Schwinger confinement mechanism [1, 2] in the works of [27–34], while and the deconfinement conclusion arises from the absence of the Schwinger confinement mechanism in lattice calculations [17, 18]. Therefore, it is worth constructing a plausible "stretch (2+1)D" flux tube model to demonstrate the importance of the Schwinger confinement mechanism in compact QED in (3+1)D.

In such a demonstration, we note first of all that the Schwinger confinement mechanism occurs in (1+1)D space-time, whereas the physical world is in (3+1)D. For the Schwinger confinement mechanism to be operative, the quark-QED system must possess transverse confinement as a flux tube in the (3+1)D space-time before the flux tube can be idealized as a one-dimensional string in the (1+1)D space-time. In this regard, we note from Polyakov's previous results that electric charges of opposite signs interacting in compact QED in (2+1)D are confined and that the confinement persists for all non-

vanishing coupling constants, no matter how weak [5, 6]. We can combine Schwinger's longitudinal confinement in (1+1)D QED with Polyakov's transverse confinement in (2+1)D compact QED to study QED confinement in a flux tube environment in (3+1)D.

Before we come to the "stretch (2+1)D" flux tube model of $q\bar{q}$ production in compact QED in (3+1)D, it is necessary to clarify the concept of compactness in the QED interaction.

There are two different types of QED $U(1)$ gauge interactions possessing different confinement properties [5, 6, 16]. There is the compact QED $U(1)$ gauge theory in which the gauge fields A^μ are angular variables with a periodic gauge field action which allows transverse photons to self-interact among themselves. The gauge field action in the compact QED $U(1)$ gauge theory, in the lattice gauge units and notations of Refs. [5, 6, 16], is

$$S = \frac{1}{2g^2}\sum_{x,\alpha\beta}(1-\cos F_{x,\alpha\beta}), \tag{76}$$

where g is the coupling constant and the gauge fields $F_{x,\alpha\beta}$ are

$$F_{x,\alpha\beta} = A_{x,\alpha}+A_{x+\alpha,\beta}-A_{x+\beta,\alpha}-A_{x,\beta}, \text{with } -\pi \le A_{x,\alpha} \le \pi. \tag{77}$$

There is also the non-compact QED $U(1)$ gauge theory with the gauge field action [5, 6, 16]

$$S = \frac{1}{4g^2}\sum_{x,\alpha\beta}F^2_{x,\alpha\beta}, \quad \text{with} \quad -\infty \le A_{x,\alpha} \le +\infty. \tag{78}$$

In non-compact QED gauge theories, the photons do not interact with other photons and the fermions in non-compact QED gauge theories are always de-confined. In compact QED in (2+1)D, the photons interact among themselves because the gauge fields are angular variables. Static charges of opposite signs are confined for all strength of the coupling constant in compact QED in (2+1)D. In compact QED in (3+1)D, however, static opposite charges are confined only for strong coupling but de-confined for weak coupling [5, 6, 16]. Even though the compact and the non-compact QED gauge theories in Eqs. (76) and (77) have the same continuum limit, they have different confinement properties. On the other hand, in the Schwinger confinement mechanism in QED in (1+1)D, massless fermions are confined for all coupling strengths in the continuum limit, which does not distinguish between compact and non-compact QED [1, 2].

We need to ascertain the type of the QED $U(1)$ gauge interaction between a quark and an antiquark in a QED meson. As pointed out by Yang [217], the quantization and the commensurate properties of the electric charges of the interacting particles imply the compact property of the underlying QED gauge theory. Because (i) quark and antiquark electric charges are quantized and commensurate, (ii) quarks and antiquarks are confined, and (iii) there are pieces of experimental evidence for possible occurrence of confined $q\bar{q}$ QED meson states as we mentioned in the Introduction, it is therefore reasonable to propose that quarks and antiquarks interact in the compact QED $U(1)$ interaction.

In compact QED, Polyakov [5, 6] showed previously that a pair of opposite electric charges and their gauge fields in $(2+1)\mathrm{D}_{\{x^1,x^2,x^0\}}$ are confined, and that the confinement persists for all non-vanishing coupling constants, no matter how weak. As explained by Drell and collaborators [16], such a confinement in (2+1) $\mathrm{D}_{\{x^1,x^2,x^0\}}$ arises from the angular-variable property of A_ϕ and the periodicity of the gauge field action as indicated in Eq. (76). The gauge action periodicity in the neighborhood of the produced opposite electric charges leads to self-interacting transverse gauge photons. These transverse gauge photons interact among themselves, they do not radiate away, and they join the two opposite electric charges and their associated gauge fields by a confining interaction.

6.3 The stretch (2+1)D model

To construct a "stretch (2+1)D" flux tube model [33, 34] for the production of a quark and an antiquark in a QED meson in (3+1)D, we take the Polyakov's transverse confinement configuration in compact QED in (2+1)D as input. We envisage the production of the nascent $q\bar{q}$ pair at the origin $(x^1,x^2,x^3)=0$ in the center-of-mass system, at the eigenenergy $\sqrt{s}(q\bar{q})$ of a QED meson[8)] as shown in Fig. 12(a). We take for simplicity the quark charge to be positive, which can be easily generalized to other cases of negatively-charged quark and flavor mixing. At birth and born to be in a QED meson state, the quark and the antiquark must possess an equal and opposite momenta in the center-of-mass system[8)]. The quark momentum defines the longitudinal direction from which we can define the transverse coordinates (x^1,x^2) and the transverse planes at $x^3=$ (constant). The quark and the antiquark produced at birth are located in the vicinity of the origin, and they are separated by an infinitesimal longitudinal separation Δx^3 and an infinitesimal transverse separation $\Delta \boldsymbol{r}_\perp$ as in Fig. 12(a). Polyakov's transverse confinement of the quark and the antiquark in compact QED in (2+1)D is realized on the transverse (x^1,x^2)-plane at $x^3\sim 0$, at the birth of the q–$\bar{q}$ pair. The creation of the charge q–$\bar{q}$ pair will be accompanied by the associated creation of their gauge fields $\boldsymbol{A}$,

[8)] As discussed in the Introduction, states of a quark and an antiquark do not exist except in a confined $q\bar{q}$ eigenstate, so we can study the confinement dynamics of a quark and an antiquark only when the quark and the antiquark under consideration here are constituents of a confined system such as a QED meson. Such a logical circularity arises because of the peculiar property of quark confinement.

$\boldsymbol{E}$, and $\boldsymbol{B} = \nabla \times A$, which by causality can only be in the neighborhood of the created charges initially with the created $\boldsymbol{E}$ and $\boldsymbol{B}$ fields lying along the longitudinal x^3 direction.

Subsequent to their births, the quark and the antiquark will execute stretching and contracting "yo–yo" motion along the longitudinal x^3 direction, appropriate for the QED meson bound state in question. As the quark and antiquark stretch outward in the longitudinal x^3 directions, we can construct a longitudinal tube structure of gauge fields in the stretch (2+1)D configuration by duplicating longitudinally the transversely-confined gauge fields that exist on the transverse (x^1, x^2)-plane at $x^3 \sim 0$ initially at their birth, for the longitudinal region between the stretching quark and antiquark. A snap shot of the stretch (2+1)D flux tube configurations at an early moment in the longitudinal stretching motion is shown in Fig. 12(b). The transcription of Fig. 12(b) in terms of the lattice link and plaquette variables is shown in Fig. 12(c), by following the Hamiltonian formulation and the notations of Drell *et al.* [16]. Specifically, in the $A^0 = 0$ gauge we specify the canonical conjugate gauge fields $\boldsymbol{A}$ and $\boldsymbol{E}$ at the links in Fig. 12(c), where we display only the A^1, A^2 and E^3 values of the conjugate gauge fields. The $\boldsymbol{B}$ and $\boldsymbol{E}$ fields are aligned along the longitudinal x^3 axis as shown in Fig. 12(b). These gauge field configurations are the ones that lead to Polyakov's transverse confinement of the quarks. They maintain the cylindrical symmetry of the stretch (2+1)D flux tube. They will lead to the desirable full confinements of the quark and the antiquark, as the magnetic field $\boldsymbol{B}$ sends the quark and antiquark charges into the appropriate Landau orbitals to execute confined transverse zero-mode harmonic oscillator zero-point motions on their respective $\{x^1, x^2\}$ planes. At the QED meson eigenenergy, the electric field $\boldsymbol{E}$ along the longitudinal x^3 direction send the quark and the antiquark in longitudinal 3D longitudinal stretching and contracting "yo–yo" motion. The electric charge densities obey the Gauss law associated with the divergence of the electric field $\boldsymbol{E}$. The positive electric quark charge fractions [solid circles in Fig. 12(c)] reside at the $-x^3/2$ plaquette vertices and the negative electric antiquark charge fractions [open circles in Fig. 1(c)] at the antiquark plaquette vertices at their $x^3/2$ planes. In the stretch (2+1)D configuration, the transverse gauge fields $\boldsymbol{A}$ on the transverse links are copies of those on the quark and the antiquark plaquettes at $x^3(q) = -x^3/2$ and at $x^3(\bar{q}) = x^3/2$ respectively, and they are unchanged in the stretching motion, while the longitudinal links are all $E^3 = |\boldsymbol{E}|/4$.

By the duplication of the initial transversely-confined gauge fields along the longitudinal direction, we obtain a longitudinal tube with a cylindrical symmetry in (3+1)D. The property of the transverse confinement at one longitudinal coordinate at birth is thereby extended to the whole tube, and the longitudinal tube will likely be a transversely-confining flux tube.

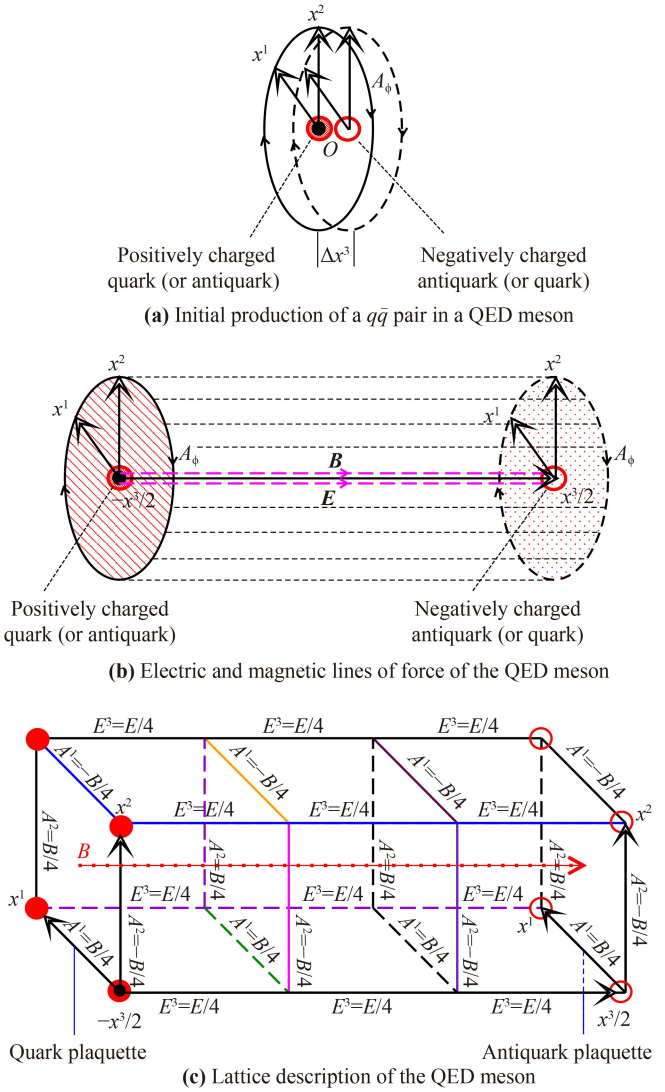

Fig. 12 **(a)** depicts the initial production of the $q\bar{q}$ pair of a QED meson, with an infinitesimal longitudinal separation Δx^3. **(b)** gives a snapshot of the configuration of the quark charge, the antiquark charge, gauge fields $\boldsymbol{A}, \boldsymbol{E}$, and $\boldsymbol{B} = \nabla \times \boldsymbol{A}$ during the dynamical longitudinal yo–yo motion of the $q\bar{q}$ pair interacting in compact QED in a QED meson, starting from a (2+1)D transversely confined $q\bar{q}$ system. **(b)** is the "stretch (2+1)D" configuration. **(c)** is the corresponding lattice transcription, following the Hamiltonian formulation of Drell *et al.* [16].

We show in the stretch (2+1)D model [34] that the longitudinal $\boldsymbol{B}$ field that is present initially to confine quarks and antiquarks on the transverse plane at their birth continues to confine quarks and antiquarks transversely, because of the Landau level dynamics. The cloud of transverse gauge fields continue to interact with each other to maintain the transverse confinement on their transverse planes. As a consequence, quarks, antiquarks, and gauge fields will be transversely confined in the stretch (2+1)D flux tube.

With the attainment of transverse confinement and $\boldsymbol{E}$ and $\boldsymbol{B}$ aligned along the longitudinal direction in the flux tube, it remains necessary to examine the question of longitudinal confinement. Therefore, we idealize the flux tube in the stretch (2+1)D configuration as a longitudinal string in $(1+1)\mathrm{D}_{\{x^3,x^0\}}$ and approximate the quarks to be massless, with the information on the transverse degrees of freedom stored as input parametric quantities in the idealized $(1+1)_{\{x^3,x^0\}}$ space-time. In the longitudinal dynamics with massless quarks in QED in $(1+1)\mathrm{D}_{\{x^3,x^0\}}$, there is a gauge-invariant relation between the quark current j^μ and the gauge field A^μ as given by [1, 2, 20]

$$j^\mu = \frac{g_{2\mathrm{D}}}{\pi}(A^\mu - \partial^\mu \frac{1}{\partial_\lambda \partial^\lambda}\partial_\nu A^\nu), \tag{79}$$

where $g_{2\mathrm{D}}$ is the coupling constant in (1+1)D space-time which is related to the coupling $g_{4\mathrm{D}}$ in (3+1)D by Eq. (11). On the other hand, the gauge field A^μ depends on the quark current j^ν through the Maxwell equation,

$$\partial_\nu(\partial^\nu A^\mu - \partial^\mu A^\nu) = -g_{2\mathrm{D}} j^\mu. \tag{80}$$

For the longitudinal motion, Eqs. (79) and (80) lead to the Klein–Gordon equations in j^μ and A^μ for a boson with a mass $m = g_{2\mathrm{D}}/\sqrt{\pi}$,

$$-\partial_\nu\partial^\nu j^\mu = \frac{g_{2\mathrm{D}}^2}{\pi} j^\mu, \quad \text{and} \quad -\partial_\nu\partial^\nu A^\mu = \frac{g_{2\mathrm{D}}^2}{\pi} A^\mu. \tag{81}$$

Thus, the quark current j^μ and the longitudinal gauge fields A^μ self-interact among themselves and build a longitudinal confining interaction between the quark and the antiquark in (1+1)D. As a consequence, in accordance with the Schwinger confinement mechanism for massless fermions in QED in (1+1)D [1, 2], the light quark and the light antiquark interacting in QED will be longitudinally confined just as well. Possessing both transverse and longitudinal confinements as in an open-string, the quark and the antiquark will be confined and bound in a QED meson in (3+1)D.

7 Implications of quark confinement in the QED interaction

As the theoretical expositions and the accompanying experimental evidence presented in the preceding sections strongly suggest possible quark confinement in the QED interaction, it is worth examining the implications of such a new concept in order to explore further new physics on the frontier. Such an exploration will necessarily be speculative in nature. However, some educated expectations may stimulate deeper explorations into the unknown frontier, and some other expectations have measurable experimentally consequences to merits further considerations.

7.1 Confinement may be an intrinsic property of quarks

The experimental observations, if definitively confirmed under further scrutiny, will indicate that the attribute of quark confinement is not be the sole property of the QCD interaction alone and that quarks are also confined in the QED interaction. Consequently, an interesting possibility is that the confinement attribute may be an intrinsic property of quarks. This possibility is reinforced by the observational absence of free quarks, which indicates further that in the interaction of a quark and an antiquark in their many mutual interactions, there may be a quark confinement principle which holds that in the dynamics of quarks in different interactions, each interaction always leads to the confinement of quarks. That is, a quark and its antiquark may be confined and bound as a neutral boson in their many mutual interactions. Specifically, a quark and its antiquark certainly interact mutually in the weak-interaction and also in the gravitational interaction. There is no physical law that forbids a quark and an antiquark to exchange a Z^0 boson or a graviton to interact in the weak or the gravitational forces alone. What is not forbidden is allowed, in accordance with Gell-Mann's Totalitarian Principle [73]. Consequently, a quark and its antiquark may be confined and bound as a neutral boson in the weak interaction and the gravitational interaction with the exchange of a Z^0 boson or a graviton.

It is of interest to estimate the mass of such a confined neutral boson with a weak strength of the coupling constant. The quark and it antiquark reside predominantly in (1+1)D. If the work of Coleman [4] on confined fermions in QED in (1+1)D can be an approximate analogous guide, such a confined boson falls into the 2D-weak-coupling regime. In the 2D-weak-coupling regime the mass of the composite boson would be approximately their rest masses, with additional contributions from the weak coupling interaction that can be calculated in the mass perturbation theory [4]. For an interaction with a weak strength of coupling constant, we may expect the mass of the confined and bound boson to be close to the rest mass of the quark and the antiquark. Such a particle however would decay by quark–antiquark annihilations into two real photons, two virtual photons, or an e^+e^- pair. The search for such a confined $q\bar{q}$ pair may be signaled by a boson with a mass close to the sum of the rest mass of the quark and its antiquark in the region of 4–10 MeV. Experiments in high-energy hadron–hadron, nucleus–nucleus, and e^+e^- collisions in search of anomalous particles decaying into two real or virtual photons or e^+e^- in the region of a 4–10 MeV will shed light on possible $q\bar{q}$ interactions with a weak strength of coupling constants. Rigorous theoretical work on the question of quark confinement in the weak and gravitational interactions and the possibility of these weak-interaction-confined and gravitation-confined composite $q\bar{q}$ particles as dark matter material would be of great interest.

The possibility of quarks confined in the QED interaction also implies that the QED interaction between a quark and an antiquark differs from the QED interaction between an electron and a positron. It will be of great interest to find out all the differences there can be and why are they different. For example, the QED interaction between an electron and a positron may belong to the non-compact QED theory while the QED interaction between a quark and an antiquark may belong to the compact QED theory. The possibilities of the compact and non-compact QED bring with them the question whether the QED interaction is unique or endowed with a multitude of experimentally testable possibilities with different topological properties. A related question is whether the QED interaction between quarks in a nucleon may also contain the linear QED confinement component that depends on the magnitudes and signs of the electric charges in addition to the standard Coulomb component as in Eq. (84) below.

7.2 New family of QED-confined particles and dark matter

The success of the open-string description of the QCD and QED mesons leads to the search for other neutral quark systems stabilized by the QED interaction between the constituents in the color-singlet subgroup, with the color-octet QCD gauge interaction as a spectator field. Of particular interest is the QED neutron with the d, u, and d quarks [31, 32]. They form a color product group of $\mathbf{3}\otimes\mathbf{3}\otimes\mathbf{3}=\mathbf{1}\oplus\mathbf{8}\oplus\mathbf{8}\oplus\mathbf{10}$, which contains a color singlet subgroup $\mathbf{1}$ where the color-singlet currents and the color-singlet QED gauge fields reside. In the color-singlet d–u–d system with three different colors, the attractive QED interaction between the u quark and the two d quarks overwhelms the repulsion between the two d quarks to stabilize the QED neutron at an estimated mass of 44.5 MeV [31]. The analogous QED proton has been found theoretically to be unstable because of the stronger repulsion between the two u quarks, and it does not provide a bound state nor a continuum state for the QED neutron to decay onto by way of the weak interaction. Hence the QED neutron may be stable against the weak interaction. It may have a very long lifetime and may be a good candidate for the dark matter. Because QED mesons and QED neutrons may arise from the coalescence of deconfined quarks during the deconfinement-to-confinement phrase transition in different environments such as in high-energy heavy-ion collisions, neutron-star mergers [227, 229], and neutron star cores [230], the search of the QED bound states in various environments will be of great interest.

In a related matter, an assembly of the QED-confined $q\bar{q}$ mesons can also be a good candidate for a part of the dark matter [30]. Depending on its mass, the assembly can be an e^+e^- emitter, a γ emitter, or the dark matter with no particle emission if the mass exceeds their respective threshold values [30]. The dark matter models of the QED meson and the QED neutron utilize the material and the elements of the Standard Model, but with a new confining combination. Theoretical and experimental studies will be needed to examine the condense state of an assembly of QED mesons or QED neutrons.

In addition to new particles, the fact that the QED mesons are complex objects brings with them additional degrees of freedom to lead to many excited QED mesons states. For example, there can be vibrational and rotational states formed by these QED mesons. We can get some idea on the vibrational states from the spectrum of a stretched string as shown in Fig. 7 of Ref. [31]. The possibility of adding quarks with different flavors, angular momentum, and spin quantum numbers will add other dimensions to the number of species of the QED-confined $q\bar{q}$ composite particles.

7.3 Beyond the confining interaction of a quark and an antiquark in (3+1)D

A quark and an antiquark reside predominately in (1+1) D, in which the interaction between a quark and an antiquark is the linear confining interaction for both QED and quasi-Abelian QCD, as discussed in Sections 3 and 4. In the physical (3+1)D space-time, such a linear interaction is only the dominant part of the full interaction between the quark and the antiquark. There will be additional residual interactions arising from the presence of the transverse degrees of freedom. There are also contributions from the spin–spin, spin–orbit, tensor, and other higher-order terms of the Breit interaction [140–142, 252].

For a confining string with a string tension σ, Lüscher [219, 220] considered the fluctuations in the transverse direction of the flux tube as a massless bosonic field theory in two dimensions with a classical action, for which the action can be integrated out to lead to a potential between a static quark at $\boldsymbol{r}_1$ and an antiquark at $\boldsymbol{r}_2$ in the large string length limit as

$$V(\boldsymbol{r}_1\boldsymbol{r}_2)=\sigma|\boldsymbol{r}_1-\boldsymbol{r}_2|+c-\frac{\alpha}{|\boldsymbol{r}_1-\boldsymbol{r}_2|}+O\left(\frac{1}{|\boldsymbol{r}_1-\boldsymbol{r}_2|^2}\right), \quad (82)$$

where α depends on the coupling constant, and c is a constant. These are therefore long range residual interactions in both the confined QCD and QED mesons. They represent corrections that arise from expanding the potential between a quark and an antiquark in powers of their separation $|\boldsymbol{r}_1-\boldsymbol{r}_2|$. A powerful tool to study the non-perturbative behavior of the interquark potential is the "Effective String Theory" in which the confining tube contains the quark and the antiquark at the two ends [85–87, 239–242, 249, 250]. The Nambu-Goto action can be integrated exactly in all geometries that are relevant for lattice gauge theories: the rectangle

(Wilson loop) in [243], the cylinder (Polyakov loop correlators) in [244, 245] and the torus (dual interfaces) in [246].

For quarks with color charge numbers $Q_1^{\rm QCD}$ and $Q_2^{\rm QCD}$ interacting in the QCD interaction, we can match the above equation (82) with the Cornell potential [251] and the phenomenological quark–antiquark potentials in [30, 140–142] and [252]. Upon neglecting the spin–spin, spin–orbit, other higher order terms, and an unimportant potential constant, we have the linear-plus-color-Coulomb interaction of QCD

$$V^{\rm QCD}(\boldsymbol{r}_1\boldsymbol{r}_2)=Q_1^{\rm QCD}Q_2^{\rm QCD}\left(-\sigma^{\rm QCD}|\boldsymbol{r}_1-\boldsymbol{r}_2|+\frac{\alpha_s}{|\boldsymbol{r}_1-\boldsymbol{r}_2|}\right). \tag{83}$$

The quark and the antiquark also interact in the QED interaction. We can generalize the above to include both QCD ($\lambda=1$) and QED ($\lambda=0$) interactions to give

$$V(\boldsymbol{r}_1\boldsymbol{r}_2)=\sum_{\lambda=0}^{1}Q_1^\lambda Q_2^\lambda\left(-\sigma^\lambda|\boldsymbol{r}_1-\boldsymbol{r}_2|+\frac{\alpha_\lambda}{|\boldsymbol{r}_1-\boldsymbol{r}_2|}\right)\tau^\lambda,\qquad \lambda=\begin{cases}0 & \text{QED}\\ 1 & \text{QCD}\end{cases}, \tag{84}$$

where $\tau^0=t^0$ is the generator of the $U(1)$ gauge subgroup as defined in Eqs. (14), and τ^1 is a fixed generator of the $SU(3)$ subgroup oriented randomly in the eight-dimensional color-octet generator space in the quasi-Abelian approximation of the non-Abelian QCD, as defined in (23) and discussed in Section 3. The generators τ^0 and τ^1 satisfy $2{\rm tr}(\tau^\lambda\tau^{\lambda'})=\delta^{\lambda\lambda'}$.

The above equation is for a single flavor. In the case with many flavors and flavor mixing, their effects can be taken into account by replacing Q_i^λ by the effective charge $\tilde{Q}_i^\lambda$, where $\tilde{Q}_i^\lambda$ is defined by Eq. (47) in Sections 4.3 and 4.7. It can be further generalized to the case when the quark constituent and the antiquark constituent possess different flavors. For a composite $q_1\bar{q}_2$ particle with many flavors and flavor mixing, the above interaction between the quark q_q and the antiquark $\bar{q}_2$ becomes

$$V(\boldsymbol{r}_1\boldsymbol{r}_2)=\sum_{\lambda=0}^{1}\tilde{Q}_{q_1}^\lambda\tilde{Q}_{\bar{q}_2}^\lambda\left(-\sigma^\lambda|\boldsymbol{r}_1-\boldsymbol{r}_2|+\frac{\alpha_\lambda}{|\boldsymbol{r}_1-\boldsymbol{r}_2|}\right)\tau^\lambda. \tag{85}$$

When there is no flavor mixing, as in the case of the charm and the beauty quarks, the effective charge are just those of the standard quark model, with $Q^{\rm QCD}_{\{u,d,c,s,t,b\}}=1$ and $Q^{\rm QED}_{\{u,c,t\}}=2/3$, $Q^{\rm QED}_{\{d,s,b\}}=-1/3$, and $Q_{\bar{q}}^\lambda=-Q_q^\lambda$.

In addition to the above linear-plus-Coulomb-type interaction, one can include spin–spin, spin–orbit, tenor, and the full Breit interaction to study the spectroscopy of hadrons, as carried out for a $q\bar{q}$ system for example in Refs. [140–142, 252]. Such an interaction will result in an open-string-type solution of the bound meson states.

It is of interest to examine the meson–meson polarization in a many-meson system, assuming that the bound state solutions for the quark and antiquark system within each meson have already been obtained. The task is to study the color-Coulomb and electric-Coulomb interaction between constituents of different mesons to see how such perturbative interactions may affect the dynamics of the many-meson system[9].

When we work with pions as a possible molecular component, we should keep in mind however that $\tilde{Q}_q^{\rm QCD}(\pi)=\tilde{Q}_{\bar{q}}^{\rm QCD}(\pi)=0$. That is, the effective color charge of a quark or an antiquark in a pion is zero, as discussed in Section 4.7 and in Table 2. This arises because of the cancellation of color charges for two-flavor isovector QCD $q\bar{q}$ composite particles. With the absence of the effective color charges, there is no reactionary response to the confining interaction in π^0. The confinement of the constituents of π^0 comes only from the quark condensate and quark masses m_q and $m_{\bar{q}}$ (see Section 4.4). There is consequently no color-polarization of the pion under the color-Coulomb interaction with neighboring color mesons. So, in our subsequent discussions on the color-polarization of QCD mesons, such a zero effective quark and antiquark color charges of a pion need to be kept in our mind. On the other hand, for the discussions in electric charges and electric-polarization in the QED interaction between mesons, pions contain effective electric charges, and can still be polarized by QED forces between mesons. So, pions can be included when we examine QCD–QED molecular states arising from the electric-Coulomb polarization between mesons.

7.4 Dipole–dipole interaction between neutral mesons

In a single neutral meson (color-neutral with $\lambda=1$ or electric-neutral with $\lambda=0$, as the case may be), the confining interaction between the quark and its antiquark causes the constituents to execute a yo–yo motion, whose classical trajectories for massless quarks are schematically depicted in Fig. 4. There will be no net static dipole moment for a composite neutral $q\bar{q}$ system.

We consider a system with N neutral mesons and study the long-range color-Coulomb or electric-Coulomb interaction between the constituents from different mesons as perturbations, starting with the $N=2$ system of two neutral mesons. Owing to the two composite systems carrying color and electric charges, the action of the long-range color-Coulomb and electric-Coulomb interactions will polarize the mesons [256]. As a conse-

[9] The linear interaction between constituents of different mesons are screened and can be included by assuming a screening length as is done in [256]. We shall not included them in the present survey.

quence, they acquire dynamical dipole moments, leading to a dipole–dipole interaction between the composite systems as discussed in detail by Peskin and Bhanot [253, 254]. Under appropriate conditions, the polarization can lead to meson molecular states as discussed previously in [256]. Among many other descriptions, meson molecular states have been studied experimentally and theoretically since the earlier works of Refs. [255–261], and in references cited in the recent works of Refs. [262–265].

A proper way to examine the meson polarization and meson molecular states in the N-meson system is to investigate each of the neighboring 2-meson pair as a four-body problem, with the interaction of the type in Eq. (85), and reduce the problem to a two-body bound state problem as discussed in [256]. It will also be necessary to take into account the antisymmetry of the quarks if they are identical. The problem can then be generalized from the 2-meson system to the case of the N-meson system.

Following Wheeler's First Moral Principle[10] [236], it is worth studying a simple massive dipole–dipole model before we carry out extensive calculations. We can gain new insight as to interesting geometrical configurations of the N-meson phase space where interesting physics may lie, to merit further considerations.

We consider in Fig. 13 a meson A with charges $\pm|q_A|$, and meson B with charges $\pm|q_B|$, which can be color or electric, static or dynamical, pure or mixed flavor, as the case may be. For each of the mesons A and B, we presume that their linear-plus Coulomb interactions of (85) lead to their individual known bound states. In the neighborhood of each other, they are subject to the polarization interaction from the long-range interaction of the constituents of other mesons as perturbations. As a consequence, the mesons acquires dynamical dipoles $\boldsymbol{d}_A = |q_A|\boldsymbol{a}_A$ and $\boldsymbol{d}_B = |q_B|\boldsymbol{a}_B$, respectively, where the dynamical dipole $\boldsymbol{d}_i$ is directed from $-|q_i|$ to $+|q_i|$. The potential generated by the dynamical dipole $\boldsymbol{d}_A$ at a radius vector $\boldsymbol{r}_{AB}$ from meson A to meson B is given by

$$V(\boldsymbol{r}_{AB}) = -\alpha \boldsymbol{d}_A \cdot \nabla(\frac{1}{r_{AB}}), \tag{86}$$

where $\alpha = (g^\lambda)^2/(4\pi)$. The interaction energy between dipoles $\boldsymbol{d}_A$ and $\boldsymbol{d}_B$ is

$$\begin{aligned} W =& (-|q_B|)V(\boldsymbol{r}_{AB} - \frac{\boldsymbol{a}_B}{2}) + |q_B|V(\boldsymbol{r}_{AB} + \frac{\boldsymbol{a}_B}{2}) \\ =& \alpha\left[\frac{\boldsymbol{d}_A \cdot \boldsymbol{d}_B}{r_{AB}^3} - 3\frac{(\boldsymbol{d}_A \cdot \boldsymbol{r}_{AB})(\boldsymbol{d}_B \cdot \boldsymbol{r}_{AB})}{r_{AB}^5}\right]. \end{aligned} \tag{87}$$

In terms of the angle θ_A between $\boldsymbol{d}_A$ and $\boldsymbol{r}_{AB}$, the angle θ_B between $\boldsymbol{d}_A$ and $\boldsymbol{r}_{AB}$, and the azimuthal angle ϕ_{AB} between $\boldsymbol{d}_A$ and $\boldsymbol{d}_B$, when we place $\boldsymbol{d}_A$ and $\boldsymbol{d}_B$ in the polar coordinate system with $\boldsymbol{r}_{AB}$ as the polar axis, [Figs. 13(a) and (b)], the interaction energy W between A and B is

$$\begin{aligned} &W(r_{AB}, \theta_A, \theta_B, \phi_{AB}) \\ &= \alpha\frac{d_A d_B}{(r_{AB})^3}\left(\sin\theta_A \sin\theta_B \cos\phi_{AB} - 2\cos\theta_A \cos\theta_B\right). \end{aligned} \tag{88}$$

For a fixed $\boldsymbol{r}_{AB}$, we can get the equilibrium configurations with respect to angular variations by taking the first and second derivatives with respect to θ_A, θ_B and ϕ_{AB}. Assuming that at the angular equilibrium, the dynamical dipole moments $\boldsymbol{d}_A$ and $\boldsymbol{d}_B$ are weak functions of the angles, we find that for a fixed $\boldsymbol{r}_{AB}$, there are two equilibrium configurations with respect to the angular variations:

1) The linear equilibrium configuration in which the dynamical dipoles are linearly aligned along the radius vector $\boldsymbol{r}_{AB}$ between A and B as in a linear array:

$$\theta_A = 0, \quad \theta_B = 0, \quad \phi_{AB} = \text{ignorable}. \tag{89}$$

The dipole configurations shown in Fig. 13(a), with a small θ_A and θ_B, approach the linear equilibrium configuration shown in Fig. 13(c).

2) The orthogonal equilibrium configuration in which the dynamical dipoles are orthogonal to the radius vector $\boldsymbol{r}_{AB}$ between mesons A and B, with opposing dynamical dipoles:

$$\theta_A = \frac{\pi}{2}, \quad \theta_B = \frac{\pi}{2}, \quad \phi_{AB} = \pi. \tag{90}$$

The dipole configurations shown in Fig. 13(b), with opposing dipoles orthogonal to the radius vector $\boldsymbol{r}_{AB}$, and θ_A and θ_B close to right angles, approach the orthogonal equilibrium configuration shown in Fig. 13(d).

These equilibrium configurations for a fixed $\boldsymbol{r}_{AB}$ can also be figured out by elementary physics arguments.

To obtain the molecular state of mesons A and B for a given linear or an orthogonal configuration, it is necessary to solve the bound state problem involving A and B as a two-body problem in the relative coordinate r_{AB}, with the reduced mass of the two mesons in the two body potential $W(r_{AB})$ [256]. The dipole-dipole interaction $W(r_{AB})$ at the equilibrium configurations are attractive at large separations r_{AB}, at which the dipole–dipole interactions are good approximations. However, at small r_{AB}, it is necessary to forgo the dipole approximation and study the Coulomb-plus-linear interaction as a four-body problem, as is done in Ref. [256], where the two-body potential for mesons A and B is found to be negative and contain a potential pocket. In the case of mesons containing constituents of identical particles, it is necessary to take into account the antisymmetry of these

[10] Wheeler's First Moral Principle states "'*Never make a calculation until you know the answer*'. Make an estimate before every calculation, try a simple physical argument before every derivation. Guess and answer to every puzzle. A right guess reinforces the instinct. A wrong answer brings the refreshment of surprises" [236].

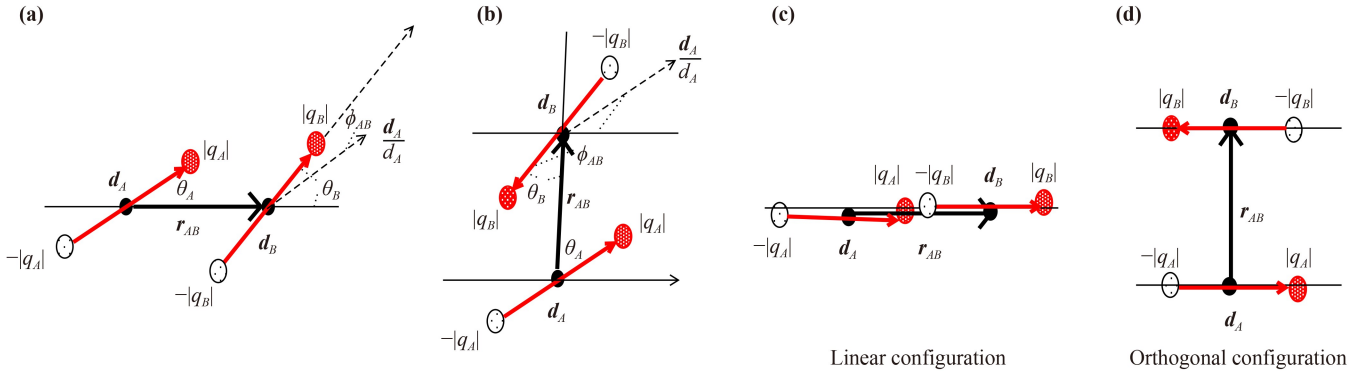

Fig. 13 The quark and antiquark configurations in the interaction between meson A and B with quark charges $\pm q_A$ and $\pm q_B$, respectively. The two mesons are separated by the radius vector $\boldsymbol{r}_{AB}$ from meson A to meson B. As a result of the long-range Coulomb interaction, mesons A and B acquire dynamical dipole moments $\boldsymbol{d}_A$ and $\boldsymbol{d}_B$, respectively. In **(a)** and **(b)**, θ_A is the angle between $\boldsymbol{d}_A$ and $\boldsymbol{r}_{AB}$, θ_B is the angle between $\boldsymbol{d}_B$ and $\boldsymbol{r}_{AB}$, and ϕ_{AB} is the azimuthal angle between $\boldsymbol{d}_A$ and $\boldsymbol{d}_B$ when we place $\boldsymbol{d}_A$ and $\boldsymbol{d}_B$ in the polar coordinates with $\boldsymbol{r}_{AB}$ as the polar axis. **(c)** and **(d)** are the linear and orthogonal equilibrium configurations with respect to angular variations at a fixed $\boldsymbol{r}_{AB}$.

constituents. The effects of antisymmetry is small when the mesons are far apart and thus such effects are not important for large r_{AB} when the dipole approximation can be approximately valid. At small r_{AB}, the antisymmetry gives rise to an effective repulsion between the mesons, and consequently a 6–12 type potential of $(a/r^{12} - b/r^6)$ with $a, b > 0$ containing a potential pocket. The potential obtained from these considerations will also be attractive at large distance and a potential pocket at short distances that will have bound meson molecular states in the limit of large meson mass.

Many QCD meson molecular states have been studied in Refs. [255–261] and in references cited in [262–265]. With QED obeying similar dynamics as the QCD mesons, there should be similar linear and orthogonal molecular states for a system of two or many QED mesons.

From the Bohr–Summerfeld quantization rule, the interaction potential such as the attractive $W(r_{AB})$ with a potential pocket would lead to a bound state if the action integral along the radial r_{AB} degree of freedom is equal to $2n\pi$. The condition for molecular bound states depends crucially on the reduced mass of the system, which depends in turn on the rest masses of the quarks. Bound molecular states will begin to appear, when the reduced mass exceeds a threshold. Quantitative calculations will need to be carried out to find out where the quark mass thresholds lie for the existence of the molecular QCD meson and QED meson states.

Given the large range of the quark masses of different flavors from a few MeV to hundreds of GeV, it is useful to consider a massive dipole–dipole model in the large mass limit such that the masses of interacting dipoles are assumed to exceed the threshold for bound molecular states, for systems with an attractive interaction potential $W(r_{AB})$ as a function of the dipole–dipole separation r_{AB}, with the mesons oriented at angles of angular equilibrium [such as the linear or the orthogonal equilibrium of Figs. 13(c) and (d)]. Our interest is to have an idea on the geometric configurations of the meson dipoles in the large mass limit so as to point to possible configurations that merit further analysis. Such a massive dipole–dipole model is not the ultimate definitive determination of stable configurations. On the other hand, the large range of quark masses ensure however that it is not just of academic interest. The model serves as a guide to interesting meson geometrical configurations that may be possible when the quark masses are large enough to exceed the mass threshold for molecular formation, and therefore worthy of further considerations with more rigorous analysis.

7.5 Interesting molecular configurations in the massive dipole–dipole model

We can consider N neutral mesons in the massive dipole–dipole model to explore different molecular configurations of interest. The mesons will interact with each other to lead to dynamical dipole moments, resulting in many different equilibrium configurations. The interactions are operative in the τ^0 and τ^1 color space, as the color charge densities generates color potentials while the electric charge densities generates electric potentials. The dipole–dipole interaction energy W of N mesons is given by

$$W(\{\boldsymbol{r}^\lambda_{i,j}\},\{\theta^\lambda_i\},\{\phi^\lambda_{i,j}\}) = \frac{1}{2}\sum_{\lambda=0}^{1}\sum_{i=1}^{N}\sum_{j=1,j\neq i}^{N}\left[\frac{\alpha_\lambda d^\lambda_i d^\lambda_j}{r^3_{ij}}(\sin\theta^\lambda_i \sin\theta^\lambda_j \cos\phi^\lambda_{i,j} - 2\cos\theta^\lambda_i \cos\theta^\lambda_j)\right]\tau^\lambda. \quad (91)$$

If we consider the approximation of only pairwise dipole–dipole interaction between neighboring dipoles, then the potential energy W of N mesons is given by

$$W(\{\boldsymbol{r}^{\lambda}_{i,i+1}\},\{\theta^{\lambda}_{i}\},\{\phi^{\lambda}_{i,i+1}\}) = \sum_{\lambda=0}^{1}\sum_{i=1}^{N}\left[\frac{\alpha_{\lambda} d^{\lambda}_{i} d^{\lambda}_{i+1}}{r^{3}_{i,i+1}}(\sin\theta^{\lambda}_{i}\sin\theta^{\lambda}_{i+1}\cos\phi^{\lambda}_{i,i+1} - 2\cos\theta^{\lambda}_{i}\cos\theta^{\lambda}_{i+1})\right]\tau^{\lambda}, \tag{92}$$

where in the case of a closed figure such as a polygon, the index $N+1$ reverts to be 1.

With the linear and the orthogonal equilibrium configurations, there can be many different configurations for a system of many neutral mesons (color-neutral or electric neutral, as the case may be). Some examples of the possible configurations of molecular states are depicted in Fig. 14.

One can build the linear chain as in Fig. 14(a), the orthogonal chain as in Fig. 14(b), the extension both longitudinally and transversely, as in Fig. 14(c), or turning in a right angle $\theta_1 = \pi/2$ at a corner, as in Fig. 14(d). By extending such chains and building up an orthogonal configuration into a third direction, it is possible to construct molecular states in three dimensions as in organic chemistry.

In addition to these linear and orthogonal configurations in two dimensions and perhaps also in three dimensions, there may be molecular polygon meson systems. There may be regular polygons if all the meson dipoles are the same, with $d_i = d$. There may also be irregular if some of the meson dipoles are different. We can consider the regular polygon as an simple illustration. Such regular polygon configurations arise in the massive dipole–dipole model because the interaction energy $W^{(N)}(r)$ as a function of the separation r between the nearest neighboring dipoles are always negative and attractive for $N \geq 2$. For example for $N = 3$, the molecular state in the form of a regular triangle as shown in Fig. 14(e) has an interaction energy

$$W^{(3)}(r) = -\frac{3}{4}\frac{d^2}{r^3}. \tag{93}$$

For $N = 4$, the molecular state in the form of a square as shown in Fig. 14(f) has the interaction energy

$$W^{(4)}(r) = \left(-9 - \frac{1}{\sqrt{2}}\right)\frac{d^2}{r^3}. \tag{94}$$

These interaction energies are always negative and attractive, and in the massive dipole–dipole model, a negative interaction energy with a potential pocket will lead to a bound state in the large mass limit. For the case of a polygon with N dipoles, the interaction energy from the contributions from the nearest neighboring dipoles is

$$\begin{aligned} &W^{(N)}(\text{all nearest neighboring pairs}) \\ &= \frac{N(N-1)}{2}\frac{d^2}{r^3}[1 - 5\cos^2(\frac{\pi}{N})], \end{aligned} \tag{95}$$

which is also always negative, and the contribution from next-to-next neighbors diminishes in strength. In the massive dipole–dipole model, such a negative interaction energy will lead to a stable bound molecular state of a polygon with N mesons in the massive dipole–dipole model.

It is interesting to take note the recent results on the stable $D^*D^*D^*$ triangular molecular state from a quantitative analysis in Ref. [265]. The $D^*D^*D^*$ triangular state for $N = 3$, together with the molecular state X(3872) for $N = 2$, may indicate that the molecular state mass threshold in the large mass limit of the dipole-dipole model may have been reached already with the charm quark mass. If this is the case, we should expect the massive dipole–dipole model to be approximately valid for other $N \geq 3$ cases for open charm mesons. Open charm mesons in the form of square, pentagon, hexagon, and higher polygons may be possible. Future experimental and theoretical research on these exotic open charm meson polygons will be of interest.

7.6 Molecular states with both QCD and QED mesons

The QCD and QED configurations in the massive dipole–dipole model considered in the last subsection deal with color-neutral QCD mesons or electric-neutral QED mesons by themselves in their respective τ^1 and τ^0 color subspace. In addition to these purely QCD and purely QED mesons, there may be molecular states in

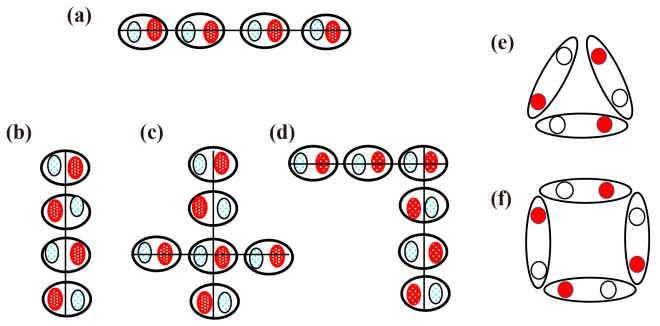

Fig. 14 Interesting configurations of QCD and QED neutral mesons in the massive dipole–dipole model that may merit further considerations. In these configurations, a meson is depicted with its positive charge constituent in a solid eclipse, and its negative charge constituent in an open eclipse. Examples shown here include: a linear chain in **(a)**, an orthogonal chain as in **(b)**, the extension both longitudinally and transversely in **(c)**, a linear chain turning in a right angle $\theta_1 = \pi/2$ in **(d)**, a triangle in **(e)**, and a square in **(f)**.

the τ^0 sector comprising of both QCD and QED mesons interacting the QED interaction in the massive dipole-dipole model.

In such a mixture of QCD and QED mesons, we can include both electric-neutral and charged QCD mesons. A charged QCD meson arises from a quark and an antiquark possessing electric charges of the same sign. For such a charged QCD meson, we assume that the forces leading to quark confinement in the QCD meson is dominated by the strong QCD interaction. Thus, even though there occurs a repulsive linear electric interaction between electric constituent charges of the same sign, such a QED electric-linear repulsion will be overwhelmed by the attractive QCD confining color-linear interaction between the quark and the antiquark and the confining force from the quark condensate. The QCD interaction is expected to lead to the confined QCD meson state. As a consequence, a charged QCD meson A with constituents q_A and $\bar{q}_A$ possesses a charge electric monopole with a net electric charge Q_A

$$Q_A = \frac{Q_{q_A} + Q_{\bar{q}_A}}{2}. \tag{96}$$

The charged meson also possesses electric dipole charges $\pm|Q_{q_A} + Q_{\bar{q}_A}|/2$ and a static electric dipole $\boldsymbol{d}_A(\text{static})$,

$$\boldsymbol{d}_A(\text{static}) = \frac{|Q_{q_A} + Q_{\bar{q}_A}|}{2}\boldsymbol{a}_A, \tag{97}$$

where $\boldsymbol{a}_A$ is the open-string length vector of meson A from the lesser-charged quark to the greater-charged quark of A. In the presence of neighboring mesons with electric dipole moments, the charged meson will also be polarized to acquire an additional dynamical dipole moment. While the quantitative magnitude of the total dipole moment needs to be worked out in detail, it suffice to consider here that the QCD meson possesses a total electric dipole vector sum $\boldsymbol{d}_A$ in its interaction with the neighboring QED meson. The effect of the electric monopole leads to an additional electric monopole-dipole interaction energy with a neighboring dipole $\boldsymbol{d}_B$, and the total electric interaction energy W is given by

$$W = \alpha_c\left[\frac{Q_A\boldsymbol{d}_B\cdot\boldsymbol{r}_{AB}}{r_{AB}^3} + \frac{\boldsymbol{d}_A\cdot\boldsymbol{d}_B}{r_{AB}^3} - 3\frac{(\boldsymbol{d}_A\cdot\boldsymbol{r}_{AB})(\boldsymbol{d}_B\cdot\boldsymbol{r}_{AB})}{r_{AB}^5}\right]. \tag{98}$$

With an additional monopole–dipole interaction, the orientation angles at the linear equilibrium configuration are unchanged. That is, they remain to be $\theta_A = \theta_B = 0$, with ignorable ϕ_{AB}. So, the linear molecular state configurations for mixed QCD and QED mesons are unchanged as in the case of neutral QCD and QED mesons. However, the orientation angles at the orthogonal equilibrium configuration are modified by the presence of the monopole-dipole interaction. For this reason, we shall not consider the orthogonal configuration in the present survey.

An interesting (QED meson)-(QCD quarkonium)-(QED meson) combination as depicted in Fig. 15(a). In such a configuration, the positive charge of the QCD quarkonium will attract a QED meson dipole pointing away from the quarkonium while the negative charge of the quarkonium will attract a QED dipole pointing into the heavy quarkonium. Such a chain of QED–QCD–QED mesons is a molecular state in the massive dipole-dipole model at large mass limit. Whether such a structure with the X17 or E38 as the QED meson have reduced masses exceeded the mass thresholds for the occurrence of molecular states will need to be worked out quantitatively in detail.

Other interesting combinations involve charged or neutral QCD and QED mesons as depicted in Figs. 15 (b)–(d). In the meson chain in (b)–(d), the QCD meson can be either neutral or charged with electric charge of the appropriate sign. These configurations are the equilibrium configurations in the massive dipole–dipole model.

Even though quarks in pions does not carry color charges because of the cancellation of their color charges in the isovector state, they carry electric charges. As a consequence, pion can be electrically polarized by other mesons and they in turn can polarize other mesons. The possible equilibrium configurations in Figs. 15(b)–(d) in the massive dipole–dipole model provides impetus to explore whether the π-(QED meson)–(QED meson)-π or the (QED meson)-π–π-(QED meson) molecules may be related to the perplexing ABC anomaly [75–80] and the R360 anomaly [53, 196]. If the molecular states can resolve these anomalies, they will provide additional support for the description of the anomalous X17 and E38 particles as QED mesons.

In exploring the molecular description of the ABC and R360 resonances, we need to estimate the masses in these linear QCD–QED meson molecules. In a molecular state of the type in Fig. 15, the molecular binding energy of the mesons would be of order of a few MeV (see for example the molecular state in Ref. [256]). So, the mass of the molecular states consisting of

$$\begin{aligned}&(\text{mass of molecular state})\\ &= \sum_i m_i - (\text{molecular binding energy}),\end{aligned} \tag{99}$$

where m_i are the mass of the meson i constituents of the molecular state. Within an error of the order of a few MeV, the mass of a molecular state is approximately

$$(\text{mass of a molecular state}) \approx \sum_i m_i. \tag{100}$$

We can use the above approximate molecular-state relation to estimate the masses of the molecular states in Figs. 15(b)–(d). If the QED mesons in these figures are the X17 particles each with a mass of 17 MeV, then the

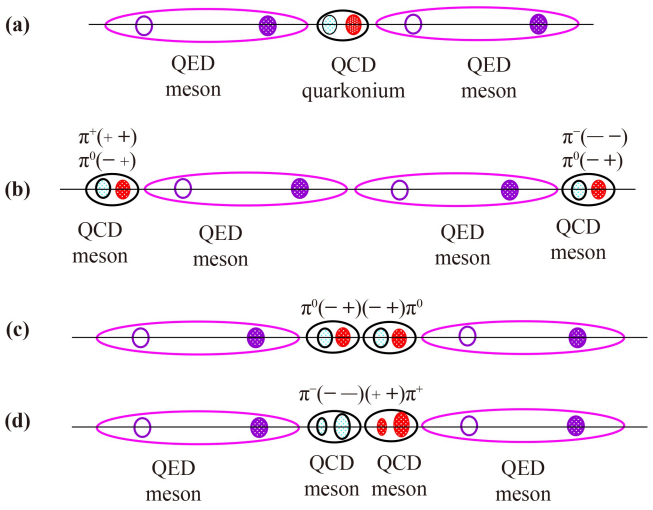

Fig. 15 Examples of interesting linear molecular configurations in the massive dipole–dipole model of QCD–QED mesons that may merit further considerations. In these configurations, a solid eclipse stands a positive charge and an open eclipse for a negative charge. Examples shown here include a linear chain for (QED meson)–(QCD quarkonium)–(QED meson) in **(a)**, the (QCD meson)–(QED meson)–(QED meson)–(QCD meson) in **(b)**, and the (QED meson)–(QCD meson)–(QCD meson)–(QED meson) in **(c)** and **(d)**. Pions as examples of the QCD mesons are indicated schematically.

masses in these linear QCD-QED meson molecules will be

$$\begin{aligned} &m_{\pi^+}+m(\mathrm{X17})+m(\mathrm{X17})+m_{\pi^-}=314\ \mathrm{MeV},\ \text{and}\\ &m_{\pi^0}+m(\mathrm{X17})+m(\mathrm{X17})+m_{\pi^0}=304\ \mathrm{MeV}, \end{aligned} \tag{101}$$

which fall within the energy of the ABC resonance at $M_{\mathrm{ABC}}=310$ MeV with a width of $\Gamma_{\mathrm{ABC}}=10$ MeV [75]. Other measurements gave the masses as $M_{\mathrm{ABC}}=316\pm 10$ MeV with a width $\Gamma_{\mathrm{ABC}}=55\pm10$ MeV in $d+p\rightarrow{}^3$He+ X collisions with a deuteron beam at 2.83 MeV at a scattering angle of 0.3^o of the fused ^{3}He [77]. Another measurement gives $M_{\mathrm{ABC}}=298\pm5$ MeV to 319 ± 8 MeV with a width from $\Gamma_{\mathrm{ABC}}=38\pm5$ MeV to $44+\pm9$ MeV [80]. There is thus an approximate relation

$$m(X17)\approx\frac{1}{2}(m_{\mathrm{ABC}}-2m_\pi). \tag{102}$$

If the QED mesons in Fig. 15(b) are E38 particles each with a mass of 38 MeV, then the masses in these linear QCD-QED meson molecules will be

$$\begin{aligned} &m_{\pi^+}+m(\mathrm{E38})+m(\mathrm{E38})+m_{\pi^-}=354\ \mathrm{MeV},\ \text{and}\\ &m_{\pi^0}+m(\mathrm{E38})+m(\mathrm{E38})+m_{\pi^0}=344\ \mathrm{MeV}, \end{aligned} \tag{103}$$

which fall within the energy of the R360 resonance of $M_{\mathrm{R360}}=360\pm7\pm9$ MeV with a width of $\Gamma_{\mathrm{R360}}=63.7\pm17.8$ MeV observed by Dubna [196]. The SACLAY group also observed similarly an anomalous resonance at $M_X=365\pm23$ MeV with a width of $\Gamma_{\mathrm{X}}=51\pm10$ MeV in the reaction of $d+p\rightarrow{}^3$He+ X for a deuteron beam at 3.82 MeV at a scattering angle of 0.3^o [77]. There is thus an approximate relation

$$m(E38)\approx\frac{1}{2}(m_{\mathrm{R360}}-2m_\pi). \tag{104}$$

Equations (102) and (104) relating the ABC and R360 resonances with the X17 and E38 resonances suggests that the proposed description of QED-confined mesons have the prospect of linking the five anomalies of (i) the anomalous soft photons, (ii) the X17 particle, (iii) the E38 particle, (iv) the ABC resonance, and (v) the R360 resonance in as single consistent QED meson framework.

As the masses of the configurations in Figs. 16(c) and (d) falling within the measured ABC and R360 resonances, it is thus worth exploring whether the molecular states may provide the appropriate descriptions for these two anomalous resonances. The ABC resonance is produced in nuclear collisions with the following characteristics occurring near the threshold of two pion production [75–80]:

1) the ABC resonance occurs at energies near but slightly beyond the threshold for two pion production (of 270–280 MeV) at $M_{\mathrm{ABC}}\sim310$ MeV with a relatively narrow width of order 50–60 MeV;

2) most likely observed in the forward and backward directions;

3) isoscalar nature of the $\pi\pi$(X) pair;

4) the occurrence of the ABC resonance is accompanied by the fusion of the colliding nuclei into a fused nuclear system [75–80] as in $d+p\rightarrow{}^3$He+X^0, $d+p\rightarrow{}^3$H+X$^+$ [75, 77], and $d+d\rightarrow{}^4$He+X^0 [78];

5) no occurrence of the ABC resonance when there is no fusion of the colliding nuclei, as in $pn\rightarrow pp\pi^0\pi^-$ and $pn\rightarrow pn\pi^0\pi^0$ even though the $d^*(2380)$ resonance appears in these reactions. Thus, the occurrence of the ABC resonance may be independent of the $d^*(2380)$ resonance [79].

We can attempt to interpret the molecular state description of the ABC and the R360 resonances by describing the possible production mechanism in the following way. The basic process may be the collision of a projectile nucleon p and a target nucleon n as depicted in Fig. 16, entering as a sub-process in the more complicated nuclear collisions. In such a $p+n$ collision, we may envisage the emission of a gluon from n at the vertex V and a gluon from p at the vertex V' as in Fig. 16. The fusion of the two gluons lead to a q_1 and $\bar{q}_2$ string which pull apart from each other. The fragmentation of the receding $q_1\bar{q}_2$ string in the inside-outside cascade picture of Bjorken, Casher, Kogut, and Susskind [83, 84] produces the pions and other particles, X_1,π_1,π_2,X_2, as depicted in Fig. 16. Because the produced particles arise by pulling the receding $q_1\bar{q}_2$ open string apart from the

colliding nucleons, the fragmentation process will be facilitated in the forward and backward direction of the colliding baryon system. Hence, the productions of the ABC and R360 resonances may be favored in the forward and backward directions.

The isospin properties and the parity of the X17 as an isoscalar particle and E38 particles as an isovector particle require that they must be produced in pairs in order to have the quantum number of the vacuum. The produced $\pi^0\pi^0$ or $\pi^+\pi^-$ pair can also form a coupled isoscalar, even-parity state in the QCD sector. The pair of X17 or E38 QED mesons can combine with two pions to form an isoscalar, even-parity object, depicted schematically in Fig. 16. The narrowness of the widths of the ABC and R360 resonances indicates that they may likely be molecular resonances with a weak binding and long-range interactions, with the mesons far separated. They may not likely be resonances from the exchange of the strong-interaction scalar QCD meson for which the width would be much greater.

The requirement that the ABC resonance must necessarily accompany the fusion reaction may perhaps be understood in terms of the color flow of the projectile and target nucleons in Fig. 16. The incident p and n are initially in a colorless color-single state. After p and n each emits a virtual gluon at V and V', the scattered nucleons p' and n' will be colored objects. With the produced $q\bar{q}$ open string materializing as the ABC resonance of the colorless molecular state of π-X17-X17-π, the process would not be observable if the scattered p' and n' remain as colored objects and cannot combine with other colored objects to form a colorless state. The scattered colored p' and n' can bleach their colors by exchanging a virtual gluon and fusing together into a colorless bound state of the fused nuclei. Hence, the fusion reaction always accompany the production of the molecular state of the ABC resonance. Such a fusion of the baryons and the fusion of the gluons with the subsequent production of the ABC resonance can take place in conjunction because they occur in different parts of the three-dimensional space.

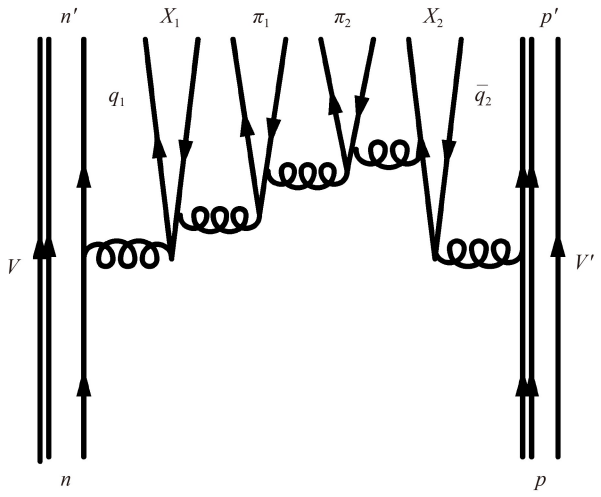

Fig. 16 The possible mechanism of the production of the molecule state π–(QED meson)–(QED meson)–π in the collision of n and p near the two-pion threshold by the fusion of two virtual gluons, with the subsequent string fragmentation of the q_1–$\bar{q}_2$ open string into the four mesons, X_1, π_1, π_2, X_2, near the $\pi\pi$ threshold.

It is interesting to note the similarity of the proposed mechanism for the production of the ABC resonance in Fig. 16 and the proposed mechanism for the production of the X17 particle in $p+{}^3\mathrm{H}_{\mathrm{ground\ state}}$ in Fig. 3(a), because the process of color bleaching leading to a fused nucleus are the same, as discussed in Section 2.

If the molecular states of π-X17-X17-π and π-E38-E38-π are proper descriptions of such resonances, we would expect that X17 particles may appear as decay products of the ABC resonance, and E38 particles may appear as decay products of the R360 resonance. A search for these particles accompanying the ABC resonance and the R360 resonance in these reactions in the forward and backward directions will be of interest. In this regard, it is interesting to note the possible mutual evidential support that reactions involved in the production of R360 are also the reactions where the E38 particle has been observed [53, 196]. Further research on these interesting suggestions with regard to the ABC and the R360 resonances will be of great interest.

7.7 Molecular states with baryons

The consideration of molecular mesons can be generalized to include the discussions on baryons when we approximate a baryon as a confined state of a quark and a diquark, with the diquark playing the role of an antiquark. In such a picture, a charged baryon possesses an electric monopole in addition to an electric dipole moment. The color and electric charges in the presence of neighboring mesons or baryons will be polarized and they will acquire additional dynamical dipole moments. Likewise, we need to consider both the dynamical color and electric polarization in the molecular states involving baryons. Because a baryon that carry an electric charge repel another baryon with electric charges of the same sign, molecular states with baryons would be favorable with a charged baryon with a neutral baryon or an antibaryon with a charge of opposite signs. In this regard, molecular states consisting of a baryon and an antibaryon opens a new degree of freedom to the construction of hadron molecular states as discussed in Ref. [264].

An example of particular interest is the $d^*(2380)$ resonance [266–269] that occur often with the ABC effect. Although a 6-quark description is possible [270] and chiral quark model [271, 272] is used to describe the baryon–baryon resonance, it can also be depicted equivalently as a molecular state of $\Delta^+[IJ = (1/2)(3/2)^+]$-

$\Delta^0[IJ = (1/2)(3/2)^0]$ state with a $D_{03}(I = 0, J^\pi = 3^+)$ dipole–dipole molecule. The molecular state binds its two Δ resonances by a binding energy of $E_{\text{binding}} = 2 \times 1232 - 2380 = 84$ MeV. Because of the molecular binding, the two Δ constituents lie below their rest mass energies, and as a result, the decay life time is lengthened with a narrower width of about 70 MeV, much smaller than the expected width of twice the Δ decay width of 110 MeV. They are formed in the collision of a proton and a neutron so that they can occur as a stretched configuration between the Δ^+ and Δ^0 predominantly in the forward and backward directions. It will be interesting to examine the molecular properties of the $d^*(2380)$, in addition to the other descriptions.

8 Conclusions and discussion

As advised by the late J. A. Wheeler on many occasions, "In the exploration on the new frontiers of physics, we make progress by walking on two legs, with one leg on firm grounds, and the other in a venturing spirit". On the question of quark confinement in QED, on firm grounds are (i) the non-isolation of quarks, (ii) a quark and its antiquark interaction in the QED interaction, and (iii) a quark and its antiquark are confined in the QED interaction in (1+1)D (Schwinger). In venturing spirit is the question whether they might be confined in the physical world of (3+1)D, when they interact in the QED interaction alone.

A prerequisite for asking such a question is to inquire whether there are experimental circumstances in which a $q\bar{q}$ pair may be produced and may interact in QED interaction alone. We find that in hadron–hadron, AA, e^+e^-, and e^-A collisions, there can be situations in which a quark and an antiquark may be produced with a center-of-mass energy below the pion mass gap m_π for collective QCD excitation, and the quark and its antiquark can interact non-perturbatively in the QED interaction alone.

It is well known that in the Schwinger confinement mechanism, massless fermions interacting in the Abelian QED gauge interactions in (1+1)D are confined for all strengths of the gauge interaction, as in an open string, leading to a confined and bound neutral boson with a mass proportional to the magnitude of the coupling constant.

Light quarks have masses of only a few MeV and they can be approximated as massless. A quark and an antiquark cannot be isolated, so they reside predominantly in (1+1)D. They can produced and interact in the QED interaction alone. The conditions under which the Schwinger confinement mechanism can be applicable are met when a light quark and a light antiquark are produced and interact with the QED interaction alone. Consequently, we can apply the Schwinger mechanism to quarks to conclude that a light quark and its antiquark are confined in the QED interaction in (1+1)D. The requirement of the massless condition for quarks is actually not as restrictive as it may appear to be because Coleman, Jackiw & Susskind [3] showed that the Schwinger confinement persist even when quarks are massive in (1+1)D. Therefore, a quark and its antiquark are confined in the QED interaction for all flavors and gauge interaction strength in (1+1)D.

On questions of quark confinement and $q\bar{q}$ QCD bound states, the non-Abelian QCD interaction can also be approximated as a quasi-Abelian interaction. As a consequence, the Schwinger confinement mechanism can be applied to quarks interacting in both the QED interaction and the QCD interaction, leading to confined $q\bar{q}$ pairs in QED and QCD open string states in (1+1)D, with the composite boson masses depending on the magnitudes of the QCD and QED coupling constants. Such a viewpoint is consistent with the QCD string description of hadrons in the Nambu [85] and Goto [85] string model, the string fragmentation models of particle production of Bjorken, Casher, Kogut, and Susskind [84, 123, 125–128], the Abelian projection model [88], and the Abelian dominance model [90, 91].

In a phenomenological analysis, we inquire whether an open string in the phenomenological open string model of QCD and QED $q\bar{q}$ systems in (1+1)D can be the idealization of a flux tube in (3+1)D and can show up as a bound and confined boson. In such a phenomenological open string model, we need an important relationship to ensure that the boson mass calculated in the lower (1+1)D can properly represent the mass of a physical boson in (3+1)D. The open string in (1+1)D can describe a physical meson in (3+1)D if the structure of the flux tube is properly taken into account. This can be achieved by relating the coupling constant in (1+1)D with the coupling constant in (3+1)D and the flux tube radius R_T [27, 32, 81, 82]. Using such a relationship, we find that that π^0, η, and η' can be adequately described as open string $q\bar{q}$ QCD mesons. By extrapolating into the $q\bar{q}$ QED sector in which a quark and an antiquark interact with the QED interaction, we find an open string isoscalar $I(J^\pi) = 0(0^-)$ QED meson state at 17.9 ± 1.5 MeV and an isovector $(I(J^\pi) = 1(0^-), I_3 = 0)$ QED meson state at 36.4 ± 3.8 MeV.

On the experimental front, it has been observed that anomalous soft photons with a transverse momentum of many tens of MeV/c are proportionally produced when hadrons are produced and are not produced when hadrons are not produced, indicating that the production of hadrons are always accompanied by the production of neutral particles with masses in the region of many tens of MeV/c^2. In search of axion with a mass of many tens of MeV, anomaly pointing to the production of an X17 particle with a mass of about 17 MeV has been observed in the decay of ^{4}He, ^{8}Be, and ^{12}C excited states. There have been also observation of the E38 particle at Dubna

with a mass of 38 MeV. The predicted masses of the isoscalar and isovector QED mesons in the open-string model of the QCD and QED mesons are close to the masses of the reported X17 and E38 particles observed recently, making them good candidates for these particles. Experimental confirmation of the reported X17 and the E38 particles in the same experimental setup will shed light on the question of quark confinement for quarks interacting in the Abelian $U(1)$ QED interaction.

On the theoretical front, there is a need for theoretical clarification on the question of confinement with regard to lattice gauge calculations. The lattice gauge calculations indicate that a static quark and a static antiquark interacting in the compact QED interaction will not be confined in (3+1)D. However, the deconfined solution for static quark and static antiquark in compact QED in (3+1)D in lattice gauge calculations contradicts the experimental absence of fractional charges. This indicates that the present lattice gauge calculations for compact QED in (3+1)D may not be complete and definitive, because the important Schwinger dynamical quark effects associated with light quarks has not been included.

We have constructed a "stretch (2+1)D" flux tube model to investigate the importance of the Schwinger mechanism on quark confinement in QED in (3+1)D [31] by utilizing the Polyakov's transverse confinement in conjunction with Schwinger's longitudinal confinement, We find that the stretch (2+1)D flux tube model leads to quark confinement in compact QED in (3+1)D [32]. Such a quark confinement result of the stretch (2+1)D flux tube model is consistent with the experimental absence of fractional charges. Furthermore, it gives predictions on the masses of neutral QED mesons and QED mesons in agreement with the experimental QCD and QED meson spectra. It is therefore worthy of further considerations. It is important to find out whether future lattice gauge calculations with dynamical light quarks, in a configuration such as the stretch (2+1) D flux tube configuration, will lead to confined quarks in compact QED in (3+1)D.

The success of the open-string description of the QCD and QED mesons leads to the search for other neutral quark systems stabilized by the QED interaction between the constituents in the color-singlet subgroup, with the color-octet QCD gauge interaction as a spectator field. Of particular interest is the QED neutron with the d, u, and d quarks [34]. They form a color product group of $\mathbf{3} \otimes \mathbf{3} \otimes \mathbf{3} = \mathbf{1} \oplus \mathbf{8} \oplus \mathbf{8} \oplus \mathbf{10}$, which contains a color singlet subgroup $\mathbf{1}$ where the color-singlet current and the color-singlet QED gauge field reside. In the color-singlet d–u–d system with three different colors, the attractive QED interaction between the u quark and the two d quarks overwhelms the repulsion between the two d quarks to stabilize the QED neutron at an estimated mass of 44.5 MeV. The analogous QED proton has been found theoretically to be unstable, and it does not provide a bound state nor a continuum state for the QED neutron to decay onto by way of the weak interaction. Hence the QED neutron may be stable against the weak interaction. It may have a very long lifetime and may be a good candidate for the dark matter. Because QED mesons and QED neutrons may arise from the coalescence of deconfined quarks during the deconfinement-to-confinement phrase transition in different environments such as in high-energy heavy-ion collisions, neutron-star mergers [227, 229], and neutron star cores [230], the search of the QED bound states in various environments will be of great interest.

It is necessary to address the question why the QCD mesons and the QCD neutron have not been observed to decay to the lower energy QED counterparts, even though the QCD hadrons lie higher in energy than those of the QED mesons and the QED neutron. The QCD meson and neutron and their analogous QED counterparts lie at different local energy minima in the configuration space. The QCD mesons have a flux tube radius of about 0.4 fm and a longitudinal length $L_{\rm QCD}$ of about a Fermi, as one can infer from the lattice gauge calculations and phenomenological considerations. For the QED meson, a flux tube radius about the same as that of the QCD meson appears to be a reasonable concept, because such a flux tube radius gives the QED meson masses in agreement with the observed X17 and E38 masses. The longitudinal lengths $L_{\rm QED}$ of the QED mesons are an order of magnitude greater than those of the QCD mesons [34]. The QCD mesons and their analogous QED meson have different local energy minima in the longitudinal length space L. In between the two energy minima, there is a barrier between the QCD meson and the analogous QED counterpart. To make a transition from a QCD meson energy minimum at $L_{\rm QCD}$ so as to come to the region of the analogous QED meson in the local energy minimum at $L_{\rm QED}$, the QCD meson needs to tunnel under a barrier from $L_{\rm QCD}$ to $L_{\rm QED}$ with a barrier height of order $(L_{\rm QCD} - L_{\rm QED}) \times 1$ GeV/fm, where 1 GeV/fm is the magnitude of the QCD string tension coefficient. This gives a barrier height of order 10 GeV. Such a high barrier makes the transition probability prohibitively small. Similarly, a QCD neutron has a spatial length scale of order 1 fm, whereas the QED neutron has a spatial length scale of order 20–30 fm [34]. They lie in different local energy minima in the length scale space L. The high barrier between the QCD neutron energy minimum and the QED neutron energy minimum makes the transition probability prohibitively small.

Experimentally, in the environment in which a pair of color-singlet quark and an antiquark are produced, such as by the fusion of two virtual photons or two virtual gluons at the eigenenergy of a QED meson (e.g., 17 or 38 MeV, with the proper quantum numbers), as shown in Figs. 1, 2 and 3, the color-singlet q and $\bar{q}$ pair created at a local point will expand to the full longitudinal extension to become a QED meson and will carry out a

longitudinal yo–yo motion appropriate for the QED meson eigenstate, as described in Fig. 12 and in Ref. [34]. Similarly, in the surface region of a quark–gluon plasma during the confinement-to-deconfinement phase transition in high-energy heavy-ion collisions, deconfined u and d quarks with low energies may search for partners to form a low-energy d–u–d bound state. A color-singlet combination of low-energy u and d quarks may form a d–u–d QED neutron eigenstate by their mutual QED interactions, if these quarks posses the proper eigenenergy. A search for the QED neutron in high-energy heavy-ion collisions may be of great interest.

Acknowledgements The author is indebted to Prof. V. F. Perepelitsa whose talk at the International Symposium on Multiparticle Dynamics, in 2009 introduced the author to the subject of anomalous soft photons which raised author's interest on the question of quark confinement in the QED interaction. The author would like to thank Profs. Y. Jack Ng, A. Koshelkin, H. Sazdjian, Soren Sorensen, D. Blaschke, Kh. U. Abraamyan, Gang Wang, Xi-Guang Cao, G. Wilk, Y. Sharon, L. Zamick, and I-Yang Lee for helpful communications. The research was supported in part by the Division of Nuclear Physics, U.S. Department of Energy under Contract No. DE-AC05-00OR22725 with UT-Battelle, LLC.

References and notes

1. J. Schwinger, Gauge invariance and mass II, *Phys. Rev.* 128(5), 2425 (1962)
2. J. Schwinger, Gauge theory of vector particles, in: Theoretical Physics, Trieste Lectures, 1962 (IAEA, Vienna, 1963), page 89
3. S. Coleman, R. Jackiw, and L. Susskind, Charge shielding and quark confinement in the massive Schwinger model, *Ann. Phys.* 93(1–2), 267 (1975)
4. S. Coleman, More about the massive Schwinger model, *Ann. Phys.* 101(1), 239 (1976)
5. A. M. Polyakov, Quark confinement and topology of gauge theories, *Nucl. Phys. B* 120(3), 429 (1977)
6. A. M. Polyakov, Gauge Fields and Strings, Hardwood Academic Publishers, Switzerland, 1987
7. K. G. Wilson, Confinement of quarks, *Phys. Rev. D* 10(8), 2445 (1974)
8. J. Kogut and L. Susskind, Hamiltonian formulation of Wilson's lattice gauge theories, *Phys. Rev. D* 11(2), 395 (1975)
9. S. Mandelstam, Vortices and quark confinement in non-Abelian gauge theories, *Phys. Lett. B* 53(5), 476 (1975)
10. T. Banks, B. Myerson, and J. Kogut, Phase transitions in Abelian lattice gauge theories, *Nucl. Phys. B* 129(3), 493 (1977)
11. J. Glimm and A. Jaffe, Instantons in a $U(1)$ lattice gauge theory: A Coulomb dipole gas, *Commun. Math. Phys.* 56(3), 195 (1977)
12. M. E. Peskin, Mandelstam–'t Hooft duality in Abelian lattice models, *Ann. Phys.* 113(1), 122 (1978)
13. A. Guth, Existence proof of a nonconfining phase in four-dimensional $U(1)$ lattice gauge theory, *Phys. Rev. D* 21(8), 2291 (1980)
14. K. I. Kondo, Existence of confinement phase in quantum electrodynamics, *Phys. Rev. D* 58(8), 085013 (1998)
15. G. Magnifico, T. Felser, P. Silvi, and S. Montangero, Lattice quantum electrodynamics in (3+1)-dimensions at finite density with tensor networks, *Nat. Commun.* 12(1), 3600 (2021), arXiv: 2011.10658
16. S. D. Drell, H. R. Quinn, B. Svetitsky, and M. Weinstein, Quantum electrodynamics on a lattice: A Hamiltonian variational approach to the physics of the weak-coupling region, *Phys. Rev. D* 19(2), 619 (1979)
17. G. Arnold, B. Bunk, T. Lippert, and K. Schilling, Compact QED under scrutiny: It's first order, *Nucl. Phys. B Proc. Suppl.* 119, 864 (2003), arXiv: hep-lat/0210010
18. L. C. Loveridge, O. Oliveira, and P. J. Silva, Lattice pure gauge compact QED in the Landau gauge: The photon propagator, the phase structure, and the presence of Dirac strings, *Phys. Rev. D* 104(11), 114511 (2021), and references cited therein
19. J. Schwinger, On Gauge Invariance and Vacuum Polarization, *Phys. Rev.* 82(5), 664 (1951)
20. C. Y. Wong, Introduction to High-Energy Heavy-Ion Collisions, World Scientific Publisher, 1994
21. H. Georgi, The Schwinger point, *J. High Energy Phys.* 11, 057 (2019), arXiv: 1905.09632
22. H. Georgi and B. Noether, Non-perturbative effects and unparticle physics in generalized Schwinger models, arXiv: 1908.03279v3 (2019)
23. H. Georgi and B. Warner, Generalizations of the Sommerfield and Schwinger models, *J. High Energy Phys.* 01, 047 (2020), arXiv: 1907.12705v2
24. H. Georgi, Automatic fine-tuning in the two-flavor Schwinger model, *Phys. Rev. Lett.* 125(18), 181601 (2020), arXiv: 2007.15965
25. H. Georgi, Mass perturbation theory in the 2-flavor Schwinger Model with opposite masses, *J. High Energy Phys.* 2022(10), 119 (2022), arXiv: 2206.14691
26. R. Dempsey, I. R. Klebanov, S. S. Pufu, and B. Zan, Discrete chiral symmetry and mass shift in lattice Hamiltonian approach to Schwinger model, arXiv: 2206.05308 (2022)
27. C. Y. Wong, Anomalous soft photons in hadron production, *Phys. Rev. C* 81(6), 064903 (2010), arXiv: 1001.1691
28. C. Y. Wong, Anomalous soft photons associated with hadron production in string fragmentation, Talk presented at the IX International Conference on Quark Confinement and Hadron Spectrum, Madrid, Spain, Aug. 30–Sep. 3, 2010, *AIP Conf. Proc.* 1343, 447 (2011), arXiv: 1011.6265
29. C. Y. Wong, An overview of the anomalous soft photons in hadron production, Talk presented at International Conference on the Structure and the Interactions of the Photon, 20–24 May 2013, Paris, France, *PoS Photon* 2013, 002 (2014), arXiv: 1404.0040
30. C. Y. Wong, Open string QED meson description of the X17 particle and dark matter, *J. High Energy Phys.* 2020(8), 165 (2020), arXiv: 2001.04864
31. C. Y. Wong, On the stability of the open-string QED neutron and dark matter, *Europhys. J. A* 58, 100

(2022), arXiv: 2010.13948
32. C. Y. Wong, QED mesons, the QED neutron, and the dark matter, in: Proceedings of the 19th International Conference on Strangeness in Quark Matter, *EPJ Web Confer.* 259, 13016 (2022), arXiv: 2108.00959
33. C. Y. Wong, QED meson description of the X17 and other anomalous particles, in: Proceedings of the Workshop of "Shedding Light on X17", September 6–8, 2021, Centro Ricerche Enrico Fermi, Rome, Italy, arXiv: 2201.09764
34. C. Y. Wong and A. Koshelkin, Dynamics of quarks and gauge fields in the lowest-energy states in QCD and QED, arXiv: 2111.14933 (2021)
35. A. Koshelkin and C. Y. Wong, Dynamics of quarks and gauge fields in the lowest-energy states in QCD and QED, in Proceedings of the 41st International Conference in High Energy Physics, 6–13 July, 2022, Bologna, Italy, *PoS* 414, 302 (2022), arXiv: 2212.11749
36. P. V. Chliapnikov, E. A. De Wolf, A. B. Fenyuk, L. N. Gerdyukov, Y. Goldschmidt-Clermont, V. M. Ronjin, and A. Weigend, Observation of direct soft photon production in π^-p interactions at 280 GeV/c, *Phys. Lett. B* 141(3–4), 276 (1984)
37. F. Botterweck, et al. (EHS-NA22 Collaboration), Direct soft photon production in K^+p and π^+p interactions at 250 GeV/c, *Z. Phys. Chem.* 51, 541 (1991)
38. S. Banerjee, et al. (SOPHIE/WA83 Collaboration), Observation of direct soft photon production in π^-p interactions at 280 GeV/c, *Phys. Lett. B* 305(1–2), 182 (1993)
39. A. Belogianni, W. Beusch, T. J. Brodbeck, D. Evans, B. R. French, A. Jacholkowski, J. B. Kinson, A. Kirk, V. Lenti, R. A. Loconsole, V. Manzari, I. Minashvili, V. Perepelitsa, N. Russakovich, P. Sonderegger, M. Spyropoulou-Stassinaki, G. Tchlatchidze, G. Vassiliadis, I. Vichou, and O. Villalobos-Baillie (WA91 Collaboration), Confirmation of a soft photon signal in excess of QED expectations in π^-p interactions at 280 GeV/c, *Phys. Lett. B* 408(1–4), 487 (1997)
40. A. Belogianni, et al. (WA102 Collaboration), Further analysis of a direct soft photon excess in π^-p interactions at 280-GeV/c, *Phys. Lett. B* 548(3–4), 122 (2002)
41. A. Belogianni, W. Beusch, T. J. Brodbeck, F. S. Dzheparov, B. R. French, P. Ganoti, J. B. Kinson, A. Kirk, V. Lenti, I. Minashvili, V. F. Perepelitsa, N. Russakovich, A. V. Singovsky, P. Sonderegger, M. Spyropoulou-Stassinaki, and O. Villalobos Baillie (WA102 Collaboration), Observation of a soft photon signal in excess of QED expectations in pp interactions, *Phys. Lett. B* 548(3–4), 129 (2002)
42. V. Perepelitsa, Anomalous soft photons in hadronic decays of Z^0, Proceedings of the XXXIX International Symposium on Multiparticle Dynamics, Gomel, Belarus, September 4–9, 2009, published in: *Nonlin. Phenom. Complex Syst.* 12, 343 (2009)
43. J. Abdallah, et al. (DELPHI Collaboration), Evidence for an excess of soft photons in hadronic decays of Z^0, *Eur. Phys. J. C* 47(2), 273 (2006), arXiv: hep-ex/0604038
44. J. Abdallah, et al. (DELPHI Collaboration), Observation of the muon inner bremsstrahlung at LEP1, *Eur. Phys. J. C* 57(3), 499 (2008)
45. J. Abdallah, et al. (DELPHI Collaboration), Study of the dependence of direct soft photon production on the jet characteristics in hadronic Z^0 decays, *Eur. Phys. J. C* 67(3–4), 343 (2010)
46. A. J. Krasznahorkay, M. Csatlós, L. Csige, Z. Gácsi, J. Gulyás, M. Hunyadi, I. Kuti, B. M. Nyakó, L. Stuhl, J. Timár, T. G. Tornyi, Z. Vajta, T. J. Ketel, and A. Krasznahorkay, Observation of anomalous internal pair creation in ^{8}Be: A possible indication of a light, neutral boson, *Phys. Rev. Lett.* 116(4), 042501 (2016), arXiv: 1504.01527
47. A. J. Krasznahorkay, et al., New evidence supporting the existence of the hypothetical X17 particle, arXiv: 1910.10459 (2019)
48. A. J. Krasznahorkay, M. Csatlós, L. Csige, J. Gulyás, A. Krasznahorkay, B. M. Nyakó, I. Rajta, J. Timár, I. Vajda, and N. J. Sas, New anomaly observed in ^{4}He supports the existence of the hypothetical X17 particle, *Phys. Rev. C* 104(4), 044003 (2021), arXiv: 2104.10075
49. A. J. Krasznahorkay, et al., X17: Staus and experiments on ^{8}Be and ^{4}He, presented at the Workshop of "Shedding Light on X17", September 6–8, 2021, Centro Ricerche Enrico Fermi, Rome, Italy
50. N. J. Sas, A. J. Krasznahorkay, M. Csatlós, J. Gulyás, B. Kertész, A. Krasznahorkay, J. Molnár, I. Rajta, J. Timár, I. Vajda, and M. N. Harakeh, Observation of the X17 anomaly in the ^{7}Li(p, e^+e^-)^{8}Be direct proton-capture reaction, arXiv: 2205.07744 (2022)
51. A. J. Krasznahorkay, et al., New anomaly observed in ^{12}C supports the existence and the vector character of the hypothetical X17 boson, arXiv: 2209.10795 (2022)
52. K. Abraamyan, A. B. Anisimov, M. I. Baznat, K. K. Gudima, M. A. Nazarenko, S. G. Reznikov, and A. S. Sorin, Observation of the $E(38)$-boson, arXiv: 1208.3829v1 (2012)
53. K. Abraamyan, C. Austin, M. Baznat, K. Gudima, M. Kozhin, S. Reznikov, and A. Sorin, Check of the structure in photon pairs spectra at the invariant mass of about 38 MeV/c^2, *EPJ Web of Conferences* 204, 08004 (2019)
54. Proceedings of the Workshop on "Shedding Light on X17", September 6–8, 2021, Centro Ricerche Enrico Fermi, Rome, Italy; Eds.: M. Raggi, P. Valente, M. Nardecchia, A. Frankenthal, G. Cavoto, published in: D. S. M. Alves, et al., *Eur. Phys. J. C* 83, 230 (2023)
55. A. J. Krasznahorkay (for the ATOMKI Collaboration), X17: Status of the experiments on ^{8}Be and ^{4}He, Talk presented at the Workshop on "Shedding Light on X17", September 6, 2021, Rome, Italy, in Ref. [54]
56. Kh. U. Abraamyan, Ch. Austin, M. I. Baznat, K. K. Gudima, M. A. Kozhin, S. G. Reznikov, and A. S. Sorin (Dubna Collaboration), Private communications
57. Y. S. Cheng, H. Z. Huang, and G. Wang (STAR Collaboration), Private communications
58. A. Papa (for the MEGII Collaboration), X17 search with the MEGII apparatus, Talk presented at the Workshop on "Shedding Light on X17", September 6, 2021, Rome, Italy, in Ref. [54]
59. H. N. da Luz (for the TU Prague Collaboration), Measurements of internal pair creation with a time projection chamber-based setup, Talk presented at the Workshop on "Shedding Light on X17", September 6,

2021, Rome, Italy, in Ref. [54]
60. C. Gustavino (for the nTOF Collaboration), The search for 4 He anomaly at n_TOF experiment, Talk presented at the Workshop on "Shedding Light on X17", September 6, 2021, Rome, Italy, in Ref. [54]
61. E. Depero (for the NA64 Collaboration), X17 in the NA64 experiment, Talk presented at the Workshop on "Shedding Light on X17", September 6, 2021, Rome, Italy, in Ref. [54]
62. L. Darmé, M. Raggi, and E. Nardi, (for the INFNRome Collabration), X17 production mechanism at accelerators, Talk presented at the Workshop on "Shedding Light on X17", September 6, 2021, Rome, Italy, in Ref. [54]
63. E. Goudzovski (for the NA48 Collaboration), Search for dark photon in π^0 decays by NA48/2 at CERN, Talk presented at the Workshop on "Shedding Light on X17", September 6, 2021, Rome, Italy, in Ref. [54]
64. A. K. Perrevoort (for the Mu3e Collaboration), Prospects for Dark Photon Searches in the Mu3e Experiment, Talk presented at the Workshop on "Shedding Light on X17", September 6, 2021, Rome, Italy, in Ref. [54]
65. L. Doria (for the MAGIX Collaboration), Dark Matter and X17 Searches at MESA 4.4. 2 Light Dark Matter, Talk presented at the Workshop on "Shedding Light on X17", September 6, 2021, Rome, Italy, in Ref. [54]
66. A. Gasparian (for the JLAB-PAC50 Collaboration), A Direct Detection Search for Hidden Sector New Particles in the 3–60 MeV Mass Range, Talk presented at the Workshop on "Shedding Light on X17", September 6, 2021, Rome, Italy, in Ref. [54]
67. A. Ahmidouch, et al. (for the JLAB-PAC50 Collaboration), A Direct Detection Search for Hidden Sector New Particles in the 3–60 MeV Mass Range, arXiv: 2108.13276 (2021)
68. V. Kozhuharov (for the PADME Collaboration), Searching X17 with positrons at PADME, Talk presented at the Workshop on "Shedding Light on X17", September 6, 2021, Rome, Italy, in Ref. [54]
69. E. Cline, et al. (for the DarkLight Collaboration), Searching for New Physics with DarkLight at the ARIEL Electron-Linac, arXiv: 2208.04120 (2022)
70. P. Navrátil, ARIEL experiments and theory, arXiv: 2210.08438 (2022)
71. S. Huang (for the LUXE Collaboration), Probing new physics at the LUXE experiment, Proceedings of 41st International Conference on High Energy physics - ICHEP2022, 6–13 July, 2022, arXiv: 2211.11045
72. G. Azuelos, D. Bryman, W. C. Chen, H. de Luz, L. Doria, A. Gupta, L. A. Hamel, M. Laurin, K. Leach, G. Lefebvre, J. P. Martin, A. Robinson, N. Starinski, R. Sykora, D. Tiwari, U. Wichoski, and V. Zacek, Status of the X17 search in Montreal, *J. Phys. Conf. Ser.* 2391(1), 012008 (2022)
73. M. Gell-Mann, The interpretation of the new particles as displaced charge multiplets, *Nuovo Cim.* 4(S2), 848 (1956)
74. M. Tanabashi, et al. (Particle Data Group), Review of particle physics, *Phys. Rev. D* 98, 030001 (2019)
75. A. Abashian, N. E. Booth, and K. M. Crowe, Possible anomaly in meson production in $p+d$ collisions, *Phys. Rev. Lett.* 5(6), 258 (1960)
76. N. E. Booth, A. Abashian, and K. M. Crowe, Anomaly in meson production in $p+d$ collisions, *Phys. Rev. Lett.* 7(1), 35 (1961)
77. J. Banaigs, J. Berger, L. Goldzahl, T. Risser, L. Vu-Hai, M. Cottereau, and C. Le Brun, "ABC" and "DEF" effects in the reaction $d + p \to \mathrm{He}^3 + (mm)^0$: Position, width, isospin, angular and energy distributions, *Nucl. Phys. B* 67(1), 1 (1973)
78. P. Adlarson, et al., Abashian–Booth–Crowe effect in basic double-pionic fusion: A new resonance? *Phys. Rev. Lett.* 106(24), 242302 (2011)
79. M. Bashkanov, H. Clement, and T. Skorodko, Examination of the nature of the ABC effect, *Nucl. Phys. A* 958, 129 (2017)
80. V. I. Komarov, et al., Resonance-like coherent production of a pion pair in the reaction $pd\to pd\pi\pi$ in the GeV region, *Eur. Phys. J. A* 54, 206 (2018), arXiv: 1805.01493
81. C. Y. Wong, The Wigner function of produced particles in string fragmentation, *Phys. Rev. C* 80(5), 054917 (2009)
82. A. V. Koshelkin and C. Y. Wong, The compactification of QCD4 to QCD2 in a flux tube, *Phys. Rev. D* 86(12), 125026 (2012), arXiv: 1212.3301
83. J. D. Bjorken, Lectures presented in the 1973 Proceedings of the Summer Institute on Particle Physics, edited by Zipt, SLAC-167 (1973)
84. A. Casher, J. Kogut, and L. Susskind, Vacuum polarization and the absence of free quarks, *Phys. Rev. D* 10(2), 732 (1974)
85. Y. Nambu, Quark model of the factorization of the Veneziano Amplitude, in Lectures at the Copenhagen Symposium: Symmetry and Quark Models, edited by R. Chand, Gordon and Breach, 1970, page 269
86. Y. Nambu, Strings, monopoles, and gauge fields, *Phys. Rev. D* 10(12), 4262 (1974)
87. T. Goto, Relativistic quantum mechanics of one-dimensional mechanical continuum and subsidiary condition of dual resonance model, *Prog. Theor. Phys*, 46, 1560 (1971), arXiv: hep-th/9302104
88. G. 't Hooft, Topology of the gauge condition and new confinement phases in non-Abelian gauge theories, *Nucl. Phys. B* 190(3), 455 (1981)
89. L. V. Belvedere, J. A. Swieca, K. D. Rothe, and B. Schroer, Generlaized two-dimensional Abelian gauge theories and confinement, *Nucl. Phys. B* 153, 112 (1979)
90. T. Sekido, K. Ishiguro, Y. Koma, Y. Mori, and T. Suzuki, Abelian dominance and the dual Meissner effect in local unitary gauges in $SU(2)$ gluodynamics, *Phys. Rev. C* 75, 064906 (2007), arXiv: hep-ph/0703002
91. T. Suzuki, K. Ishiguro, Y. Koma, and T. Sekido, Gauge-independent Abelian mechanism of color confinement in gluodynamics, *Phys. Rev. D* 77, 034502 (2008), arXiv: 0706.4366
92. H. Suganuma and H. Ohata Local correlation among the chiral condensate, monopoles, and color magnetic fields in Abelian projected QCD, arXiv: 2108.08499 (2021)

93. G. 't Hooft, A planar diagram theory for strong interactions, *Nucl. Phys. B* 72(3), 461 (1974)
94. G. 't Hooft, A two-dimensional model for mesons, *Nucl. Phys. B* 75(3), 461 (1974)
95. S. Huang, J. W. Negele, and J. Polonyi, Meson structure in QCD2, *Nucl. Phys. B* 307(4), 669 (1988)
96. G. S. Bali, H. Neff, T. Duessel, T. Lippert, and K. Schilling (SESAM), Observing long colour flux tubes in $SU(2)$ lattice gauge theory, *Phys. Rev. D* 71, 114513 (2005)
97. L. Cosmai, P. Cea, F. Cuteri, and A. Papa, Flux tubes in QCD with (2+1) HISQ fermions, Pos, 4th annual International Symposium on Lattice Field Theory, 24–30 July 2016, University of Southampton, UK, arXiv: 1701.03371 (2017)
98. N. Cardoso, M. Cardoso, and P. Bicudo, Inside the $SU(3)$ quark–antiquark QCD flux tube: Screening versus quantum widening, *Phys. Rev. D* 88, 054504 (2013), arXiv: 1302.3633
99. P. Bicudo and N. Cardoso, Colour field densities of the quark–antiquark excited flux tubes in $SU(3)$ lattice QCD, *Phys. Rev. D* 98 (2018) 11, 114507, arXiv: 1808.08815
100. P. Bicudo, N. Cardoso, and M. Cardoso, Pure gauge QCD flux tubes and their widths at finite temperature, *Nucl. Phys. B* 940, 88 (2019), arXiv: 1702.03454
101. M. E. Peskin and D. V. Schroeder, An Introduction to Quantum Field Theory, Addison-Wesley Publishing Company, 1995
102. M. B. Halpern, Quantum "solitons" which are $SU(N)$ fermions, *Phys. Rev. D* 12(6), 1684 (1975)
103. J. Kogut and L. Susskind, Quark confinement and the puzzle of the ninth axial-vector current, *Phys. Rev. D* 10(10), 3468 (1974)
104. J. Kogut and L. Susskind, How quark confinement solve the $\eta \to 3\pi$ problem, *Phys. Rev. D* 11(12), 3594 (1975)
105. J. Kogut and D. K. Sinclair, Quark Confinement and the evasion of the Goldestone's theorem in 1 + 1 dimensions, *Phys. Rev. D* 12(6), 1742 (1975)
106. E. Witten, Non-Abelian bosonization in two dimensions, *Commun. Math. Phys.* 92(4), 455 (1984)
107. D. Gepner, Non-abelian bosonization and multiflavor QED and QCD in two dimensions, *Nucl. Phys. B* 252, 481 (1985)
108. J. Ellis, Y. Frishman, A. Hanany, and M. Karliner, Quark solitons as constituents of hadrons, *Nucl. Phys. B* 382(2), 189 (1992)
109. Y. Frishman and J. Sonnenschein, Bosonization and QCD in two dimensions, *Phys. Rep.* 223(6), 309 (1993)
110. Y. Frishman, A. Hanany, and J. Sonnenschein, Subtleties in QCD theory in two dimensions, *Nucl. Phys. B* 429(1), 75 (1994)
111. A. Armoni and J. Sonnenschein, Mesonic spectra of bosonized QCD2 models, *Nucl. Phys. B* 457(1–2), 81 (1995)
112. A. Armoni, Y. Frishman, J. Sonnenschein, and U. Trittmann, The spectrum of multi-flavor QCD2 and the non-Abelian Schwinger equation, *Nucl. Phys. B* 537(1–3), 503 (1999)
113. A. Abrashkin, Y. Frishman, and J. Sonnenschein, The spectrum of states with one current acting on the adjoint vacuum of massless, *Nucl. Phys. B* 703(1–2), 320 (2004)
114. D. J. Gross, I. R. Klebanov, A. V. Matytsin, and A. V. Smilga, Screening vs. confinement in 1+1 dimensions, *Nucl. Phys. B* 461(1–2), 109 (1996), arXiv: hep-th/9511104
115. J. P. Vary, T. J. Fields, and H. J. Pirner, Chiral perturbation theory in the Schwinger model, *Phys. Rev. D* 53(12), 7231 (1996)
116. Y. Hosotani and R. Rodriguez, Bosonized massive N-flavour Schwinger model, *J. Phys. Math. Gen.* 31(49), 9925 (1998)
117. E. Abdalla, M. C. B. Abdalla, and K. D. Rothe, Two Dimensional Quantum Field Theory, World Scientific Publishing Company, Singapore, 2001
118. S. Nagy, Massless fermions in mutiflavor QED, *Phys. Rev. D* 79(4), 045004 (2009)
119. J. Kovács, S. Nagy, I. Nandori, and K. Sailer, Renormalization of QCD2, *J. High Energy Phys.* 2011(1), 126 (2011)
120. S. Weinberg, Phenomenological Lagrangians, *Physica A* 96(1–2), 327 (1979)
121. E. Witten, Current algebra theorems for the $U(1)$ Goldstone boson, *Nucl. Phys. B* 156(2), 269 (1979)
122. G. Veneziano, Construction of a crossing-simmetric, Regge-behaved amplitude for linearly rising trajectories, *Nuovo Cim. A* 57(1), 190 (1968)
123. X. Artru and G. Mennessier, String model and multiproduction, *Nucl. Phys. B* 70(1), 93 (1974)
124. A. M. Polyakov, Quantum geometry of bosonic strings, *Phys. Lett. B* 103(3), 207 (1981)
125. B. Andersson, G. Gustafson, and T. Sjöstrand, A general model for jet fragmentation, *Zeit. für Phys. C* 20, 317 (1983)
126. B. Andersson, G. Gustafson, G. Ingelman, and T. Sjöstrand, Parton fragmentation and string dynamics, *Phys. Rep.* 97(2–3), 31 (1983)
127. T. Sjöstrand and M. Bengtsson, The Lund Monte Carlo for jet fragmentation and e^+e^- physics – jetset version 6.3 – an update, *Comput. Phys. Commun.* 43(3), 367 (1987)
128. B. Andersson, G. Gustafson, and B. Nilsson-Almqvist, A model for low-p_T hadronic reactions with generalizations to hadron–nucleus and nucleus–nucleus collisions, *Nucl. Phys. B* 281(1–2), 289 (1987)
129. G. Gatoff and C. Y. Wong, Origin of the soft p_T spectra, *Phys. Rev. D* 46(3), 997 (1992)
130. C. Y. Wong and G. Gatoff, The transverse profile of a color flux tube, *Phys. Rep.* 242(4–6), 489 (1994)
131. C. Y. Wong, R. C. Wang, and C. C. Shih, Study of particle production using two-dimensional bosonized QED, *Phys. Rev. D* 44(1), 257 (1991)
132. H. Aihara, et al. (TPC/Two_Gamma Collaboration), Charged hadron production in e^+–e^- annihilation at $\sqrt{s} = 29$ GeV, Lawrence Berkeley Laboratory Report LBL-23737 (1988)
133. W. Hofmann, Particle composition in hadronic jets in e^+–e^- annihilation, *Annu. Rev. Nucl. Part. Sci.* 38(1), 279 (1988)
134. A. Petersen, et al. (Mark II Collaboration), Multihadronic

events at $E_{\rm CM}$ = 29 GeV and predictions of QCD models from $E_{\rm CM}$ = 29 GeV to $E_{\rm CM}$ = 93 GeV, *Phys. Rev. D* 37, 1 (1988)
135. K. Abe, et al. (SLD Collaboration), Production of π^+, K^+, K^0, $K_*{}^0$, ϕ, p, and Λ^0 in hadronic Z^0 decays, *Phys. Rev. D* 59, 052001 (1999)
136. K. Abreu, et al. (DELPHI Collaboration), Energy dependence of inclusive spectra in e^+–e^- annihilation, *Phys. Lett. B* 459, 397 (1999)
137. H. Yang (BRAHMS Collaboration), Rapidity densities of $\pi^\pm$, $K^\pm$, p and $\bar{p}$ in p+p and d+Au collisions at $\sqrt{s_{\rm NN}}$ = 200 GeV, *J. Phys. G.* 35, 104129 (2008)
138. K. Hagel (BRAHMS Collaboration), APS DNP 2008, Oakland, California, USA, Oct. 23–27, 2008
139. M. Gell-Mann, R. J. Oakes, and B. Renner, Behavior of current divergences under $SU(3)$*$SU(3)$, *Phys. Rev.* 175(5), 2195 (1968)
140. T. Barnes and E. S. Swanson, Diagrammatic approach to meson–meson scattering in the nonrelativistic quark potential model, *Phys. Rev. D* 46(1), 131 (1992)
141. C. Y. Wong, E. S. Swanson, and T. Barnes, Cross sections for π- and ρ-induced dissociation of J/ψ and ψ', *Phys. Rev. C Nucl. Phys.* 62, 045201 (2000)
142. C. Y. Wong, E. S. Swanson, and T. Barnes, Heavy quarkonium dissociation cross sections in relativistic heavy-ion collisions, *Phy. Rev. C* 65, 014903 (2002), arXiv: nucl-th/0106067
143. M. Baldicchi, A. V. Nesterenko, G. M. Prosperi, and C. Simolo, QCD coupling below 1 GeV from quarkonium spectrum, *Phys. Rev. D* 77(3), 034013 (2008)
144. A. Deur, S. J. Brodsky, and G. F. de Téramond, The QCD running coupling, *Prog. Part. Nuc. Phys.* 90, 1 (2016), arXiv: 1604.08082
145. F. Low, Bremsstrahlung of very low-energy quanta in elementary particle collisions, *Phys. Rev.* 110(4), 974 (1958)
146. V. N. Gribov, Bremsstrahlung of hadrons at high energies, *Yad. Fiz.* 5, 399 (1967) [*Sov. J. Nucl. Phys.* 5, 280 (1967)]
147. L. Van Hove, Cold quark–gluon plasma and multiparticle production, *Ann. Phys.* 192(1), 66 (1989)
148. P. Lichard, and L. Van Hove, The cold quark–gluon plasma as a source of very soft photons in high energy collisions, *Phys. Lett. B* 245(3–4), 605 (1990)
149. P. Lichard, Consistency of data on soft photon production in hadronic interactions, *Phys. Rev. D* 50(11), 6824 (1994)
150. E. Kokoulina, A. Kutov, and V. Nikitin, Gluon dominance model and cluster production, *Braz. J. Phys.* 37(2c), 785 (2007)
151. M. Volkov, E. Kokoulina, and E. Kuraev, Gluon dominance model and cluster production, *Ukr. J. Phys.* 49, 1252 (2003)
152. S. Barshay, Anomalous soft photons from a coherent hadronic phase in high-energy collisions, *Phys. Lett. B* 227(2), 279 (1989)
153. E. Shuryak, The soft photon puzzle and pion modification in hadronic matter, *Phys. Lett. B* 231(1–2), 175 (1989)
154. V. Balek, N. Pisutova, and J. Pisut, The puzzle of very soft photon production in hadronic Interactions, *Acta Phys. Pol. B* 21, 149 (1990)
155. W. Czyz and W. Florkowski, Soft photon production in the boost invariant color flux tube model, *Z. Phys. Chem.* 61, 171 (1994)
156. O. Nachtmann, Nonperturbative QCD effects in high-energy collisions, arXiv: hep-ph/9411345 (1994)
157. G. W. Botz, P. Haberl, and O. Nachtmann, Soft photons in hadron hadron collisions: Synchrotron radiation from the QCD vacuum? *Z. Phys. Chem.* 67, 143 (1995)
158. P. Lebiedowicz, O. Nachtmann, and A. Szczurek, Soft-photon radiation in high-energy proton–proton collisions within the tensor-Pomeron approach: Bremsstrahlung, *Phys. Rev. D* 106, 034023 (2022), arXiv: 2206.03411
159. Y. Hatta and T. Ueda, Soft photon anomaly and gauge /string duality, *Nucl. Phys. B* 837(1–2), 22 (2010)
160. S. M. Darbinian, K. A. Ispirian, and A. T. Margarian, Unruh radiation of quarks and the soft photon puzzle in hadronic interactions, *Sov. J. Nucl. Phys.* 54, 364 (1991)
161. Yu. A. Simonov, Di-pion decays of heavy quarkonium in the field correlator method, *Phys. Atom. Nucl.* 71, 1049 (2008), arXiv: hep-ph/07113626
162. Yu. A. Simonov, Di-pion emission in heavy quarkonia decays, *JETP Lett.* 87(3), 121 (2008)
163. Yu. A. Simonov and A. I. Veselov, Bottomonium $\Upsilon(5S)$ decays into BB and $BB\pi$, *JETP Lett.* 88(1), 5 (2008)
164. Yu. A. Simonov and A. I. Veselov, Strong decays and di-pion transitions of $\Upsilon(5S)$, *Phys. Lett. B* 671(1), 55 (2009)
165. D. E. Kharzeev and F. Loshaj, Anomalous soft photon production from the induced currents in Dirac sea, *Phys. Rev. D* 89(7), 074053 (2014)
166. R. Hagedorn, Statistical thermodynamics of strong interactions at high energies, *Nuo. Cim. Suppl.* 3, 147 (1965)
167. I. Abelev, et al. (STAR Collaboration), Strange particle production in p^+p collisions at $\sqrt{s}$ = 200 GeV, *Phys. Rev. C* 75(6), 064901 (2007)
168. I. Abelev, et al. (STAR Collaboration), Systematic measurements of identified particle spectra in pp, d+Au, and Au+Au collisions at the STAR detector, *Phys. Rev. C* 79, 034909 (2009)
169. A. Adare, et al. (PHENIX Collaboration), Measurement of neutral mesons in pp collisions at $\sqrt{s}$=200 GeV, *Phys. Rev. D* 83, 052004 (2011)
170. A. T. D'yachenko and E. S. Gromova, Detection of particles of dark matter from the spectrum of secondary particles in high-energy proton–proton collisions in a thermodynamic model, *J. Phys. Conf. Series* 2131, 022 (2021)
171. A. T. D'yachenko, A. A. Verisokina, and M. A. Verisokina, High-energy collisions of protons and nuclei and the possibility of detecting dark matter particles in the spectra of soft photons, *Acta Phys. Pol. B Proc. Suppl.* 14(4), 761 (2021)
172. F. W. N. de Boer, O. Fröhlich, K. E. Stiebing, K. Bethge, H. Bokemeyer, A. Balanda, A. Buda, R. van Dantzig, T. W. Elze, H. Folger, J. van Klinken, K. A. Müller, K. Stelzer, P. Thee, and M. Waldschmidt, A deviation in internal pair conversion, *Phys. Lett. B* 388(2), 235 (1996)

173. F. W. N. de Boer, R. van Dantzig, J. van Klinken, K. Bethge, H. Bokemeyer, A. Buda, K. A. Müller, and K. E. Stiebing, Excess in nuclear pairs near 9 MeV/c^2 invariant mass, *J. Phys. G* 23(11), L85 (1997)
174. F. W. N. de Boer, K. Bethge, H. Bokemeyer, R. van Dantzig, J. van Klinken, V. Mironov, K. A. Müller, and K. E. Stiebing, Further search for a neutral boson with a mass around 9 MeV/c^2, *J. Phys. G* 27(4), L29 (2001), arXiv: hep-ph/0101298v2
175. A. Vitéz, A. Krasznahorkay, J. Gulyás, and M. Csatlós, L. Csige Z. Gácsi, A. Krasznahorkay Jr., B. M. Nyakó, F. W. N. de Boer, T. J. Ketel, 33 anomalous internal pair creation in ^{8}Be as a signature of the decay of a new particle, *Acta Phys. Pol.* B39, 483 (2008)
176. X. Zhang and G. A. Miller, Can nuclear physics explain the anomaly observed in the internal pair production in the Beryllium-8 nucleus? *Phys. Lett. B* 773, 159 (2017)
177. J. Feng, et al., Protophobic fifth force interpretation of the observed anomaly in ^{8}Be nuclear transitions, *Phys. Rev. Lett.* 117, 071803 (2016) (2016)
178. J. Feng, B. Fornal, I. Galon, S. Gardner, J. Smolinsky, T. M. P. Tait, and P. Tanedo, Particle physics models for the 17 MeV anomaly in beryllium nuclear decays, *Phys. Rev. D* 95(3), 035017 (2017)
179. B. Fornal, Is there a sign of new physics in beryllium transitions? *Int. J. Mod. Phys. A* 32(25), 1730020 (2017)
180. J. Batley, et al. (NA48/2 Collaboration), Search for the dark photon in π^0 decays, *Phys. Lett. B* 746, 178 (2015)
181. L. D. Rose, S. Khalil, and S. Moretti, Explanation of the 17 MeV Atomki anomaly in a $U(1)$-extended two Higgs doublet model, *Phys. Rev. D* 96(11), 115024 (2017)
182. L. Delle Rose, S. Khalil, S. J. D. King, S. Moretti, and A. M. Thabt, Atomki anomaly in family-dependent $U(1)$ extension of the standard model, *Phys. Rev. D* 99(5), 055022 (2019)
183. L. Delle Rose, S. Khalil, S. J. D. King, and S. Moretti, New physics suggested by Atomki anomaly, *Front. Phys. (Lausanne)* 7, 73 (2019)
184. J. Bordes, H. M. Chan, and T. S. Tsun, Accommodating three low-scale anomalies (g-2, Lamb shift, and Atomki) in the framed standard model, *Int. J. Mod. Phys. A* 34 (25), 1830034 (2019), and references cited therein
185. H. M. Chan and S. T. Tsou, Two variations on the theme of Yang and Mills - the SM and the FSM Invited contribution to the "Festschrift for the Yang Centenary" (edited by F. C. Chen, et al.), arXiv: 2201.12256 (2022)
186. U. Ellwanger and S. Moretti, Possible explanation of the electron positron anomaly at 17 MeV in ^{8}Be transitions through a light pseudoscalar, *J. High Energy Phys.* 11(11), 39 (2016)
187. D. S. M. Alves and N. J. Weiner, A viable QCD axion in the MeV mass range, *J. High Energy Phys.* 07(7), 92 (2018)
188. V. Kubarovsky and J. Rittenhouse West, and S. J. Brodsky, Quantum chromodynamics resolution of the ATOMKI anomaly in ^{4}He nuclear transitions, arXiv: 2206.14441 (2022)
189. M. Viviani, L. Girlanda, A. Kievsky, and L. E. Marcucci, n+^{3}H, p+^{3}He, p+^{3}H, and n+^{3}He scattering with the hyper-spherical harmonic method, *Phys. Rev. C* 102(3), 034007 (2020)
190. M. Viviani, E. Filandri, L. Girlanda, C. Gustavino, A. Kievsky, L. E. Marcucci, and R. Schiavilla, X17 boson and the $H^3(p, e^+ e^-)He^4$ and $He^3(n, e^+ e^-)He^4$ processes: A theoretical analysis, *Phys. Rev. C* 105(1), 014001 (2022)
191. M. Munch, O. Sølund Kirsebom, J. A. Swartz, K. Riisager, and H. O. U. Fynbo, Measurement of the full excitation spectrum of the ^{7}Li(p, γ)αα reaction at 441 keV, *Phys. Lett. B* 782, 779 (2018)
192. D. Banerjee, et al. (NA64 Collaboration), Search for a hypothetical 16.7 MeV gauge boson and dark photons in the NA64 Experiment at CERN, *Phys. Rev. Lett.* 120(23), 231802 (2018)
193. D. Banerjee, et al. (NA64 Collaboration), Improved limits on a hypothetical X(16.7) boson and a dark photon decaying into e^+e^- pairs, arXiv: 1912.11389 (2019)
194. C. Taruggi, A. Ghoshal, and M. Raggi (for the PADME Collaboration), Searching for dark photons with the PADME experiment (Conference: C18-05-07.4, pp 17–21, pp 28–34, and pp 337–344), *Frascati Phys. Ser.* 67, 17, 28, and 334 (2018)
195. D. Barducci and C. Toni, An updated view on the ATOMKI nuclear anomalies, arXiv: 2212.06453 (2022)
196. Kh. U. Abraamyan, et al., Resonance structure in the γγ invariant mass spectrum in pC and dC interactions, *Phys. Rev. C* 80, 034001 (2009)
197. Kh. U. Abraamyan, A. B. Anisimov, M. I. Baznat, K. K. Gudima, M. A. Kozhin, V. I. Kukulin, M. A. Nazarenko, S. G. Reznikov, and A. S. Sorin, Diphoton and dipion productions at the Nuclotron/NICA, *Eur. Phys. J. A* 52(8), 259 (2016)
198. W. T. Donnelly, S. J. Freedman, R. S. Lytel, R. D. Peccei, and M. Schwartz, Do axions exist? *Phys. Rev. D* 18(5), 1607 (1978)
199. M. E. El-Nadi and O. E. Badawy, Production of a new light neutral boson in high-energy collisions, *Phys. Rev. Lett.* 61(11), 1271 (1988)
200. M. E. El-Nadi, et al, External electron pair production in high-energy collisions, *Nuo. Cim. A* 109, 1517 (1996)
201. P. L. Jain and G. Singh, Search for new particles decaying into electron pairs of mass below 100 MeV/c^2, *J. Phys. G* 34(1), 129 (2007)
202. F. W. N. de Boer, and C. A. Fields, A re-evaluation of evidence for light neutral bosons in nuclear emulsions, *Int. J. Mod. Phys. E* 20(8), 1787 (2011), arXiv: 1001.3897
203. J. Bernhard, and K. Schönning, Test of OZI violation in vector meson production with COMPASS, arXiv: 1109.0272v2 (2011)
204. J. Bernhard, Exclusive vector meson production in pp collisions at the COMPASS experiment, Ph. D. Thesis, University of Mainz, 2014
205. T. Schlüter, The exotic $\eta\pi^-$ wave in 190 GeV π–$p \rightarrow \pi$–$\eta' p$ at COMPASS, arXiv: 1108.6191v2 (2011)
206. T. Schlüter, The π–η and π–η′ systems in exclusive 190

GeV/c π–p Reactions at COMPASS, Ph. D. Thesis, Univ. München, 2012
207. J. Bernhard, J. M. Friedrich, T. Schlüter, and K. Schönning, Comment on "Material evidence of a 38 MeV boson", arXiv: 1204.2349 (2012)
208. E. van Beveren, and G. Rupp, First indications of the existence of a 38 MeV light scalar boson arXiv: 1102.1863 (2011)
209. E. van Beveren, and G. Rupp, Material evidence of a 38 MeV boson, arXiv: 1202.1739 (2012)
210. E. van Beveren and G. Rupp, Reply to Comment on "Material evidence of a 38 MeV boson", arXiv: 1204.3287 (2012)
211. E. van Beveren and G. Rupp, $Z^0(57)$ and $E(38)$: possible surprises in the Standard Model, arXiv: 2005.08559 (2020) (accepted for publication in *Acta Physica Polonica B Proc. Suppl.*)
212. C. Y. Wong, Shells in a simple anisotropic harmonic oscillator, *Phys. Lett. B* 14(8), 668 (1970)
213. C. Y. Wong, Interaction barrier in charged-particle nuclear reactions, *Phys. Rev. Lett.* 31(12), 766 (1973)
214. T. G. Lee, O. Bayrak, and C. Y. Wong, Pocket resonances in low-energy antineutrons reactions with nuclei, *Phys. Lett. B* 817, 136301 (2021), arXiv: 2102.06691
215. J. A. Wheeler, Molecular viewpoints in nuclear structure, *Phys. Rev.* 52(11), 1083 (1937)
216. D. R. Tilley and H. R. Weller, Energy levels of light nuclei A=4, *Nucl. Phys. A* 541, 1 (1992)
217. D. R. Tilley, J. H. Kelley, J. L. Godwin, D. J. Millener, J. Purcell, C. G. Sheu, and H. R. Weller, Energy levels of light nuclei, *Nucl. Phys. A* 745(3–4), 155 (2004)
218. J. L. Feng, T. M. P. Tait, and C. B. Verharen, Dynamical evidence for a fifth force explanation of the ATOMKI nuclear anomalies, *Phys. Rev. D* 102(3), 036016 (2020)
219. W. B. He, Y. G. Ma, X. G. Cao, X. Z. Cai, and G. Q. Zhang, Dipole oscillation modes in light alpha-clustering nuclei, *Phys. Rev. C* 94(1), 014301 (2016), arXiv: 1602.08955
220. B. L. Berman and S. C. Fultz, Measurements of the giant dipole resonance with monoenergetic photons, *Rev. Mod. Phys.* 47(3), 713 (1975)
221. J. H. Kelley, J. E. Purcell, and C. G. Sheu, Energy levels of light nuclei A = 12, *Nucl. Phys. A* 968, 71 (2017)
222. L. D. Landau, The moment of a 2-photon system, *Dokl. Akad. Nauk SSSR* 60, 207 (1948)
223. C. N. Yang, Selection rules for the dematerialization of a particle into two photons, *Phys. Rev.* 77(2), 242 (1950)
224. E. van Beveren and G. Rupp, First indications of the existence of a 38 MeV light scalar boson, arXiv: 1102.1863 (2011)
225. E. van Beveren and G. Rupp, Material evidence of a 38 MeV boson, arXiv: 1202.1739 (2012)
226. E. Guido (BaBar Collaboration), Lepton universality test in Upsilon(1S) decays at BABAR, Proceedings of the DPF-2009 Conference, Detroit, MI, July 27–31, 2009, arXiv: 0910.0423
227. A. Bauswein, N. U. F. Bastian, D. Blaschke, K. Chatziioannou, J. A. Clark, T. Fischer, and M. Oertel, Identifying a first-order phase transition in neutron-star mergers through gravitational waves, *Phys. Rev. Lett.* 122(6), 061102 (2019)
228. A. Bauswein, S. Blacker, V. Vijayan, N. Stergioulas, K. Chatziioannou, J. A. Clark, N. U. F. Bastian, D. B. Blaschke, M. Cierniak, and T. Fischer, Equation of state constraints from the threshold binary mass for prompt collapse of neutron star mergers, *Phys. Rev. Lett.* 125(14), 141103 (2020)
229. L. R. Weih, M. Hanauske, and L. Rezzolla, Postmerger gravitational-wave signatures of phase transitions in binary mergers, *Phys. Rev. Lett.* 124(17), 171103 (2020)
230. E. Annala, T. Gorda, A. Kurkela, J. Naettilae, and A. Vuorinen, Evidence for quark-matter cores in massive neutron stars, *Nat. Phys.* 16(9), 907 (2020)
231. R. Barate, et al. (ALPEPH Collaboration), Inclusive production of neutral pions in hadronic Z decays, *Z. Phys. C* 74, 451 (1997)
232. C. Amsler, et al. (Particle Data Group), Review of particle physics, *Phys. Lett. B* 667(1–5), 1 (2008)
233. V. M. Aulchenko, et al. (CMD-2 Collaboration), Measurement of the pion form factor in the range 1.04–1.38 GeV with the CMD-2 detector, *JETP Lett.* 82(12), 743 (2005) (*Pisma Zh. Eksp. Teor. Fiz.* 82, 841 (2005), arXiv: hep-ex/0603021
234. T. Aaltonen, et al. (CDF Collaboration), Precision measurement of the X(3872) mass in $J/\psi\ \pi^+\pi^-$ decays, *Phys. Rev. Lett.* 103, 152001 (2009), arXiv: 0906.5218
235. B. Aubert, et al. (BarBar Collaboration), Study of hadronic transitions between Υ states and observation of $\Upsilon(4S)\to\eta\,\Upsilon(1S)$ decay, *Phys. Rev. D* 78, 112002 (2008), arXiv: 0807.2014
236. E. F. Taylor and J. A. Wheeler, Space-time Physics, W. H. Freeman and Co., 2nd Ed., 1992, page 20
237. C. N. Yang, Charge quantization, compactness of the gauge group, and flux quantization, *Phys. Rev. D* 8(8), 2360 (1970)
238. A. C. Hayes, J. Friar, G. M. Hale, and G. T. Garvey, Angular correlations in the e^+e^- decay of excited states in ^{8}Be, *Phys. Rev. C* 105(5), 055502 (2022), arXiv: 2106.06834
239. M. Lüscher, Symmetry breaking aspects of the roughening transition in gauge theories, *Nucl. Phys. B* 180(2), 317 (1981)
240. M. Lüscher, K. Symanzik, and P. Weisz, Anomalies of the free loop wave equation in the WKB approximation, *Nucl. Phys. B* 173(3), 365 (1980)
241. J. Polchinski and A. Strominger, Effective string theory, *Phys. Rev. Lett.* 67(13), 1681 (1991)
242. C. Bonati, M. Caselle, and S. Morlacchi, The unreasonable effectiveness of effective string theory: The case of the 3D $SU(2)$ Higgs model, *Phys. Rev. D* 104(5), 054501 (2021), arXiv: 2106.08784
243. M. Billo, M. Caselle, and R. Pellegrini, New numerical results and novel effective string predictions for Wilson loops, *J. High Energy Phys.* 01(1), 104 (2012) [Erratum: *J. High Energy Phys.* 04, 097 (2013)], arXiv: 1107.4356
244. M. Lüscher and P. Weisz, String excitation energies in $SU(N)$ gauge theories beyond the free-string approxi-

mation, *J. High Energy Phys.* 0407, 014 (2004), arXiv: hep-th/0406205
245. M. Billo and M. Caselle, Polyakov loop correlators from D^0-brane interactions in bosonic string theory, *J. High Energy Phys.* 0507, 038 (2005), arXiv: hep-th/0505201
246. M. Billo, M. Caselle, and L. Ferro, The partition function of interfaces from the Nambu–Goto effective string theory, *J. High Energy Phys.* 0602, 070 (2006), arXiv: hep-th/0601191
247. H. Georgi, Unparticle physics, *Phys. Rev. Lett.* 98(22), 221601 (2007)
248. H. Georgi and Y. Kats, Unparticle examples in 2D, *Phys. Rev. Lett.* 101(13), 131603 (2008)
249. S. Hellerman, S. Maeda, J. Maltz, and I. Swanson, Effective string theory simplified, *J. High Energy Phys.* 09(9), 183 (2014), arXiv: 1405.6197
250. O. Aharony and Z. Komargodski, The effective theory of long strings, *J. High Energy Phys.* 05(5), 118 (2013), arXiv: 1302.6257
251. E. Eichten, K. Gottfried, T. Kinoshita, J. B. Kogut, K. B. Lane, and T. M. Yan, Spectrum of charmed quark–antiquark bound states, *Phys. Rev. Lett.* 34(6), 369 (1975)
252. H. W. Crater, J. H. Yoon, and C. Y. Wong, Singularity structures in Coulomb-type potentials in two body Dirac equations of constraint dynamics, *Phys. Rev. D* 79(3), 034011 (2009), arXiv: 0811.0732
253. M. Peshkin, Short distance analysis for heavy quark systems. 1. Diagrammatics, *Nucl. Phys. B* 156(3), 365 (1979)
254. G. Bhanot and M. Peshkin, Short distance analysis for heavy quark systems. 2. Applications, *Nucl. Phys. B* 156(3), 391 (1979)
255. S. K. Choi, et al., Observation of a narrow charmonium-like state in exclusive $B^{\pm} \to K^{\pm}\pi^{+}\pi^{-}$ J/ψ decays, *Phys. Rev. Lett.* 91, 262001 (2003)
256. C. Y. Wong, Molecular states of heavy quark mesons, *Phys. Rev. C* 69(5), 055202 (2004), arXiv: hep-ph/0311088
257. N. A. Tornqvist, Isospin breaking of the narrow charmonium state of Belle at 3872 MeV as a deuson, *Phys. Lett. B* 590(3–4), 209 (2004)
258. F. E. Close and P. R. Page, The $D^{*0}D^0$ threshold resonance, *Phys. Lett. B* 578(1–2), 119 (2004)
259. S. Pakvasa and M. Suzuki, On the hidden charm state at 3872 MeV, *Phys. Lett. B* 579(1–2), 67 (2004)
260. E. S. Swanson, Diagnostic decays of the $X(3872)$, *Phys. Lett. B* 598(3–4), 197 (2004)
261. M. B. Voloshin, Interference and binding effects in decays of possible molecular component of $X(3872)$, *Phys. Lett. B* 579(3–4), 316 (2004)
262. F. K. Guo, C. Hanhart, U. G. Meißner, Q. Wang, Q. Zhao, and B. S. Zou, Hadronic molecules, *Rev. Mod. Phys.* 90, 015004 (2018) [Erratum: *Rev. Mod. Phys.* 94(2), 029901 (2022)], arXiv: 1705.00141
263. B. Yang, L. Meng, and S. L. Zhu, Possible molecular states composed of doubly charmed baryons with coupled-channel effect, *Eur. Phys. J. A* 56(2), 67 (2020), arXiv: 1906.04956
264. X. K. Dong, F. K. Guo, and B. S. Zou, A survey of heavy–antiheavy hadronic molecules, *Progr. Phys.* 41(2), 65 (2021), arXiv: 2101.01021
265. S. Q. Luo, T. W. Wu, M. Z. Liu, L. S. Geng, and X. Liu, Triple-charm molecular states composed of D^*D^*D and $D^*D^*D^*$, *Phys. Rev. D* 105(7), 074033 (2022), arXiv: 2111.15079
266. P. Adlarson, et al. (WASA-at-COSY Collaboration and SAID Data Analysis Center), Evidence for a new resonance from polarized neutron–proton scattering, *Phys. Rev. Lett.* 112(20), 202301 (2014)
267. P. Adlarson, et al., Neutron–proton scattering in the context of the $d^*(2380)$ resonance, *Phys. Rev. C* 90(3), 035204 (2014)
268. R. Workman, Poles in the SAID NN analysis, *EPJ Web Conf.* 81, 02023 (2014)
269. R. L. Workman, W. J. Briscoe, and I. I. Strakovsky, Sensitivity of the COSY dibaryon candidate to np elastic scattering measurements, *Phys. Rev. C* 93(4), 045201 (2016)
270. M. Bashkanov, S. J. Brodsky, and H. Clement, Novel six-quark hidden-color dibaryon states in QCD, *Phys. Lett. B* 727(4–5), 438 (2013)
271. T. Goldman, K. Maltman, G. J. Stephenson, K. E. Schmidt, and F. Wang, "Inevitable" nonstrange dibaryon, *Phys. Rev. C* 39(5), 1889 (1989)
272. J. L. Ping, H. X. Huang, H. R. Pang, F. Wang, and C. W. Wong, Quark models of dibaryon resonances in nucleon–nucleon scattering, *Phys. Rev. C* 79(2), 024001 (2009)